SPINAL CORD INJURY MECHANISMS: A FINITE ELEMENT STUDY

by

CAROLYN YVONNE GREAVES

B.A.Sc, The University of Waterloo, 2001

A THESIS SUBMITTED IN PARTIAL FULFILMENT OF
THE REQUIREMENTS FOR THE DEGREE OF

MASTER OF APPLIED SCIENCE

in

THE FACULTY OF GRADUATE STUDIES
DEPARTMENT OF MECHANICAL ENGINEERING

We accept this thesis as conforming to the required standard

THE UNIVERSITY OF BRITISH COLUMBIA

May 2004

Library Authorization

In presenting this thesis in partial fulfillment of the requirements for an advanced degree at the University of British Columbia, I agree that the Library shall make it freely available for reference and study. I further agree that permission for extensive copying of this thesis for scholarly purposes may be granted by the head of my department or by his or her representatives. It is understood that copying or publication of this thesis for financial gain shall not be allowed without my written permission.

Carolyn Greaves
Name of Author *(please print)*

21/05/2004
Date (dd/mm/yyyy)

Title of Thesis: Spinal cord injury mechanisms: a finite element study

Degree: Master of Applied Science Year: 2004

Department of Mechanical Engineering
The University of British Columbia
Vancouver, BC Canada

Abstract

Spinal cord injury is one of the most devastating medical conditions known. These injuries result from a variety of spinal column injury mechanisms; however, the mechanical relationship between column and cord injuries is not known. The objectives of this research project were to develop and validate a finite element model of the spinal cord and the surrounding structures and to use this model to compare the strain distributions in the spinal cord for three simple injury mechanisms: compression (contusion), distraction, and dislocation. The final goal was to compare linear elastic and hyperelastic constitutive models for the spinal cord in response to distraction loading.

Geometry of the model was obtained from the Visible Human Project of the National Library of Medicine and developed into a three-dimensional FE model in Ansys (Ansys User's Manual version 7.1). Three vertebrae (C4-6) and the spinal cord were modelled with brick elements, dura mater was modelled with shell elements, and ligaments and discs were modelled with cable elements. Material properties for the tissues were based on experimental data in the literature. Boundary conditions and loading were designed to simulate experimental data in the literature. The model was transferred to Abaqus (Abaqus User's Manual version 6.3 2002) for the comparison of constitutive models.

The model of spinal cord compression was validated with previous experimental data based on the reaction force at the indentor tip (Hung, Lin et al. 1979; Hung, Lin et al. 1982; Tencer, Allen et al. 1985). The distraction injury model was validated based on relative displacements of the column and cord (Maiman, Coats et al. 1989). No experimental data was available for validation of the dislocation injury mechanism.

Different strain distributions were found for compression, distraction, and dislocation injury mechanisms. The highest strains within the compression injury mechanism were in the dorsal, ventral, and central columns with critical regions in the dorsomedial and ventral white matter between the indentor and the opposing vertebral body. Strains for distraction were more uniformly distributed throughout the cord. The dislocation injury mechanism seemed to spare the lateral columns of normal strains, however all columns experienced elevated shear strains. Critical regions of strain were in the dorsolateral and ventral white matter at the level of the contacting lamina and vertebral body. Linear elastic and hyperelastic constitutive models produced similar strain distributions (difference of less than 1% strain between each maximum component strain) for axial loading of the spinal cord up to 8% axial strain. Assuming the hyperelastic model best represents the behaviour of spinal cord tissue, the linear elastic model overestimated the range of axial strains and underestimated the dorsal-ventral and transverse shear strains for axial strains between 17 and 33%.

The compression results reveal the most extensive damage peripherally, which has not been found experimentally. This highlights the possibility of a mechanical or biological susceptibility of grey matter. Results from this study suggest that dislocation injuries may result in more extensive shear strains than burst fracture injuries, which apply one-sided contusion to the cord. Extensive distraction of the spinal cord resulted in substantial shear strains. For static loading up to 8% strain, the linear elastic model may be used for FE modeling of the spinal cord.

Table of Contents

List of Tables

List of Figures

Acknowledgements

I would like to first acknowledge Dr. Tom Oxland for welcoming me into the lab and for his vision and guidance. I would also like to thank Dr. Mohamed Gadala for his patience and open-mindedness to the field of biomechanics. Dr Lynne Bilston was instrumental in the transfer of the model to Abaqus, as well as the hyperelastic material modelling. Sincere thanks also to Carolyn Sparrey and Anthony Choo who helped provide an experimental viewpoint to the model. Their valuable input was appreciated as well as their partnership in being the lone engineers in a room of neuroscientists.

I am grateful to the Michael Smith Foundation for Health Research who recognized my research potential and the value of this interdisciplinary project.

I would like to acknowledge the Visible Human Project of the National Library of Medicine who provided images for this study as well as the Visible Human, himself.

I would like to thank my ever supportive parents and my sisters who continue to motivate me. I would also like to thank my pit crew, Chris Van Toen, for his encouragement and faith in me.

Many other people have assisted my research by providing well thought-out questions, research ideas, methodology suggestions, finite element expertise, and caffeine: Christina Niosi, Juay Seng Tan, Khaled Ahmed, Hanspeter Frei, Daan Majier, Dr. Peter Cripton, Simon Sjvold, Chad Larson, Dr. Dave Wilson, Catherine Kinnaird, and Joanne Lim.

1 Introduction

1.1 Clinical Problem

Spinal cord injury (SCI) results in loss of motor or sensory function and is one of the most catastrophic medical conditions known. Injured individuals must undergo initial hospitalisation followed by a period of readjustment and rehabilitation in which they must learn a new way of life. The annual incidence rate of traumatic spinal cord injury in Canada is 52.5 per million population (Dryden, Saunders et al. 2003), while reported rates for other countries are between 14.5 and 54.8 per million population (Griffin, O'Fallon et al. 1985; Griffin, Opitz et al. 1985; Dixon, Danesh et al. 1993; O'Connor 2002). Each year, approximately 1,700 new spinal cord injuries occur in Canada (Dryden, Saunders et al. 2003), while 16,000 new spinal cord injuries occur in the United States (Kraus, Franti et al. 1975; Griffin, Opitz et al. 1985). These injuries are devastating to the injured individuals, their families, and to society, where the annual economic cost is over $9.7 billion in the United States (Berkowitz, O'Leary et al. 1998). SCI usually removes a young, previously healthy individual from society as most patients are below 30 years of age (Tator, Duncan et al. 1993). Indirect costs due to loss in productivity have been estimated at $2.6 billion in the United States (Berkowitz, O'Leary et al. 1998). Although significant advances in care and rehabilitation have increased longevity for paraplegic and quadriplegic individuals, hospital costs due to traumatic SCI are increasing (DeVivo, Rutt et al. 1992). Improved treatment for SCI would have immense personal, familial, and socioeconomic impact.

The most common causes of SCI are motor vehicle accidents, falls, sports, and violence (Myers and Winkelstein 1995). Motor vehicle accidents, including pedestrian, motorcycle and bicycle accidents, are the leading cause of injury and account for 41 to 66% of all SCI's (Griffin, Opitz et al. 1985; Dixon, Danesh et al. 1993; Tator, Duncan et al. 1993; O'Connor 2002; Dryden, Saunders et al. 2003; Pickett, Simpson et al. 2003). SCI also commonly results from sports, such as surfing, snowmobiling, rugby, football, trampoline, shallow water diving, skiing, waterskiing, track and field, skydiving, ice

hockey, and wrestling (Shields, Fox et al. 1978; Reid and Saboe 1989; Dixon, Danesh et al. 1993; Myers and Winkelstein 1995).

It is generally accepted that SCI occurs in two stages involving primary and secondary mechanisms (Sekhon and Fehlings 2001). The primary phase is the mechanical impact to the cord causing local deformation and physical damage to the tissue. The secondary phase of injury is a series of time-dependent biochemical and cellular changes in the tissue which are initiated by primary injury and cause ongoing cellular damage and cell death. Although much work has focused on elucidating the complex pathophysiological processes involved in SCI, the complexities and inter-relationships of the secondary mechanisms are not currently fully understood.

Primary injury is a combination of the initial impact as well as subsequent persisting compression. Primary injury may be defined by a set of mechanical parameters, such as magnitude, location, and direction of the applied force, rate of force application, and duration of force application. Little is known of the mechanical insult to the spinal cord during trauma and its relationship to the resulting injury.

This study is motivated by a desire to understand the details of the mechanical loads on the spinal cord which give rise to neurological damage. Although primary injury may be considered irreversible, it could have important pathophysiological implications, since there may be an opportunity to intervene with therapeutics before extensive secondary damage has occurred. The extent and nature of primary damage incurred during an injury event provides the baseline from which treatment strategies may begin to prevent further damage (neuroprotective), optimise the function of the remaining tissue (rehabilitative), and repair neural tissue that has been damaged (regenerative). If it is determined that one injury mechanism selectively injures one region of the spinal cord, directed therapeutics may be developed to stop the progression of secondary damage and perhaps even provide an environment in which the damaged tissue may repair itself.

1.2 Background Literature

1.2.1 Anatomy

The spinal cord is the major reflex centre and conduction pathway between the brain and the body. It is a cylindrical structure that is slightly flattened anteriorly and posteriorly. Thirty-one pairs of spinal nerves extend from the spinal cord and provide conduction pathways to the rest of the body. The spinal cord is made up of specialized cells (neurons) which conduct signals throughout the nervous system. The spinal cord is protected by several layers of tissues (meninges) and it is contained inside a bony canal. The bones making up this canal (vertebrae) are separated and bound together by intervertebral (IV) discs and ligaments. This structure of bones and connecting soft tissues (the spinal column) protects the spinal cord.

1.2.1.1 Spinal Column

The spine is a mechanically and geometrically complex structure. The human vertebral column consists of 33 vertebrae arranged in five regions: seven cervical, 12 thoracic, five lumbar, five sacral, and four coccygeal (Figure 1.1).

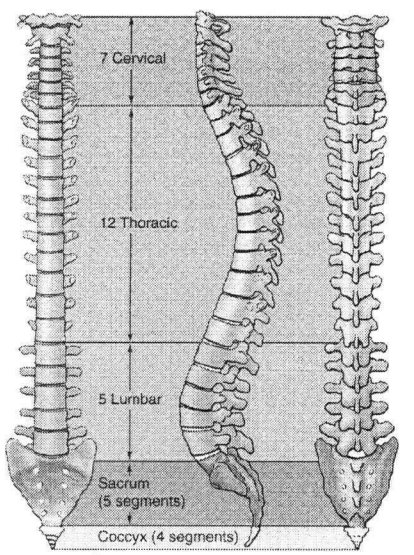

Figure 1.1: Regions of the spinal column (Figure was modified from Moore and Dalley 1999)

Vertebrae vary in size and other characteristics in different regions of the vertebral column. A typical vertebra consists of a vertebral body, a vertebral arch, and seven processes (Figure 1.2). The vertebral body is the large anterior portion of the bone that gives strength to the vertebral column and supports body weight. The vertebral arch is posterior to the body and is made up of left and right pedicles and a lamina. The pedicles are short processes that join the vertebral arch to the body. The pedicles project posteriorly to join the lamina, which is a broad, flat plate of bone. The vertebral arch and the posterior portion of the body form the walls of the vertebral foramina. The series of

vertebral foramen in the articulated column form the vertebral canal, which contains the spinal cord, meninges, fat, spinal nerve roots, and vessels. The vertebral notches are indentations above and below the pedicles. The superior vertebral notch of a vertebra and the inferior notch of the superior vertebra form an intervertebral foramen, which gives passage to the spinal nerve roots and blood vessels.

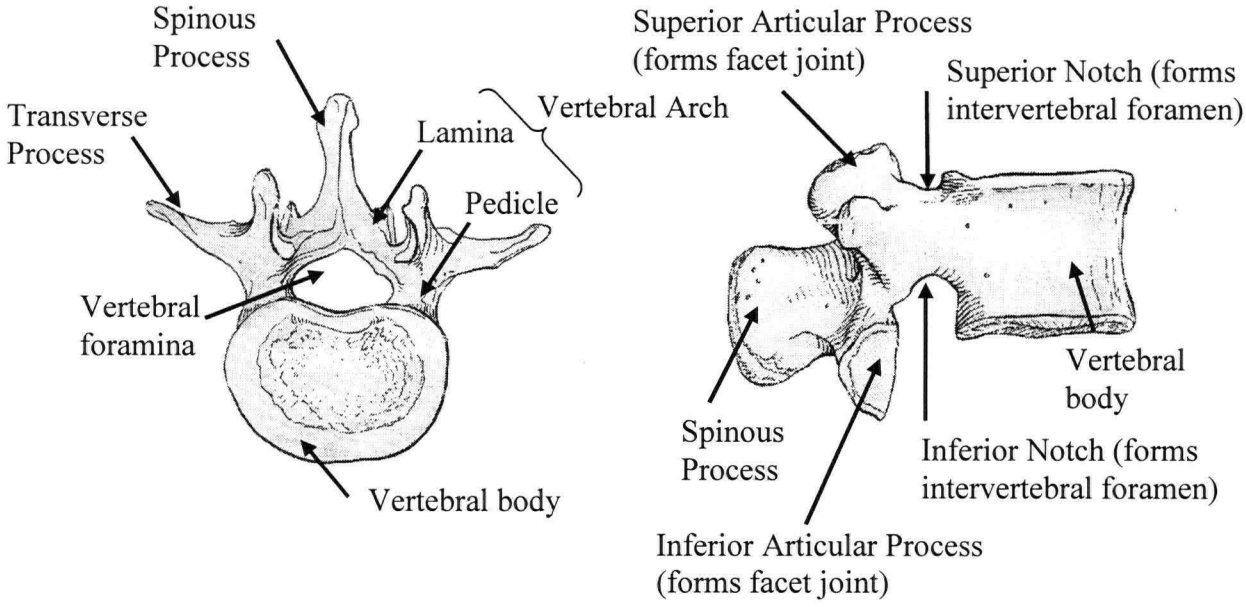

Figure 1.2: A typical vertebra (Figure was modified from Moore and Dalley 1999). A) Superior view, B) Lateral view.

Seven projections of bone arise from the vertebral arch of a typical vertebra: a spinous process, two transverse processes, and four articular processes (Figure 1.2). One spinous process attaches medially to the vertebral arch and projects posteriorly. The transverse processes project posterolaterally from the junction of the pedicles and laminae. These three processes provide attachment points for deep muscles of the back and form levers that help muscles move the vertebrae. The two superior and two inferior articular processes project from the vertebral arch and oppose the corresponding processes of the inferior and superior vertebrae, respectively. The joints formed by adjoining articular processes are called zygapophyseal (facet) joints. The facet surfaces are covered by cartilage forming an articular capsule. The function of the facet joints is to restrict

motion in certain directions, permit gliding movement between vertebrae, and to guide and control the motion.

Cervical vertebrae form the skeleton of the neck. They are relatively small bones and bear less weight than more inferior vertebrae (Figure 1.3). The most distinctive feature of vertebrae in this region is the presence of an oval foramen of the transverse process, which transmits vertebral arteries. The body of cervical vertebrae are small and wider laterally than anteroposteriorly. The superior aspect is concave, whereas the inferior aspect is convex. The vertebral foramen is large and triangular in this region. It is relatively large from the third to the seventh cervical vertebrae (C3 to C7) because the spinal cord is enlarged in this region. The superior borders of the bodies are raised posteriorly, especially at the sides, and depressed anteriorly. The raised margins are uncinate processes.

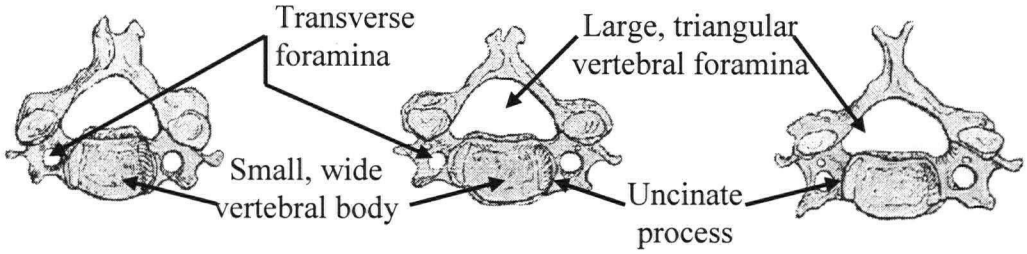

Figure 1.3: Typical cervical vertebrae (Figure was modified from Moore and Dalley 1999). A) C4, B) C5, C) C6

Cervical vertebrae have the largest range of motion in the spine. The neck is more free to move than the trunk because intervertebral discs are thick relative to the size of vertebral bodies at this level, articular surfaces of the facet joints are large and joint planes are almost horizontal, articular capsules of the facets are loose, and the neck is slender without soft tissue bulk (Moore and Dalley 1999). The cervical region is thought to be most susceptible to injury compared to the other regions of the spine due to the smaller vertebrae, reduced strength of the stabilizing structures, and the increased mobility in this region (Sekhon and Fehlings 2001).

The articulating surfaces of the vertebrae are connected by intervertebral discs and ligaments (Figure 1.4). The intervertebral discs provide strong attachment between vertebral bodies and act as shock absorbers. Their varying shapes are the main cause of the cervical and lumbar curvatures of the vertebral column (Moore and Dalley 1999) (Figure 1.1). The annulus fibrosis is the outer ring of the disc consisting of concentric lamellae of fibrocartilage. These fibres insert into the articular surfaces of the vertebral bodies, thus providing a strong bond between the disc and the adjacent vertebrae. The centre portion of the lumbar IV disc is the nucleus pulposus. It is more cartilaginous than fibrous and is normally highly elastic. It has a high water content that is maximal at birth and decreases with age.

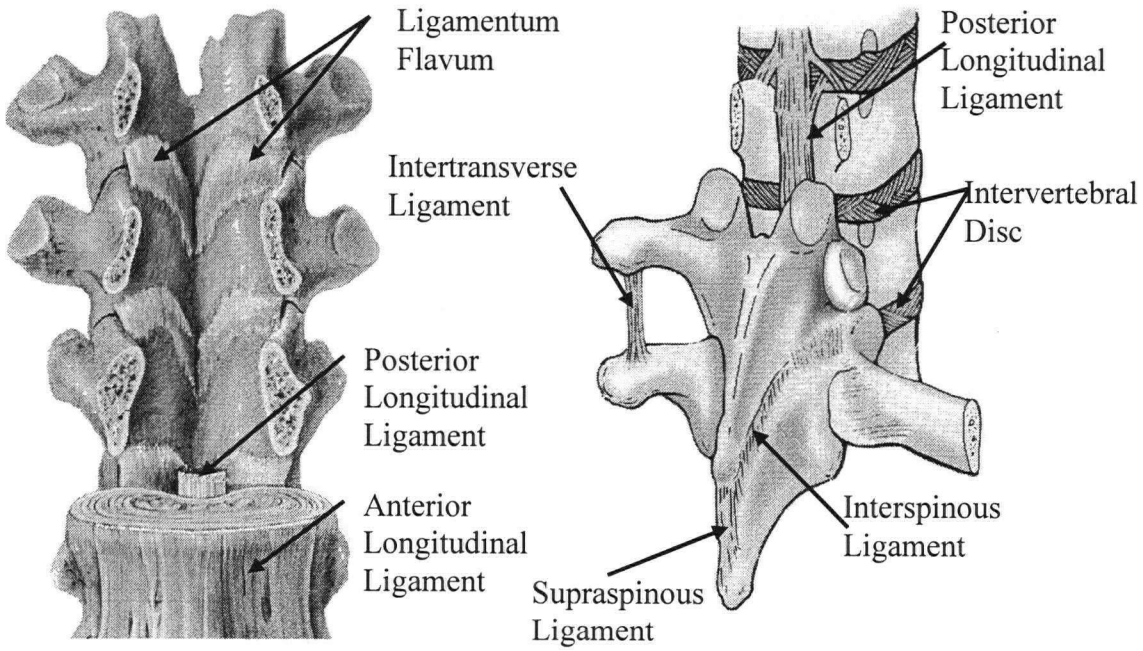

Figure 1.4: Spinal ligaments and IV disc (Figures were modified from Moore and Dalley 1999). A) Anterior view, B) Posterolateral view

Ligaments are soft connective tissues which are formed from groups of collagen fibres. Ligaments primarily resist tensile loading and their many functions relate to protecting the spinal cord and maintaining physiologic motion between vertebrae. The posterior longitudinal ligament (PLL) is a narrow band which runs within the vertebral canal along

the posterior aspect of the vertebral bodies and IV discs. Its function is to prevent hyperflexion of the spine and herniation or posterior protrusion of the discs.

The anterior longitudinal ligament (ALL) is a strong, broad fibrous band that connects the anterolateral aspects of the vertebral bodies and IV discs (Figure 1.4). It assists in maintaining the normal pattern of spinal motion and helps prevent hyperextension of the vertebral column.

The laminae of adjacent vertebrae are connected by the ligamenta flava (LF), a broad elastic fibrous tissue which extends almost vertically from the lamina above to the lamina below (Figure 1.4). The ligamentum flavum forms part of the posterior wall of the vertebral canal. The ligamenta flava are long, thin, and broad in the cervical region. Their function is to prevent separation of the vertebral lamina, which helps prevent hyperflexion of the vertebral column and protects the IV discs. They also help preserve the normal curvature of the spine and assist with straightening the column after flexing.

The spinous processes of adjacent vertebrae are joined by interspinous (ISL) and supraspinous ligaments (Figure 1.4). The interspinous ligament connects along the length of the spinous process, while the supraspinous ligament connects only the apices of the processes. The nuchal ligament extends from the posterior aspect of the cranium to the spinous processes of the cervical vertebrae. It provides attachment points for muscles in the cervical region. The intertransverse ligament joins adjacent transverse ligaments and consists of scattered fibres in the cervical region.

1.2.1.2 Meninges

The meninges provide protection to the spinal cord (Figure 1.5). The innermost layer surrounding the cord is the pia mater, which adheres to the surface of the cord and is barely visible to the unaided eye. Outside the pia mater is the arachnoid mater; a cobweb-like tissue which attaches laterally to the inner surface of the outermost meninge. The outermost layer surrounding the cord is a thick tube called the dura mater. The subarachnoid space formed between the dura mater and the pia mater is filled with cerebrospinal fluid (CSF). The CSF found in the subarachnoid space is clear and

colourless with a pressure of 8 to 18 kPa (Kiernan 1998). The epidural space formed between the vertebral canal and the dura mater is filled with epidural fat and a venous plexus. The main support and protection provided by the meninges comes from the dura mater and the CSF in the subarachnoid space.

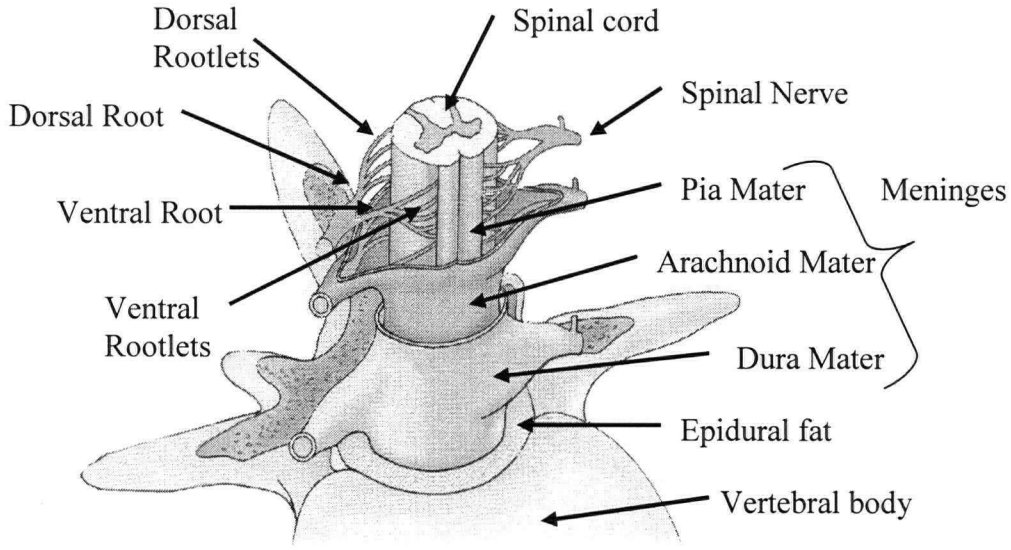

Figure 1.5: Anterolateral view of the spinal cord, spinal nerves, and spinal meninges. The denticulate ligament is not shown. (Figure was modified from Moore and Dalley 1999)

A denticulate ligament on both the right and left lateral sides of the cord suspend it in the dural sheath (Figure 1.6). These ligaments anchor the spinal cord in the CSF of the subarachnoid space and provide fixation for the cord.

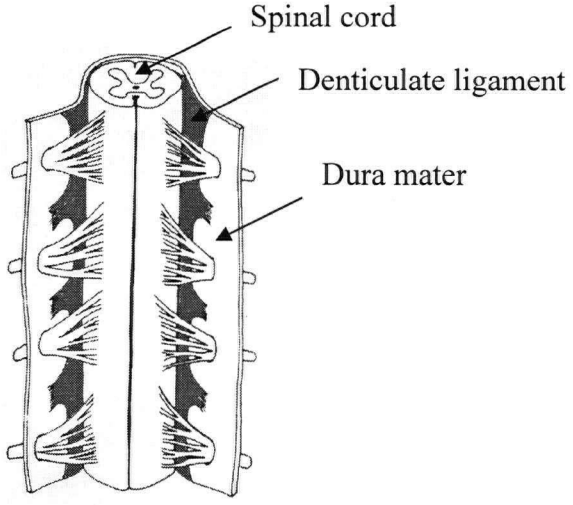

Figure 1.6: Denticulate ligaments (Figure was modified from White and Panjabi 1990)

The spinal cord and dura mater are attached to the spinal column through the spinal nerves. The spinal cord gives rise to two spinal nerves at each level which exit the cord laterally and continue to innervate tissues of the body (Figure 1.5). Each nerve consists of a dorsal and ventral root, which in turn consist of a series of rootlets that are attached to the cord. The dura mater extends into the IV foramina as it ensheathes the dorsal and ventral roots, forming dural root sleeves. The dural root sleeves adhere to the surface of the vertebrae at the IV foramina and end by blending with the sheath (epineurium) of the spinal nerves. The dura mater is also connected to the spinal column through fibrous tissue in the canal (Figure 1.7). These dural attachments are membranous formations which connect the dura mater to the PLL and other structures in the spinal canal (Hayashi, Yabuki et al. 1977; Spencer, Irwin et al. 1983; Scapinelli 1990; Wiltse, Fonseca et al. 1993; Kubo, Waga et al. 1994; Shinomiya, Sato et al. 1995).

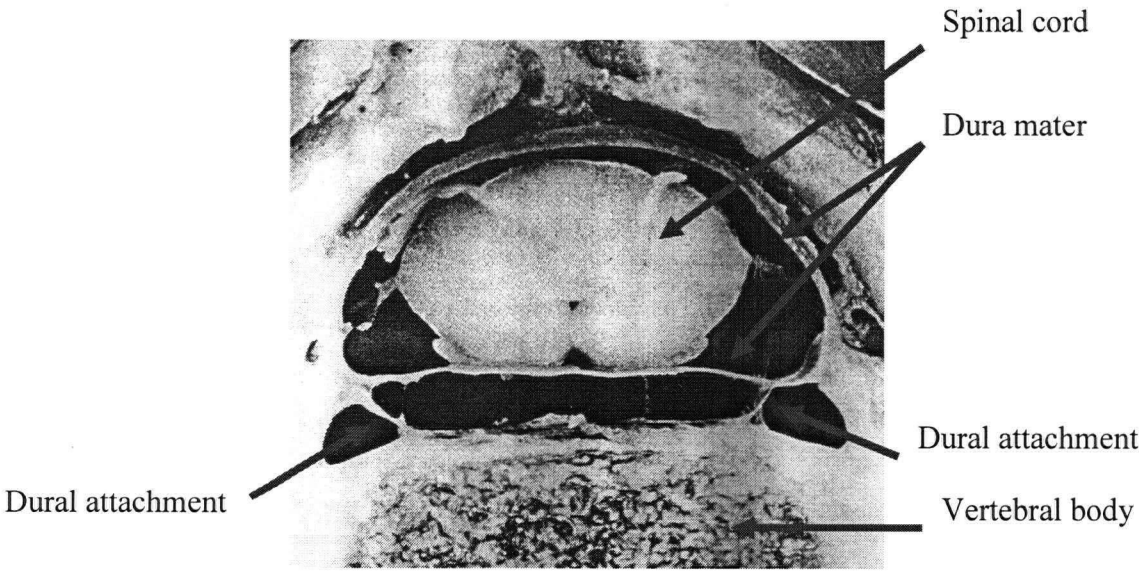

Figure 1.7: Dural attachments (Figure was modified from Hayashi, Yabuki et al. 1977)

1.2.1.3 Spinal Cord

There are two classes of cells in the spinal cord: nerve cells and neuroglial cells. Nerve cells (neurons) are specialized for the conduction of nerve impulses and are responsible for most of the functional characteristics of nerve tissue. Neurons have a cell body and two types of projections along which nerve impulses travel: dendrites and axons.

Dendrites are short projections which receive signals from other neurons and carry them towards the cell body. Each neuron has a single axon which carries impulses away from the cell body and synapses (connects) with dendrites of other neurons. The length of this projection varies greatly between neurons. Neuroglial cells (glia) have important secondary functions, such as supporting, insulating, and nourishing neurons.

The spinal cord contains two types of tissue; white and grey matter (Figure 1.8). White matter consists mainly of axons, the majority of which are surrounded by myelin sheaths that serve to increase the velocity of signal conduction. Axons in the white matter are generally oriented such that their longitudinal direction runs in a cranial-caudal direction. Grey matter consists primarily of cell bodies of neurons. Both white and grey matter also contain many neuroglial cells and a network of blood capillaries. In the transverse plane, grey matter is arranged centrally in the shape of an 'H' and the white matter surrounds the grey matter. The cross-sectional areas of the grey and white matter vary along the length of the cord. The area of white matter decreases caudally where there are fewer ascending and descending fibres. The area of grey matter indicates the number of neurons at that spinal level; therefore it is greatest for segments supplying the limbs. The surface of the spinal cord contains longitudinal furrows. The two most significant are the ventral median fissure (most deep) and the dorsal median sulcus.

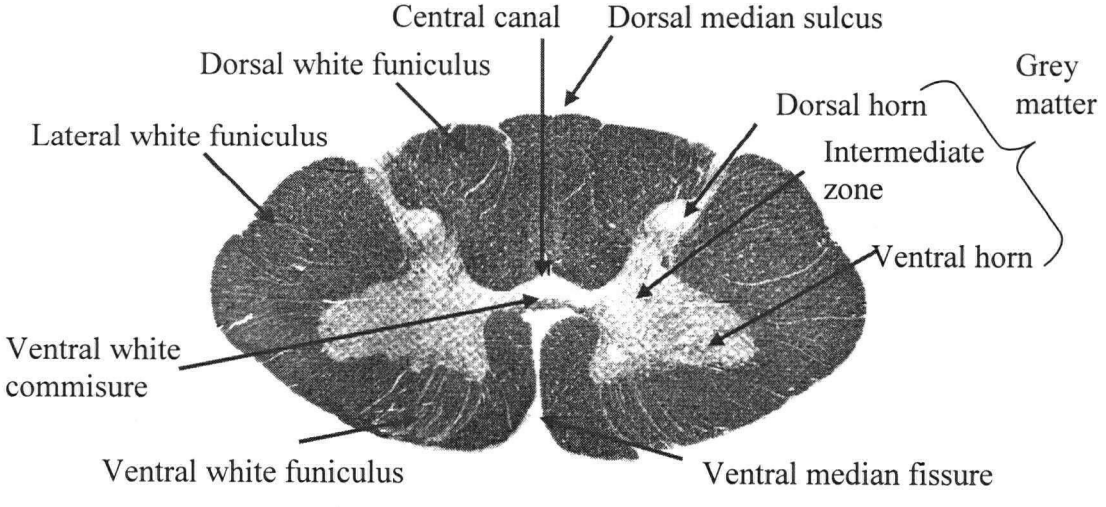

Figure 1.8: Spinal cord grey and white matter (Figure was modified from Kiernan 1998)

The grey matter on each side of the midline consists of a dorsal and ventral horn and an intermediate zone (Figure 1.8). A small central canal, lined with epithelium (membranous tissue) is located in the centre of the cord. The white matter on each side of the midline consists of three bundles of fibres (funiculi): dorsal (between the midline and the dorsal grey horn), lateral, and ventral. The lateral funiculus is further divided into dorsolateral and ventrolateral funiculi. The ventral white commisure is located ventral to the intermediate zone of grey matter. In this location, white matter tracts cross the midline to ascend or descend on the other half of the cord. Axons that connect one region with another tend to travel together and are termed tracts. The dorsolateral tract (of Lissauer) is the area between the dorsal grey horn and the dorsal surface of the cord (Figure 1.9). In this area, white matter tracts ascend or descend for several levels before terminating in grey matter.

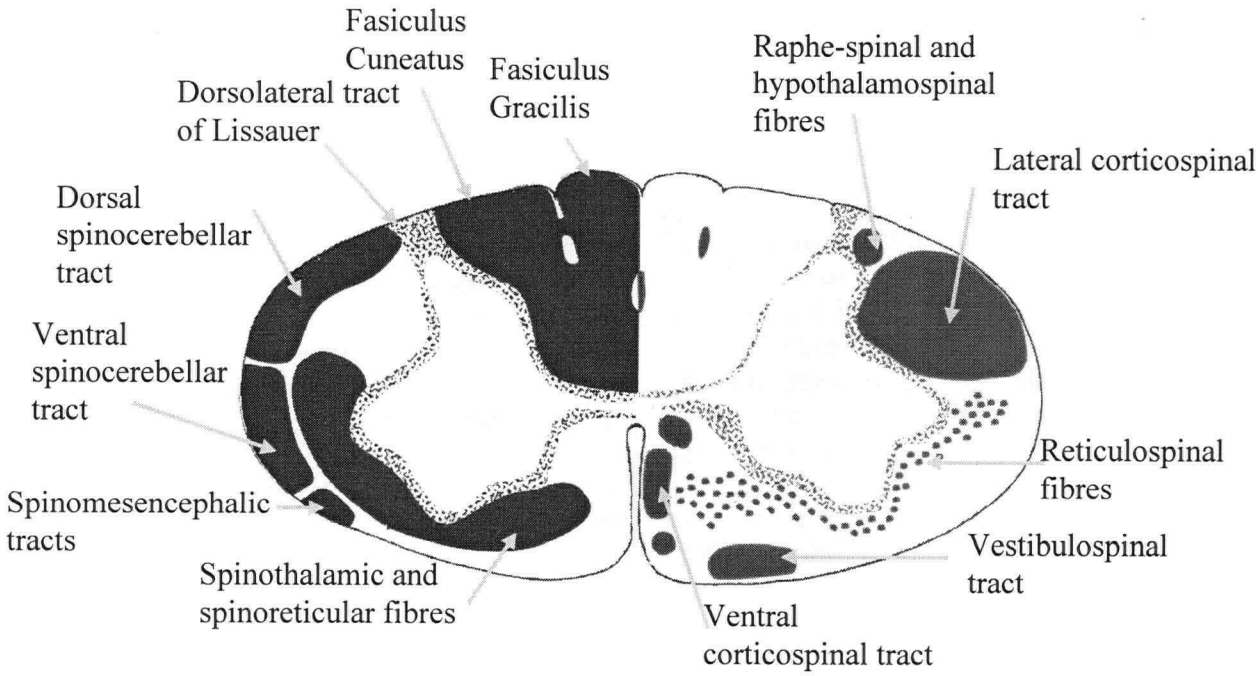

Figure 1.9: Spinal cord tract organization (Figure was modified from Kiernan 1998). Ascending tracts (blue) are on the left; descending tracts (red) are on the right.

The dorsal funiculus (Figure 1.9) consists primarily of ascending tracts of axons (sensory), which provide discriminative sensation and conscious awareness of movement. The fasciculus gracilis is located medially and it is responsible for lower limb sensations,

while the fasciculus cuneatus is located laterally, and it is responsible for upper limb sensations. These fibres provide sensory information from the ipsilateral side of the body.

The lateral funiculus (Figure 1.9) has a mix of ascending and descending tracts. Ascending fibres include the dorsal and ventral spinocerebellar tracts, spinothalamic tract, spinoreticular tract, and spinomesencephalic tracts. Descending fibres include the lateral corticospinal tract, raphe-spinal tract, hypothalamospinal tract, and reticulospinal fibres. Spinocerebellar fibres are involved in proprioception. Spinothalamic fibres conduct impulses involved in tactile, thermal, and painful sensations. Spinoreticular fibres form part of the reticular activating system (involved in sleep and consciousness, as well as sensory and motor function) and are also implicated in the perception of pain and of various sensations involving internal organs. The lateral corticospinal tract is a large grouping of fibres responsible for voluntary discrete skilled movements. The raphespinal tract modifies painful stimuli from the dorsal horn. Reticulospinal fibres compose a descending pathway through which the brain controls the activity of motor neurons and is involved in activities not requiring constant conscious effort.

The ventral funiculus (Figure 1.9) has primarily descending tracts. The ventral corticospinal tract is involved in skilled volitional movements. Also in this funiculus is the vestibulospinal tract that is responsible for balance. Some reticulospinal fibres (found in the lateral funiculus) are also found in the ventral funiculus.

Three longitudinal arteries supply the spinal cord: an anterior spinal artery and two paired posterior spinal arteries. The anterior artery lies in the ventral median fissure. Sulcal arteries arise from this artery and enter the cord by running in the transverse plane through the ventral median fissure. The sulcal arteries supply approximately two-thirds of the cross-sectional area of the spinal cord. The vertebral artery runs through the transverse foramina of the cervical vertebrae and gives rise to segmental spinal arteries which enter the vertebral canal through the intervertebral foramina. These spinal arteries supply the vertebrae and give rise to anterior and posterior radicular arteries which run along the dorsal and ventral roots of the spinal nerves and join the anterior and posterior

spinal arteries. In general, the veins of the spinal cord have a distribution similar to the arteries.

The tracts of spinal cord white matter consist primarily of bundles of parallel fibres formed by axons, which conduct impulses away from cell bodies. They have a uniform diameter throughout their length. Almost all axons with diameters above 0.2 μm in the central nervous system are surrounded by a myelin sheath (Hirano and Llena 1995). The function of myelin is to increase the speed of signal conduction along axons. Myelin sheathes begin near the origin of the axon and end short of its terminal branching. Myelin is laid down by oligodendrocytes (glial cells). Regions formed by different oligodendrocytes are joined by nodes of Ranvier.

The primary constituents of brain and spinal cord tissue are the same, however their structural organisations differ somewhat. Both brain and spinal cord tissue contain white matter (consisting of axons and neuroglia cells) and grey matter (consisting of neuronal cell bodies, dendrites, and neuroglia cells). White matter of brain and spinal cord tissue is approximately 70% water whereas grey matter is 80% water (Ommaya 1968; Gadea-Ciria, Gervas-Camacho et al. 1975). Brain tissue is macroscopically isotropic (Shuck and Advani 1972), while axons within the white matter of the spinal cord are generally arranged such that their long axes run in a cranial-caudal direction. Axons in the spinal cord are slightly folded, which is exhibited most in extension of the spinal column, while in flexion they are pulled straight (Breig 1960).

Neurons have a wide range of structural diversity. The diameter of the cell body may vary from 5 to 135 μm (Kiernan 1998). The pattern of branching of the processes varies greatly and is distinctive for neurons that constitute a particular group of cells. Axons may be between 100 μm and 1 m in length, and between 1 μm and 10 μm in diameter (Kiernan 1998).

1.2.2 Mechanical Properties

Tissues of the spinal column respond differently to mechanical loading (Figure 1.10). Biological tissues, such as those in the spinal column, are subject to inherent variability

between subjects as well as within subjects; tissue from one anatomical site may have different properties than the same type of tissue from another site. Furthermore, biological tissues generally have a nonlinear and rate dependent response to loading. The stress-strain relationship of materials may be described by constitutive models; the most basic is the linear elastic model.

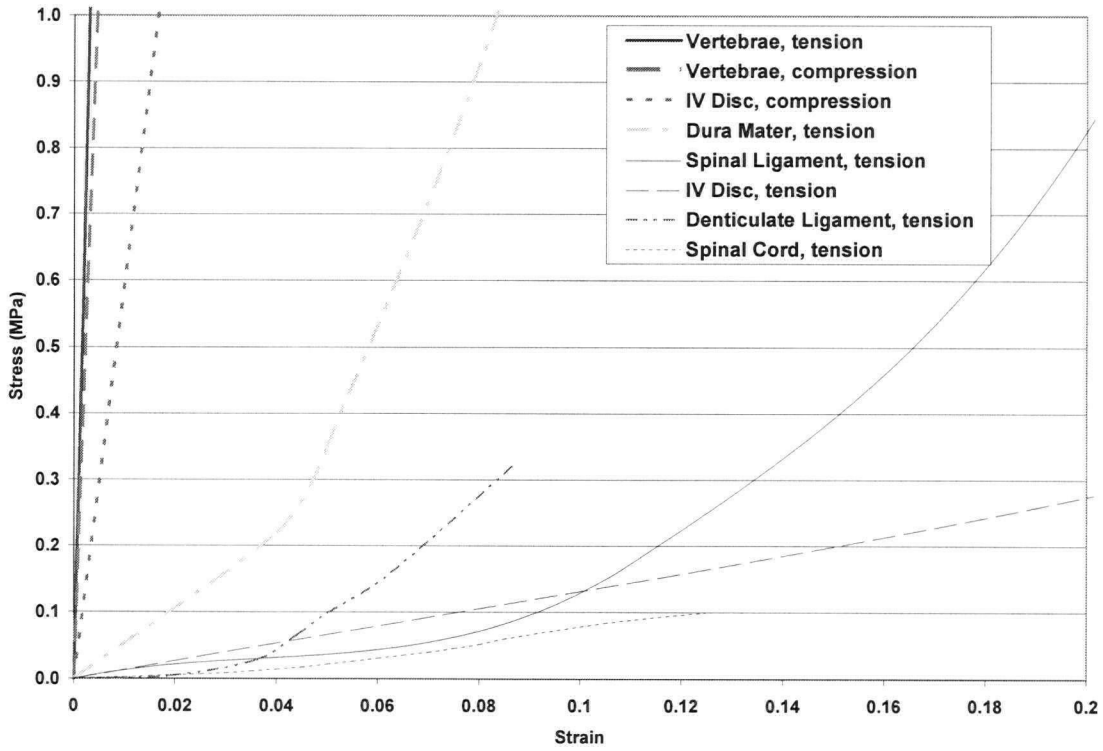

Figure 1.10: Sample mechanical response to loading of various tissues of the spinal canal (Yamada 1970; Tunturi 1978; van Noort, Black et al. 1981; Bilston and Thibault 1996; Przybylski, Carlin et al. 1996)

Experimental data exists in the literature of the mechanical properties of vertebrae, intervertebral discs, and spinal ligaments; however the lumbar region generally receives more attention than the cervical. Properties of dura mater have been reported (Galford and McElhaney 1970; van Noort, Black et al. 1981; van Noort, Martin et al. 1981; Tencer, Allen et al. 1985; Runza, Pietrabissa et al. 1999; Wilcox, Bilston et al. 2003), however their in vivo properties are not well documented. One study reported properties of the denticulate ligament (Tunturi 1978), however somewhat primitive testing methods

were employed to obtain these data. Properties of the spinal cord, which are of primary interest for this study, are not well understood.

Research into the mechanical properties of the central nervous system began with brain tissue, which has similar constituents but different structural organization than spinal cord tissue. Brain tissue was found to be extremely soft, exhibiting primarily a viscous character. Testing of such soft biological tissues has technical and ethical complications, particularly in vivo studies, which are most valuable. A noteworthy result from brain tissue testing was that death and fixation of brain tissue increased the elastic modulus, but did not change the manner in which it varied with strain (Metz, McElhaney et al. 1970). Furthermore, the elastic modulus was higher for perfused brains (those receiving a pulsed flow of liquid into the arterial vascular network) than for those without perfusion (Guillaume, Osmont et al. 1997). Linear and nonlinear viscoelastic models have been used to model the time dependent mechanical response of brain tissue (Galford and McElhaney 1970; Wang and Wineman 1972; Firoozbakhsh and DeSilva 1975; Pamidi and Advani 1978; Donnelly and Medige 1997; Peters, Meulman et al. 1997). Viscoelastic models are composed of a combination of springs, which produce instantaneous response to load, and dashpots, which produce a load proportional to the velocity at any instant. Hyperelastic models have been employed in modelling the nonlinear elastic response of brain tissue (Mendis, Stalnaker et al. 1995; Bilston, Liu et al. 1997; Miller 1999; Bilston, Liu et al. 2001; Miller and Chinzei 2002).

Spinal cord tissue is also extremely soft with a highly nonlinear response to loading and significant relaxation (Bilston and Thibault 1996) (Figure 1.11). Testing of this tissue has been limited to uniaxial tension loading using in vivo (Chang, Hung et al. 1981; Hung and Chang 1981; Hung, Chang et al. 1981; Hung, Chang et al. 1981; Chang, Hung et al. 1988) and in vitro models (Breig 1960; Tunturi 1978; Tunturi 1980; Bilston and Thibault 1996; Fiford and Bilston 1998). The stress-strain response of spinal cord tissue in vivo is linear up to small strains (5%) with an elastic modulus between 0.23 and 0.4 MPa (Chang, Hung et al. 1981; Hung and Chang 1981; Hung, Chang et al. 1981; Hung, Chang et al. 1981; Chang, Hung et al. 1988). The elastic response of spinal cord tissue has been

described using hyperelastic constitutive models (Bilston 1994; Bilston and Thibault 1996; Bilston 1998).

The viscoelastic nature of the spinal cord has been described with viscoelastic models (Chang, Hung et al. 1988; Bilston and Thibault 1996). The elastic modulus was found to increase with an increase in strain rate, ranging from 1.02 to 1.37 MPa for the human cord in vitro (Bilston and Thibault 1996). The rate at which the rat spinal cord was strained was found to affect the peak stress as well as the stress decay after 30 seconds (Fiford and Bilston 1998).

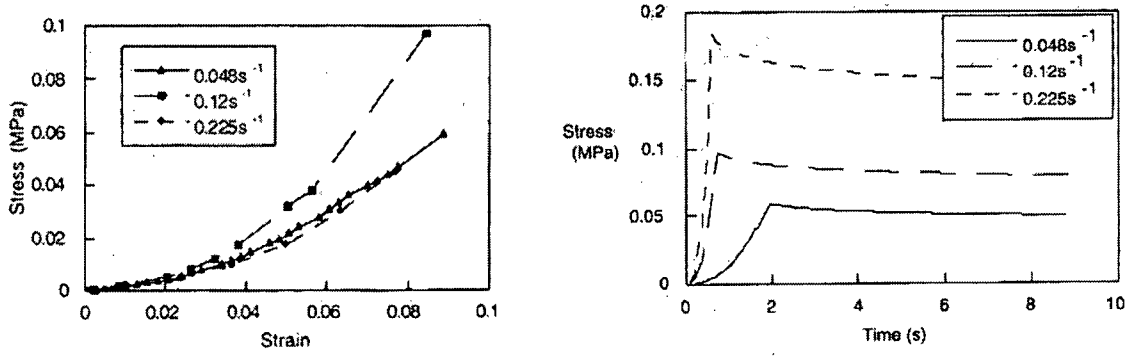

A) B)

Figure 1.11: Mechanical response of spinal cord tissue (Figures from Bilston and Thibault 1996). A) Elastic response, B) Relaxation curves

Controversy exists as to whether white matter is stiffer than grey matter, or vice versa. Historically, white matter has been considered to be stiffer than grey matter (Holbourn 1944; Kahn 1947; Schneider, Cherry et al. 1954; Panjabi and White 1988; Levine 1997), presumably due to its longitudinal orientation. Technical difficulties have precluded testing of each tissue separately, particularly because spinal cord tissue is extremely soft. Two studies that have recently investigated spinal cord white and grey matter separately have found contradictory results (Ichihara, Taguchi et al. 2001; Ozawa, Matsumoto et al. 2001). Ichihara et al. found no difference between white and grey matter at low levels of strain (0-5%), however at higher strains, grey matter was more "rigid and fragile" than white matter (Ichihara, Taguchi et al. 2001) (Figure 1.12). The coring technique used to isolate the grey matter may have disrupted connections within the tissue. Another study found no difference between the stiffnesses of white and grey matter by pipette aspiration

with finite element modelling to determine the elastic modulus (Ozawa, Matsumoto et al. 2001). The technique used for this study is novel; however it has not been proven to provide accurate results.

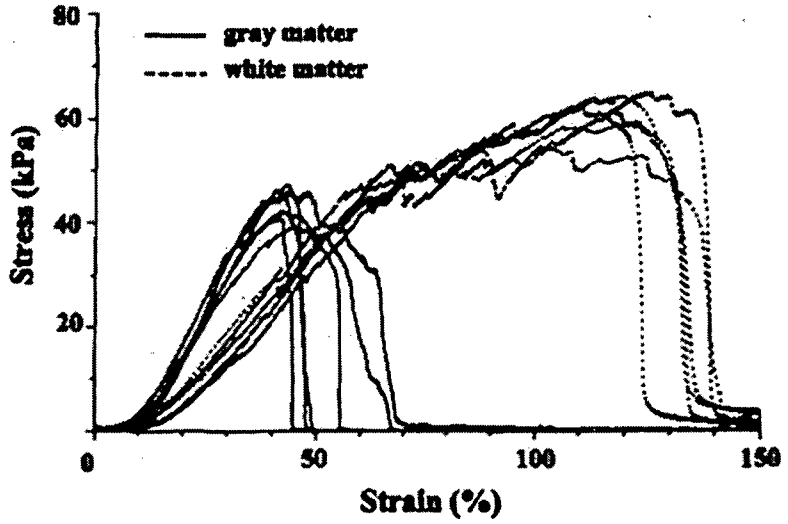

Figure 1.12: Mechanical response of white and grey matter of the spinal cord (Figure from Ichihara, Taguchi et al. 2001)

1.2.3 Clinical Aspects

Of the five regions of the spinal column, most traumatic SCI's occur in the cervical region, accounting for 52 to 62% of all cases (Griffin, Opitz et al. 1985; Fife and Kraus 1986; Dixon, Danesh et al. 1993; Tator, Duncan et al. 1993; O'Connor 2002; Dryden, Saunders et al. 2003). In the distribution of serious SCI due to motor vehicle accidents, cervical cord injuries were found to be 14 times more frequent than thoracolumbar cord injuries, even though cervical column injuries were only 1.4 times more likely than thoracolumbar column injuries (Yoganandan, Haffner et al. 1989). This indicates the importance of protecting the spinal cord in the cervical region. The cervical region is thought to be most susceptible to injury due to the smaller vertebrae, reduced strength of the stabilizing structures, and the increased mobility in this region (Sekhon and Fehlings 2001). The segment between the fifth and sixth cervical vertebrae (C5-C6 segment) is generally considered to have the greatest range of motion (Panjabi and White 1980). In addition, the spinal cord in enlarged between the third cervical vertebra (C3) and the first

thoracic vertebra (T1) due to the addition of fibres for innervation of the upper limbs. Survivors of cervical SCI are most commonly injured between the C5 and C6 vertebrae (Shields, Fox et al. 1978; Sances, Myklebust et al. 1984; Yoganandan, Haffner et al. 1989; Yoganandan, Maiman et al. 1990).

Recent advancements in care have caused an increasing trend towards incomplete SCI (partial preservation of sensory and/or motor function found below the neurological level including the lowest sacral segment), rather than complete SCI (absence of sensory and motor function below the neurological level, including the lowest sacral segment) (Tator, Duncan et al. 1993; Sekhon and Fehlings 2001). Improved initial care and retrieval systems, greater awareness of the importance of immobilization after injury, use of restraints and air bags in motor vehicles, and hospital manoeuvres to limit secondary injury have improved the prognosis of cervical SCI (Sekhon and Fehlings 2001).

A wide spectrum of injuries to the spinal cord and column may occur in the cervical region. Numerous classification systems of injury patterns in the cervical spine have been presented, but none have received widespread acceptance (Cusick and Yoganandan 2002). Comparisons of reported incidences are hindered by inconsistencies in classification systems. Allen and Ferguson developed a mechanistic classification system for lower cervical spine injuries (Allen, Ferguson et al. 1982). The advantage of a mechanistic classification system is that associated injuries as well as appropriate treatment patterns may be predicted from the mechanism of injury. These classifications are primarily based on radiological findings, which are limited since they provide a static image and do not directly correlate to the dynamic process of injury. Allen and Ferguson's classification system used a major injury vector, which produced the initial failure, to define eight types of injuries in a mechanistic clock-face classification system (Figure 1.13). Furthermore, within each injury mechanism there were a number of stages defined based on injury severity.

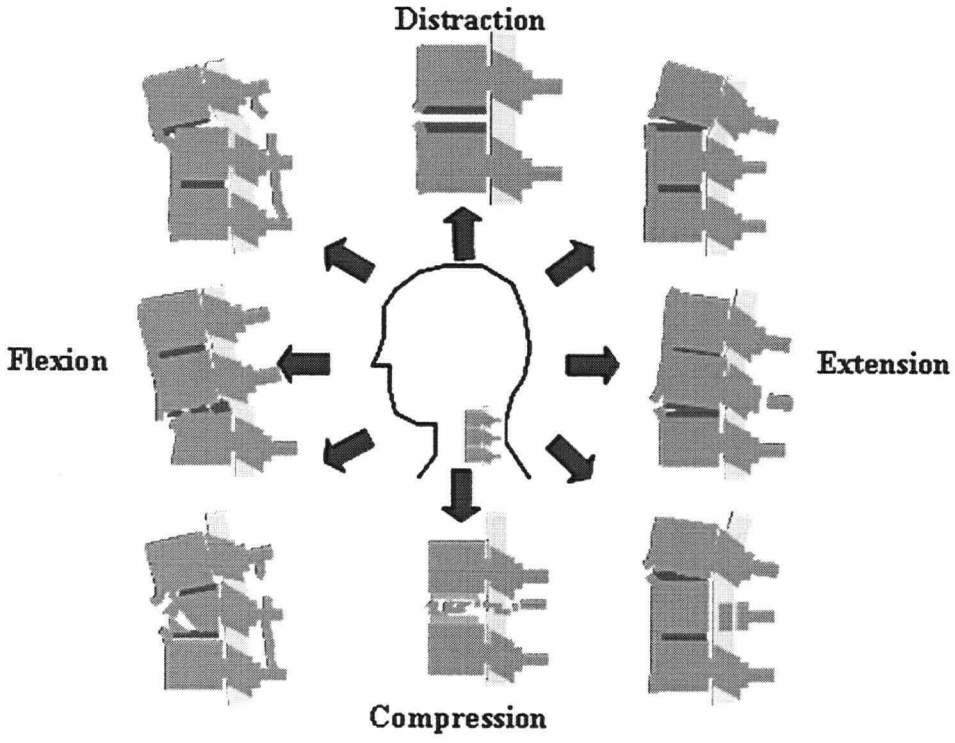

Figure 1.13: Allen and Ferguson's classification of cervical spine injuries (Allen, Ferguson et al. 1982)

Allen & Ferguson found the most common injury mechanisms in a retrospective analysis of 165 cases. The most common injury mechanisms, in order of decreasing incidence, were distractive flexion (37%), compressive extension (24%), compressive flexion (22%), vertical compression (8%), and distractive extension (5%) (Allen, Ferguson et al. 1982). Another retrospective study of 347 survivors of SCI from vehicular accidents found compressive flexion injuries to dominate the problem, accounting for 47% of all cervical SCI's (Yoganandan, Maiman et al. 1990). Other common mechanisms in motor vehicle accidents are vertical compression (14%) and distractive flexion (7%) injuries (Yoganandan, Maiman et al. 1990). Variations in injury mechanism definitions may affect their distributions; mild compressive flexion injuries may be confused with mild distractive flexion injuries (Dekutoski and Cohen-Gadol 2003). Extension and flexion mechanisms have also been identified; separate from those combined with distraction and compression, which occurred in 11 and 7% of cervical SCI, respectively (Yoganandan, Maiman et al. 1990). The extension mechanism occurred mostly in the lower cervical segments, while the flexion mechanism occurred predominantly in the upper cervical

region (Yoganandan, Maiman et al. 1990). Axial tension injuries associated with pure tension have also been recognized, however they are rare in motor vehicle accidents. These injuries are sometimes observed in pedestrian-vehicle accidents (Yoganandan, Haffner et al. 1989). Pure shear injuries are also rare in the cervical spinal column; however they often occur in conjunction with the previously described classifications.

Spinal cord lesions are classified as complete or incomplete. The extent of SCI is evaluated by neurological assessment and is classified according to functional criteria. Injuries are subdivided based on sensory loss and the amount of preserved motor function. Four syndromes are defined which describe specific incomplete spinal cord injuries: anterior cord, central cord, Brown-Séquard, and posterior cord syndromes (Figure 1.14). The topographical organization of damage to the cord for each syndrome is based on early hypothetical research and retrospective clinical findings. Furthermore, Neurological injury measures demonstrate the results of the summation of primary and secondary injury to the cord. Since damage is typically determined by neurological assessment and not by histological evaluation, it is not known which tissues are mechanically damaged for various types of SCI.

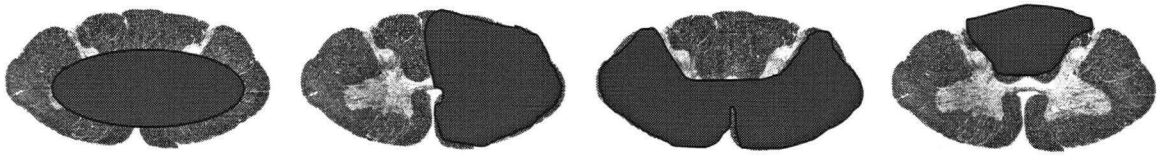

A) **B)** **C)** **D)**

Figure 1.14: Topographical organization of damage to the cord for various syndromes. Damaged areas are highlighted in red. (Figure was modified from Kiernan 1998.) A) Central cord syndrome, B) Brown-Séquard syndrome, C) Anterior cord syndrome, D) Posterior cord syndrome

Evidence exists suggesting that the injury mechanism may be related to the resulting neurologic deficit. Several retrospective studies have attempted to correlate spinal column injury to the resulting neurological deficits (Marar 1974; Allen, Ferguson et al. 1982; Tator 1983) and prognosis for recovery (Dall 1972). Although a relationship between column and cord injury is suspected, patterns and classifications of column damage have only influenced the technique to stabilize and decompress the cord

(Simpson, Sutton et al. 1994; Vaccaro 2003). Their contribution to the pattern and extent of SCI has not been adequately studied. It is expected that as new therapeutic strategies reach the stage of clinical application, they are more likely to be successful if targeted to specific injury types.

1.2.4 Experimental Aspects

Experimental strategies to identify therapeutic interventions or promote spinal cord regeneration have been developed in animal models using cord transection or cord compression (Wrathall 1992; Girardi, Khan et al. 2000) (Figure 1.15). These models inherently fail to simulate the complex biomechanical stresses of distraction, compression, bending, and shear to which the human cord is subjected during trauma (Kwon, Oxland et al. 2002). Most therapies that have gone to human clinical trials were first validated in spinal cord contusion models (Young 2002).

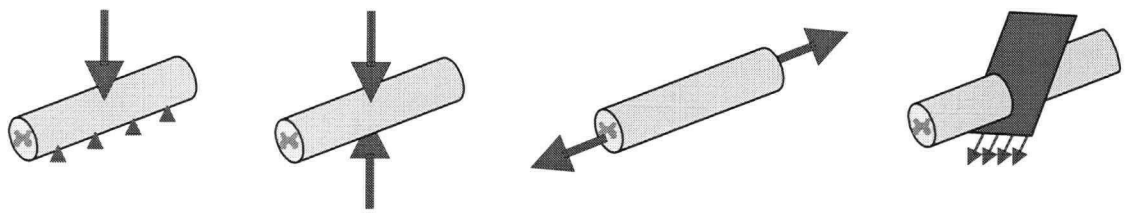

Figure 1.15: Experimental injury mechanisms applied in spinal cord injury research. A) Dorsal-ventral contusion, B) Clip compression, C) Axial tension, D) Transection (severing).

Transection models are very useful for evaluating spinal cord regeneration strategies since new axons growing across a bridge are easier to identify. This is in contrast to contusion models which may have spared axons at the lesion epicentre. Clip compression models are less clinically relevant as loads are applied at rates much lower than those seen clinically and the dynamic parameters of injury are less controlled. Axial tension models are the least commonly employed in SCI research, however they may provide important information into the mechanisms of SCI, such as the tolerance of the cord to tensile forces. Furthermore, mechanical tension on the spinal cord has been implicated as an important cause of neuronal pathology (Breig 1970; Blight 1988; Maiman, Myklebust et al. 1989).

Contusion models are designed to represent a clinically relevant injury mechanism, since SCI typically occurs by a transient blunt trauma, rather than a transection mechanism, caused by a mechanical compression of the cord due to displacement of fractured vertebrae or discs extending into the spinal canal (Kakulas 1984). Detailed pathology of human SCI suggests that the rat contusion lesion is similar to a large number of human SCI's (Kakulas 1984; Bunge, Puckett et al. 1993). The experimental contusion mechanism is a rapid anteroposterior compression typically applied on the dorsal aspect of the cord. Injury devices have been designed to allow force and displacement feedback during injury (Figure 1.16).

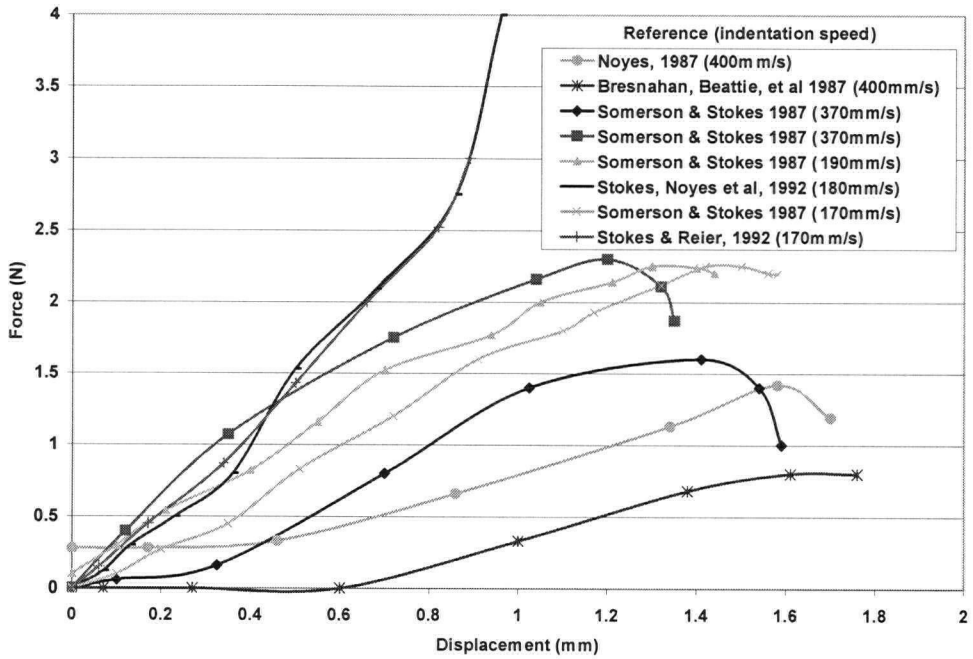

Figure 1.16: Force vs. displacement curves of contusion tests at various rates (Bresnahan, Beattie et al. 1987; Noyes 1987; Somerson and Stokes 1987; Stokes, Noyes et al. 1992; Stokes and Reier 1992)

Comparisons between studies are precluded by differences between experimental designs. For example, more recent experimental models apply more rigid fixation to the animal and apply a greater pre-load before contusing the cord (Stokes, Noyes et al. 1992; Stokes and Reier 1992), which may partially explain the increased stiffness obtained for the cord in the more recent studies illustrated in Figure 1.16. Details of the experiments which produced the results illustrated in Figure 1.16 are contained in Appendix A.

Knowledge of mechanical parameters during the dynamic injury event is useful for biomechanical models, as well as for improving the general understanding of SCI.

Variation in mechanical parameters of injury in animal contusion models has been determined to affect the functional, histological, and electrophysiological outcome; duration of force application (Carlson, Warden et al. 1997), velocity of impact and amount of compression (Kearney, Ridella et al. 1988), and contact area (Gerber and Corrie 1979) have been studied. Variations in these parameters may affect the resultant volume of damaged tissue, which suggests that a relationship does exist between the mechanics of injury and the resultant neurological outcome.

Experimental models of a distraction injury have been implemented to evaluate parameters of injury in the spinal cord. Distraction forces have been applied, in vivo, directly to the surface of the cord (Chang, Hung et al. 1981; Hung and Chang 1981; Hung, Chang et al. 1981; Hung, Chang et al. 1981; Hung, Lin et al. 1982; Chang, Hung et al. 1988) as well as indirectly using the animal's body (Cusick, Myklebust et al. 1982; Myklebust, Cusick et al. 1986; Myklebust, Maiman et al. 1988; Maiman, Coats et al. 1989; Maiman, Myklebust et al. 1989). In contrast to contusion injury, less standardized and reproducible devices have been developed for the distractive injury; however some biomechanical data of injury have been reported.

Considerable work has been done investigating the complex relationships between secondary injury pathways. Primary injury caused by mechanical impact is considered to be irreversible; therefore it is much less represented in the literature. However, the details of the mechanical injury induced on the cord in experimental models are not fully understood. Injuries that are observed by histology or neurophysiology demonstrate the final outcome of the primary injury and the time-varying complication of secondary injury. It is experimentally difficult to elucidate the effects of primary and secondary injury.

It is of interest to determine the tolerance of brain and spinal cord tissue to mechanical forces. The mechanics of a spinal cord injury are complicated, which has elucidated a need to study individual axons, or cultures of axons undergoing a simple stretch

mechanism, to dissect the effect of one simple mechanism. Single axon studies have found the extent of dysfunction is related to both the peak stretch and loading rate experienced by the tissue (Galbraith, Thibault et al. 1993). Axons may be morphologically damaged at 18% strain (Bain and Meaney 2000), electrophysiologically damaged at 21% strain (Bain and Meaney 2000), structurally damaged at 25% strain (Galbraith, Thibault et al. 1993), and severed at strains greater than 65% (Smith, Wolf et al. 1999). These tolerances have been determined through a variety of models each with their own conditions and limitations; tolerances are not directly transferable to human SCI. Results such as these may be combined with finite element models to predict regions of tissue which will be damaged. For example, shear strain has been found to be a good predictor of diffuse axonal injury in the brain (King, Ruan et al. 1995).

1.3 Injury Mechanisms Summary

Based upon the clinical and biomechanical evidence, it seems clear that there exist multiple mechanisms leading to acute SCI. Retrospective clinical studies suggest that different column injury mechanisms appear to produce different patterns of cord damage (Dall 1972; Marar 1974; Allen, Ferguson et al. 1982; Tator 1983; Yoganandan, Maiman et al. 1990; Silberstein and McLean 1994). Biomechanical studies show that variations in mechanical parameters of injury result in different levels and distributions of injury to the cord (Gerber and Corrie 1979; Kearney, Ridella et al. 1988; Carlson, Warden et al. 1997). Despite this evidence, spinal column injury mechanisms influence only the technique used to stabilize and decompress the cord. The contribution of these mechanisms to the pattern and extent of SCI has not been adequately studied. It is expected that as new therapeutic strategies reach the stage of clinical trials, they are more likely to be successful if they are strategically developed to specific injury mechanisms.

In order to begin to elucidate the relationship between injury mechanisms and immediate neurological damage caused by a mechanical insult, it was proposed to study three injury mechanisms: compression, distraction, and dislocation. These simple mechanisms are the foundations which form the clinically observed range of injuries. The compression (contusion) mechanism is experienced during vertical compression injuries, or any other injury involving material invading one side of the vertebral canal with the other side

remaining intact. Although this mechanism is experimentally produced as a spinal cord compression, it is meant to simulate the effects of a spinal column compression. Distraction of the spinal cord occurs with many other injury mechanisms; flexion of the column will induce some distraction in the cord, since it lies posterior to the centre of rotation of the column (Breig 1960). This mechanism may be considered as a distraction of the spinal cord or column. Dislocation of a vertebra commonly occurs where one vertebra is forced out of alignment anteriorly or posteriorly relative to the vertebrae below. This mechanism may be considered as a dislocation of the spinal column, or a shearing of the spinal cord.

To address this question, animal models will ultimately need to be developed. It would be more feasible, from an experimental viewpoint, to induce simple injury mechanisms, such as compression, distraction, and dislocation as opposed to complex mechanisms, such as compressive flexion injuries. Therefore, it is of primary interest to examine the effect of the simple injury mechanisms on the mechanical response of the cord.

1.4 Finite Element Modelling

To study the biomechanics of the human cervical spinal column, four types of models exist: animal, physical, cadaver, and mathematical (Yoganandan, Kumaresan et al. 1996). Each type of model is an approximation of the in vivo human situation, therefore each has inherent limitations. Animal models are advantageous since in vivo studies of injuries may be performed with physiologic responses; however, they are limited since there may be considerable variation in geometry of structures, material properties, and physiological response to injury between species. Furthermore, biologic variability may pose an obstacle. Physical models are limited in the questions they can address due to oversimplifications in geometric and structural properties. Cadaveric models are useful for studying the mechanics of the spinal column, as they are the most biofidelic; however studies including the spinal cord are limited since properties of nervous tissues change rapidly after death (Metz, McElhaney et al. 1970). Furthermore, histological, neurological, and electrophysiological parameters of cord damage require a living subject, so they cannot be obtained from cadaver models. Mathematical simulations, such as finite element modelling, allow control of parameters. They allow for the

calculation of local and internal mechanical responses which cannot be measured directly in experiments. FE models can solve geometrically complex problems with varying loading and boundary conditions. They are a complement to animal models, cadaver models, and clinical studies.

There is an abundance of finite element models which examine the response of the cervical spine to physiologic loading (Saito, Yamamuro et al. 1991; Yoganandan, Voo et al. 1995; Yoganandan, Kumaresan et al. 1996; Clausen, Goel et al. 1997; Maurel, Lavaste et al. 1997; Voo, Kumaresan et al. 1997; Goel and Clausen 1998; Kumaresan, Yoganandan et al. 1999; Ng and Teo 2001), but few relate the effects of these complex motions to the spinal cord (Hosey and Liu 1982; Bilston 1998; Scifert, Totoribe et al. 2000). Existing finite element analyses of the spinal column have focused on the physiological kinematics of the cervical spinal column segments and the effects of surgical procedures on the behaviour of the column complex (Saito, Yamamuro et al. 1991; Clausen, Goel et al. 1997; Maurel, Lavaste et al. 1997; Voo, Kumaresan et al. 1997). These models did not include the spinal cord and they did not examine conditions which would induce injury. Several studies have focused on the impact response on a functional spinal unit during vertical compression injuries (Lee, Kim et al. 2000; Whyne, Hu et al. 2003), however the spinal cord was not included in these models. Other models have included the head and the entire cervical spine for simulations of head-neck dynamics during impact (De Jager, Sauren et al. 1996; Jorst and Nurick 1996; Van der Horst, Thunnissen et al. 1997), which included muscles, but not the spinal cord. Another noteworthy study investigated the compressive flexion injury mechanism including the head and cervical spine, however the spinal cord was not included in this model (Halldin, Brolin et al. 2000).

A three-dimensional model of the head and neck including the brain and cervical spinal cord was created primarily to investigate pressure distributions in the brain during impact injury (Hosey and Liu 1982). The dura mater and CSF were also included in the model. Mid-sagittal symmetry was assumed and the geometry of the cord and vertebrae were very simplified; each vertebra was modelled by a single brick element which represented the vertebral body. Such anatomical simplifications did not capture details such as the

asymmetry of the anatomy or loading or the profile of the spinal canal that contacts the cord. Detailed strain distributions in the cord could not be evaluated using this model due to the small number of elements representing the cord resulting in significant geometric simplifications. This was the first study to explicitly include the spinal cord in addition to the brain and vertebral column. A similar model was created several years later; however the neck was included primarily for designation of the appropriate boundary conditions, since dynamic changes in pressure and shear stress throughout the brain were of primary interest (Kumaresan and Radhakrishnan 1996).

Finite element analysis was recently employed to study the effect of constitutive models for some cervical spinal cord injury modes (Bilston 1998). The effects of variations in constitutive models and material properties on the strain fields in the cord were examined for hyperflexion, hyperextension, and axial compression mechanisms. The model was validated with simulations in a physical model. This model was two dimensional with simplified geometry. Constitutive models investigated were linear elastic, orthotropic, hyperelastic, and viscoelastic. It was concluded that large changes in the spinal cord modulus had only a slight effect on the cord strains, whereas the constitutive model had a more noticeable effect on the cord stresses and strains. Furthermore, since high impact rates were modelled, the viscoelastic time-dependence did not significantly change the cord stresses and strains, since there was little time for relaxation to occur. It was suggested that the spinal cord behaves as a combination of orthotropic and hyperelastic/viscoelastic models, with the viscous effect being more important at lower loading rates (Bilston 1998). The strain distributions for each injury mechanism could not be evaluated using this model due to the lack of the third dimension and the simplified cord and vertebra geometry.

Two-dimensional finite element models of contusion injuries have been performed (Hung, Chang et al. 1987; Ichihara, Taguchi et al. 2001; Ichihara, Taguchi et al. 2003). These studies modelled a slice of the cord in the transverse plane and assume simplified geometry of the vertebral canal at one level. These two dimensional models could not evaluate axial motion of the tissue during injury; therefore they could not fully evaluate strain distributions during injury.

An abstract has recently been presented outlining the development of a FE model of the C5-C6 motion segment with spinal ligaments, IV disc, dura mater, CSF, spinal nerve with nerve sheath, denticulate ligaments, and the grey and white matter constituting the spinal cord (Scifert, Totoribe et al. 2000). The motion segment was subjected to physiologic motions (flexion and extension) and the average strains in the anterior and posterior portions of the cord and dura mater were presented. Linear elastic material properties were assumed for all components. This model was validated for column motion and not cord motion.

Despite successes in FE modelling in other aspects of biomechanics, there are relatively few studies examining spinal cord injury. The studies available are limited by simplified geometry, two-dimensionality, or they have not been used to study injury. There is no finite element model of the spinal cord with the surrounding structures which compares injury mechanisms using detailed, three-dimensional geometry.

1.5 Objective

Since the extent of dysfunction of axons is related to the peak strains they experience (Galbraith, Thibault et al. 1993), a technique which allows detailed distributions of strains to be evaluated would be useful in predicting damaged areas of the cord in SCI. Finite element modelling, which permits the calculation of strain distributions, has been used to study fracture in bones (Lotz, Cheal et al. 1991; Bozic, Keyak et al. 1994; Keyak and Rossi 2000), as well as to predict regions of damage in traumatic brain injury (King, Ruan et al. 1995). This technique is not currently being applied to its full potential in traumatic spinal cord injury research.

FE models require parameters defining the behaviour of each component (or tissue) to ensure accurate mechanical response of the model. However limited, mechanical property data of the anatomical components exist. Furthermore, experimental data is required to validate the overall response of the model. Experimental data of spinal cord compression exist for validation of the compression injury mechanism (Hung, Lin et al. 1979; Hung, Lin et al. 1982; Tencer, Allen et al. 1985). In addition, experimental data from animal models of spinal column and cord distraction exist for validation of the

distraction mechanism (Maiman, Coats et al. 1989). However, there is no mechanical data regarding the response of the spinal column complex during dislocation of the column. Therefore, it was achievable and of clinical interest to compare the strain distributions in the cord for compression, distraction, and dislocation injuries.

The goals of this study were as follows:

1. Create a comprehensive, three-dimensional finite element model of the spinal cord and the surrounding structures
2. Validate the model for compression and distraction injury mechanisms
3. Compare the strain distributions in the cord for compression, distraction, and dislocation injury mechanisms (using linear elastic constitutive model for the spinal cord)
4. Compare the mechanical response and strain distribution in the spinal cord in response to simple cord distraction using linear elastic and hyperelastic constitutive models

Researchers have developed many types of models to study spinal cord injury, with a trade-off between reproducibility and clinical relevance. Models need to be reliable, consistent, and reproducible. They need to replicate some of the important features of human spinal cord injury and should allow for some assessment of mechanistic features of damage. There is no reason to expect that any one model will provide the best material for studying widely different aspects of injury and pathophysiology.

A finite element model of the spinal cord was used to obtain internal strains throughout the cord during injury. Since many assumptions are inherent in this type of model, absolute values of strain in the cord may not be useful. However, knowledge of the areas of the cord under relatively high strain would help enhance our understanding of the injury event. Previous FE models of SCI cannot fully describe the strain distribution throughout the cord during injury (Hosey and Liu 1982; Bilston 1998; Ichihara, Taguchi et al. 2001).

A finite element model of the spinal cord could simulate the effect of deformation on the internal response of the cord, predict internal stresses and strains under impact, enhance our understanding of the injury event, and assist in the advancement or direct the development of therapeutics in specific injury patterns.

1.6 Scope

A finite element model of the human spinal cord with the surrounding structures was created. A three vertebrae segment of the cervical spine was selected for the model, since injuries are most common in this region (Sekhon and Fehlings 2001). The modelled segment (C4-6) was selected due mechanical interest; since this region is thought to have the greatest mobility (Panjabi and White 1980), an enlarged spinal cord, and because survivors of cervical SCI are most commonly injured between the C5 and C6 vertebrae (Shields, Fox et al. 1978; Sances, Myklebust et al. 1984; Yoganandan, Haffner et al. 1989; Yoganandan, Maiman et al. 1990).

Intervertebral (IV) discs and spinal ligaments were included in the model to connect the vertebrae to each other, while denticulate ligaments, dura mater, and dural attachment ligaments were included to connect the spinal cord to the vertebrae. The intervertebral discs were included in the model as a very simplified form of their anatomically and mechanically complex structure, which was appropriate for this initial development of the model. As a first approximation, the spinal cord was modelled as continuous tissue with no subdivision between white and grey matter. Furthermore, linear elastic material models were assumed for all components of the model, with the exception of the spinal cord for the material property sensitivity study. The mechanical response of the anatomical tissues in the model was determined by reviewing previous experimental work. The FE model was limited since some tissues were not well described in the literature.

The model was validated for three injury mechanisms: compression, distraction, and dislocation. As a first approximation, loads were applied statically, for ease of modelling. Compression and distraction mechanisms were modelled to replicate similar studies in animal models of SCI (Hung, Lin et al. 1982; Maiman, Coats et al. 1989). The model

was validated by comparing the results of the FE model with those found experimentally. For the dislocation mechanism, there was no data available in the literature for validation. Modelling of this mechanism was an extrapolation of the model for the other two cases.

The compression injury mechanism simulated a static dorsal-ventral force applied to the cord (Hung, Lin et al. 1982). Although this was similar to the contusion model of injury, it was referred to as compression, since the load was applied statically. Contusion models in SCI imply a rapid loading and unloading of the cord.

The development of the FE model was a considerable task in itself and it will provide the basis for further studies. For example, the effect of variation in parameters of impact may be studied with this model.

1.7 Clinical Relevance

The long-term goal of this research project, and other related projects performed at the Division of Orthopaedic Engineering Research at the University of British Columbia, is to assist in the development of clinical treatments of SCI tailored to a mechanistic pattern of injury. It is hypothesized that patients suffering a contusion injury will benefit from different treatments than those with a distraction or dislocation injury. This project is focused on the initial mechanical response of the cord during loading, which may help our understanding of the mechanical differences between contusion, distraction, and dislocation injury mechanisms. The long-term goal of this study will be achieved through the development of an appropriate animal model of injury.

Improved understanding of the relationship between mechanical loading and tissue damage would assist not only the field of traumatic injury research, but may also affect handling of patients following injury, surgical procedures, and the development of surgical tools.

2 Methods

2.1 Replication of Anatomy

The geometry of the anatomic structures was obtained from photographs of cryosection images provided by the National Library of Medicine's Visible Human Project (Spitzer, Ackerman et al. 1996). The cadaver was that of a 38 year old, 199 lb, 5'11" man who died of court-ordered lethal injection. The cadaver was perfused with approximately 19 litres of 1% formalin (used to preserve and fix tissue) and an anticoagulant 1.5 hours after death to retard deterioration. A vein was opened for drainage and an estimated 3 litres were drained. The cadaver was placed horizontally on its back in a plywood box and surrounded with a foaming agent to hold it in a fixed position. The cadaver was frozen at 26 hours after death. A milling device was used to section the cadaver in 1 mm intervals in the transverse plane. The slices were aligned by using fiducial rods and photographed providing detailed, calibrated images of the anatomy of a representative human male (Spitzer, Ackerman et al. 1996).

2.1.1 Vertebrae

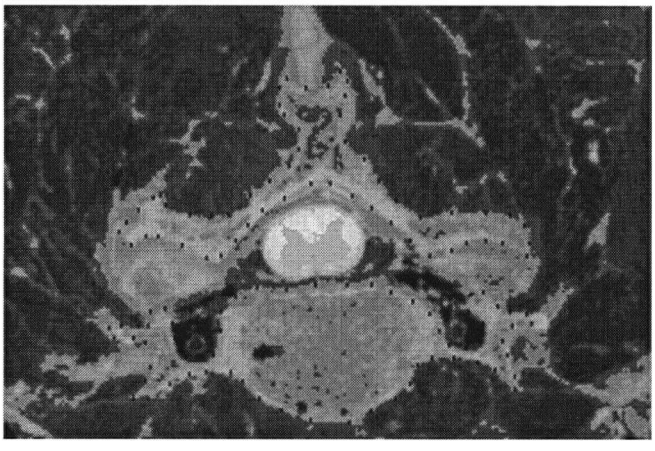

Figure 2.1: Example of the digitizing procedure used to define geometry of the C5 vertebrae (image provided by the Visible Human Project)

Images from a 6 cm segment of the cervical region were used to define the geometry of the vertebrae (C4-6). Boundary points for these structures on each transverse slice were selected using Scion Image (Scion Image for Windows 2000) and exported as two-dimensional coordinates. Figure 2.1 illustrates one transverse slice used to define some boundary points for C5. 60 images at 1 mm intervals were used to define the anatomical geometry. The two-dimensional coordinates were assembled as a three dimensional array of numbers using a program written in MatLab

5.3 (Matlab, Mathworks Inc., 1999). These points were exported in a format which allowed the finite element software Ansys 7.1 (Ansys User's Manual version 7.1, Swanson Analysis Inc., Pennsylvania, 2003) to read them as keypoints. The solid model development involved connecting keypoints to create lines, selecting lines to create areas, and selecting areas to create volumes. The vertebrae were each divided into a series of connecting six-sided blocks, to facilitate the meshing process. Each vertebra consisted of 28 volumes: three for the spinous process, four for the laminae, six for the facets, four for the pedicles, two for the transverse processes, and nine for the vertebral body. It was important to ensure that connecting volumes shared adjoining areas and lines, so that meshed volumes could share adjacent nodes. Volumes of the C5 vertebra are illustrated in Figure 2.2. Volumes representing the vertebrae were meshed using three-dimensional brick elements with eight nodes and linear shape functions (SOLID 45). Elements of C5 are illustrated in Figure 2.3. Volumes were meshed to achieve minimal element distortion by swept or mapped meshing. C4, C5, and C6 were modelled with 1794, 2000, and 1702 elements, respectively (Figure 2.4).

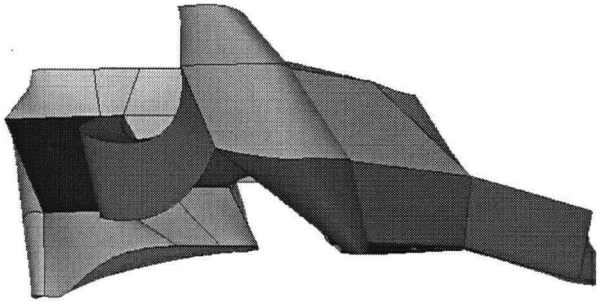

Figure 2.2: Lateral view of the volumes of C5

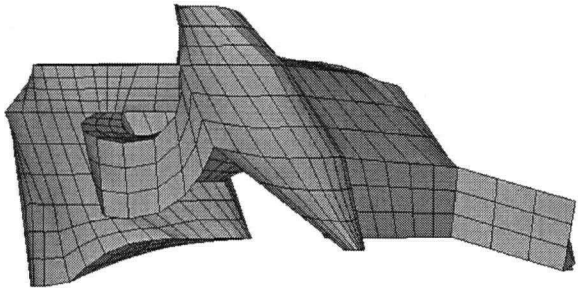

Figure 2.3: Lateral view of the elements of C5

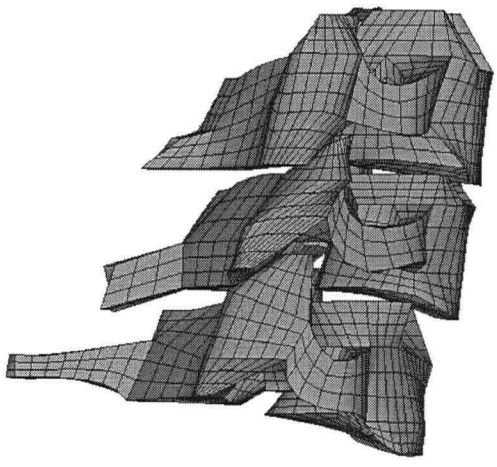

Figure 2.4: Lateral view of the elements of C4-6

2.1.2 Spinal Cord

The geometry of the spinal cord was reproduced similar to that of the vertebrae. The same transverse cryosection images were used to select boundary points for the grey and white matter, except the colour balance of the images was modified to improve the contrast between the white and grey matter (Figure 2.5). Points were digitized for the cord at intervals of 2 mm, since the geometry was less varied than that of the vertebrae. These two-dimensional points were assembled into a three-dimensional array of numbers using a program written in Matlab 5.3. Since the cadaver was placed on its back for the fixation procedure, the cord lay on the posterior wall of the canal. To model the in-vivo anatomy, the keypoints for the cord were moved anteriorly by 0.5 mm, which allowed space between the posterior wall of the canal and the spinal cord for the dura mater to be defined. The grey matter was not modelled separately from the white matter; thus only the points representing the outer surface of the white matter were used. These points

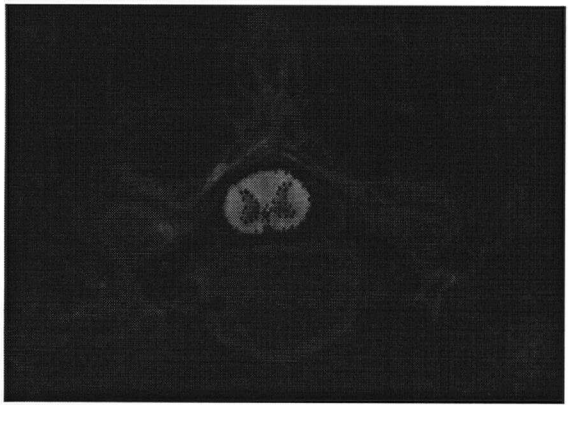

Figure 2.5: Example of the digitizing procedure used to define geometry of the spinal cord (image provided by the Visible Human Project)

were connected to create lines, the lines were connected to form areas, and areas were collected to form six-sided volumes, to facilitate meshing. Each volume was 6 mm in height and represented half of the cord segment, split in the mid-sagittal plane (Figure 2.6). The outer surface of each volume varied linearly between the top and bottom areas. Volumes representing the spinal cord were meshed using 1,920 three-dimensional brick elements with eight nodes and linear shape functions (SOLID 45). The mesh density was selected by specifying element edge lengths in the transverse plane (x-y plane) and along the axial (z) direction. Element edge lengths of 2 and 3 mm were selected for the transverse plane and the axial length, respectively. This mesh density was selected as it provided an adequate number of integration points throughout the cord with reasonable calculation time and memory requirements. Volumes were meshed to achieve minimal element distortion by swept or mapped meshing (Figure 2.7).

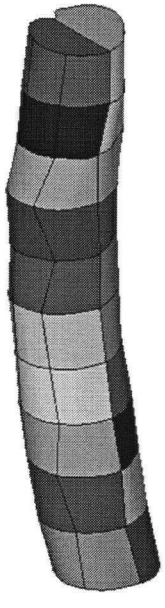

Figure 2.6: Spinal cord volumes

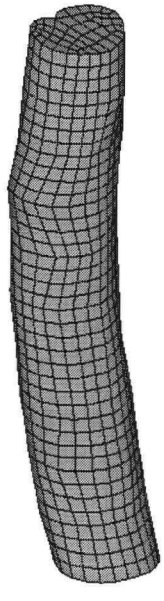

Figure 2.7: Spinal cord elements

In order to investigate more complex aspects of material modelling of the spinal cord, these elements were imported into Abaqus (Abaqus User's Manual version 6.3, Hibbitt, Karlsson & Sorensen, Inc., 2002). This program has a more extensive material library and was found to be better equipped for solving problems with complex material behaviour. The spinal cord was modelled with C3D8H elements: brick elements with

eight nodes and linear shape functions. These elements have a hybrid formulation, which allows modelling of incompressible, or nearly incompressible materials. The mesh was identical to that used in the Ansys model.

2.1.3 Dura Mater

The dura mater is a thin membrane; therefore, it is less visible in transverse sections, such as the Visible Human Project images. Keypoints for the dura mater were created in Ansys between the vertebral canal and the spinal cord in transverse planes at 6 mm intervals. These keypoints were created to fit in the small space required, based on a subset of Visible Human Project images in which the dura mater could be discerned. Ten keypoints were created for each transverse section of dura mater. Keypoints were connected to create lines and lines were combined to form areas. The dura was modelled as 20 areas, 10 anterior and 10 posterior, each with a height of 6 mm (Figure 2.8). The outer surface of dura varied linearly between transverse sections. The areas representing the dura mater were meshed using first order three-dimensional quadrilateral shell element with 4 nodes, SHELL181 (Figure 2.9), with a thickness of 0.27 mm (Tencer, Allen et al. 1985). The number of elements used to model the 6 cm segment of dura mater was 1,120.

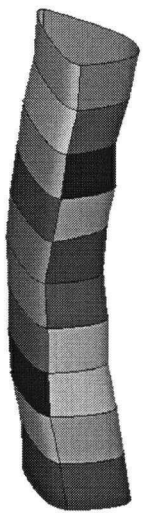

Figure 2.8: Dura mater areas

Figure 2.9: Dura mater elements

2.1.4 Spinal Ligaments

Spinal ligaments were included in the FE model to provide anatomically accurate connections between the vertebrae. The anterior longitudinal ligament (ALL), posterior longitudinal ligament (PLL), joint capsule (JC), ligamentum flavum (LF), and interspinous ligament (ISL) were modelled. The supraspinous, intertransverse, and nuchal ligaments were not included in the model.

The spinal ligaments were modelled with first order link elements with 2 nodes and linear shape functions (LINK10). The link elements are tension-only elements, meaning that they will produce zero stress in response to compressive strains and a stress that is linearly related to strain in response to tensile strains. These elements have a nonlinear stress-strain response, since the response in compression differs from that in tension. Nodes were selected on the vertebrae to form the endpoints of the ligaments. These nodes were selected to best re-create the anatomy, as described in the literature (Panjabi, Oxland et al. 1991; Przybylski, Carlin et al. 1996; Yoganandan, Kumaresan et al. 2000). For example, the anterior longitudinal ligament (ALL) is described to attach along the length of the vertebral bodies; therefore the most inferior nodes of the superior vertebrae and the most superior nodes of the inferior vertebrae were selected as the endpoints for the ALL (Figure 2.10). The width of the modelled ALL (average 7 mm) was selected to fit the modelled vertebrae and was within the range of those determined from anatomical studies (between 7 and 10 mm) (Panjabi, Oxland et al. 1991; Przybylski, Patel et al. 1998).

Histological examinations of the posterior longitudinal ligament (PLL) at the cervical level found that fibres insert along the entire length of the underlying vertebral bodies (Przybylski, Patel et al. 1998) and the PLL also has an interwoven connection with the intervertebral disc (White and Panjabi 1990). Therefore, the most inferior nodes of the superior vertebrae and the most superior nodes of the inferior vertebrae were selected as endpoints for the PLL (Figure 2.11). The width of the modelled PLL (average 10.2 mm) was selected to represent those determined in anatomical studies (between 8 and 11 mm) (Panjabi, Oxland et al. 1991; Przybylski, Patel et al. 1998).

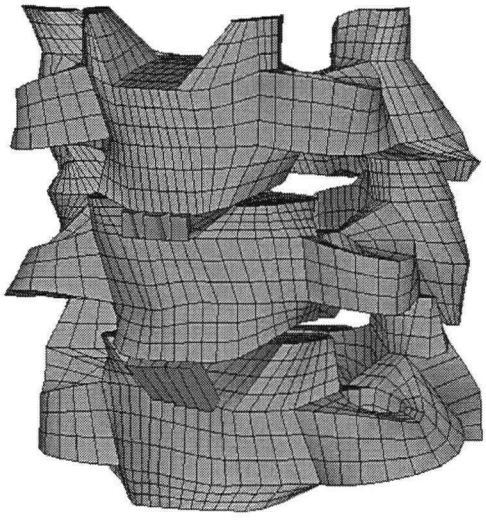

Figure 2.10: Antero-lateral view of C4-6 and anterior longitudinal ligaments (ALL)

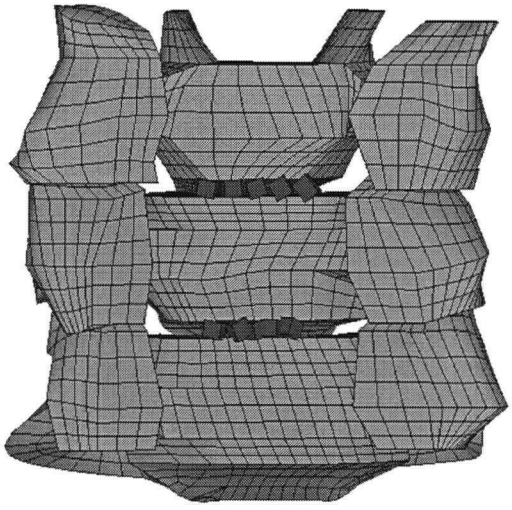

Figure 2.11: Posterior view of C4-6 (with posterior elements removed) and posterior longitudinal ligaments (PLL)

The ligamentum flavum (LF), joint capsule ligament (JC), and interspinous ligaments (ISL) were created similarly to the longitudinal ligaments; nodes were selected on adjacent vertebrae to be the endpoints for the elements (Figures 2.12-2.14).

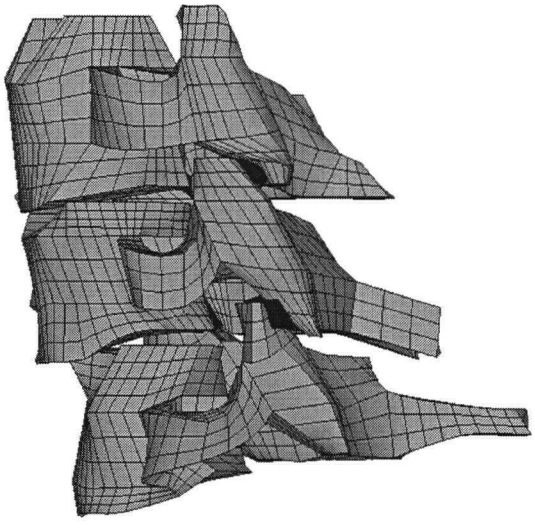

Figure 2.12: Lateral view of C4-6 and joint capsule ligament (JC)

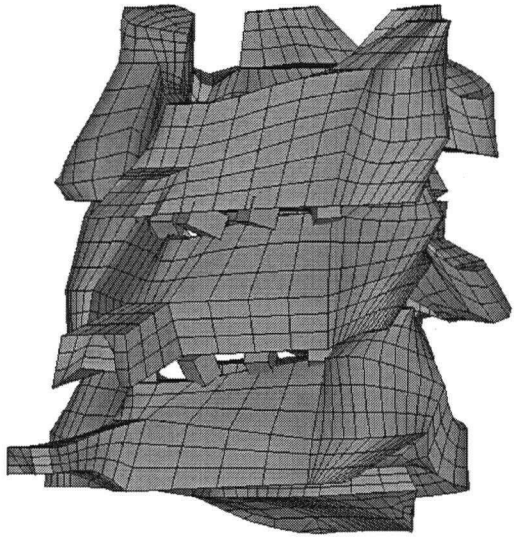

Figure 2.13: Postero-lateral view of C4-6 and ligamentum flavum (LF)

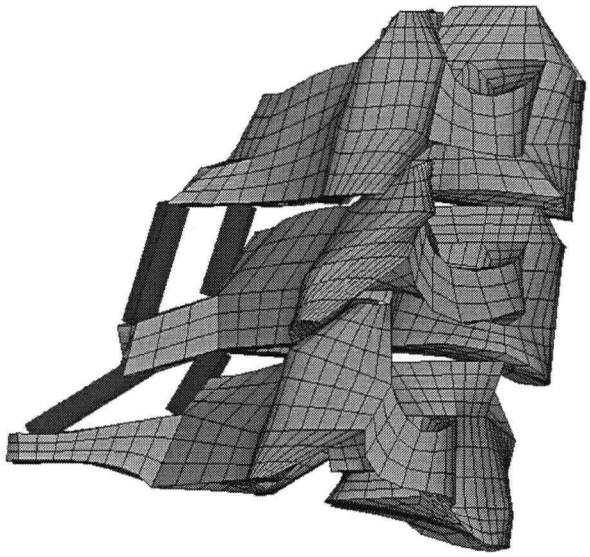

Figure 2.14: Lateral view of C4-6 and interspinous ligaments (ISL)

For this type of element (LINK10), the element cross-sectional area is required as part of the element real constants. The total area for each ligament was assumed to be the average measured area of cervical ligaments described in the literature (Figure 2.15) (Przybylski, Carlin et al. 1996; Yoganandan, Kumaresan et al. 2000). The area for each element was calculated as the total ligament area divided by the number of elements representing that ligament (Table 2.1). Spinal ligaments made up 44 elements in the C4-6 model.

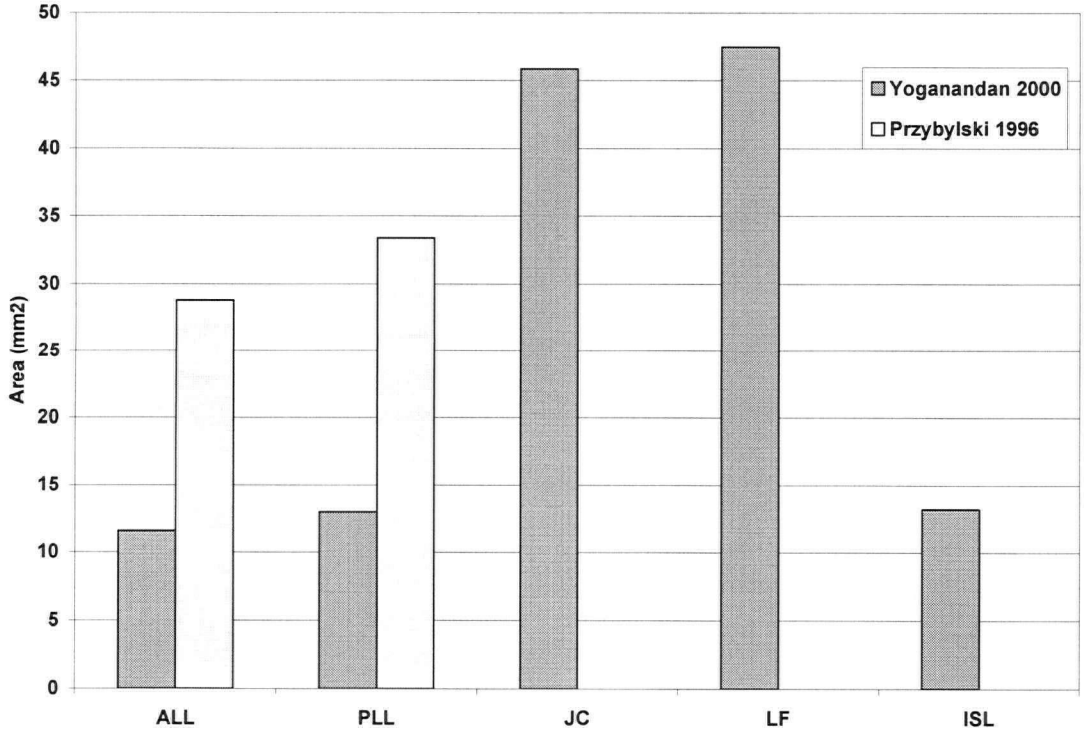

Figure 2.15: Cross sectional areas of cervical spinal ligaments from anatomical studies

Table 2.1: Spinal ligament anatomy in FE model

Ligament	# Elements / Level	Total Ligament Area (mm^2)	Area (mm^2) / Element
ALL	5	20	4
PLL	5	23	4.6
JC	4	46	11.5
LF	6	47	8
ISL	2	13	6.5

2.1.5 IV Discs

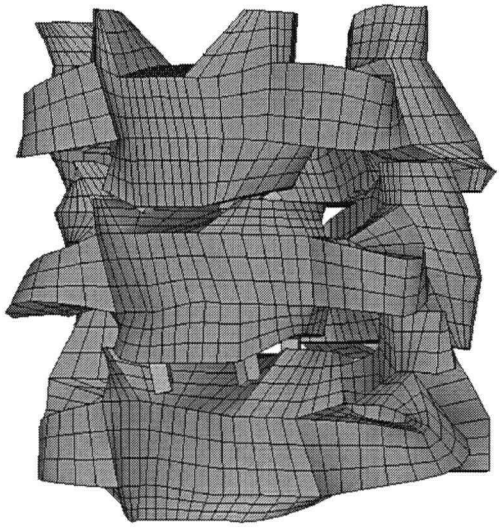

Figure 2.16: Antero-lateral view of C4-6 with IV Discs

IV discs were also included in the model to provide anatomically accurate connections between the vertebrae. IV discs were modelled with LINK8 elements, which are first order link elements with two nodes and linear shape functions (Figure 2.16). These are truss elements having linear tension/compression capabilities and no bending capabilities. The mean area of a cervical IV disc is approximately 400 mm^2 (Moroney, Schultz et al. 1988) and four elements were used to model each disc; therefore the area of each element was 100 mm^2.

2.1.6 Denticulate Ligaments

Denticulate ligaments were included in the model to provide connections between the spinal cord and the dura mater. They were modelled based on anatomic descriptions in the literature. The denticulate ligament attaches medially along the lateral surface of the cord midway beween the dorsal and ventral roots, and laterally to the arachnoid nearer to the ventral than to the dorsal aspect of the dura (Breig 1960). It has a broad base at the

cord and a narrow insertion at the dura, approximately midway between root exits (Nauta, Dolan et al. 1983). The lateral edge of the denticulate ligament is serrated (Figure 2.17).

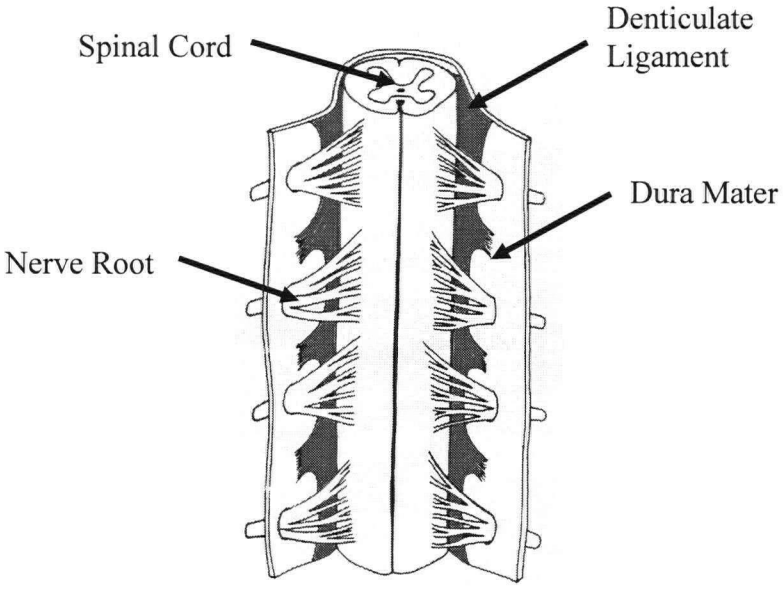

Figure 2.17: Anterior view of the spinal cord, posterior dura mater, ligaments as described in the literature (Figure modified from White and Panjabi 1990)

Denticulate ligaments connecting the spinal cord and dura mater were modelled with first order link elements with two nodes and linear shape functions (LINK10). These elements have a linear response in tension, and no response in compression; therefore they are nonlinear. These elements were created by selecting nodes on the spinal cord and dura mater as endpoints. The lateral edge of the denticulate ligament was selected to be midway between the vertebral foramen, where the nerve roots would have exited, had they been included in the model. 50 elements were created to model the denticulate ligament. Dimensions of the denticulate ligament are not available in the literature. A height and width of 0.5 mm were assumed, which gave a cross-sectional area of 0.25 mm^2. Since three elements were used to model each component of the ligament (Figure 2.18), this area was divided by three to obtain an area of 0.083 mm^2 for each element.

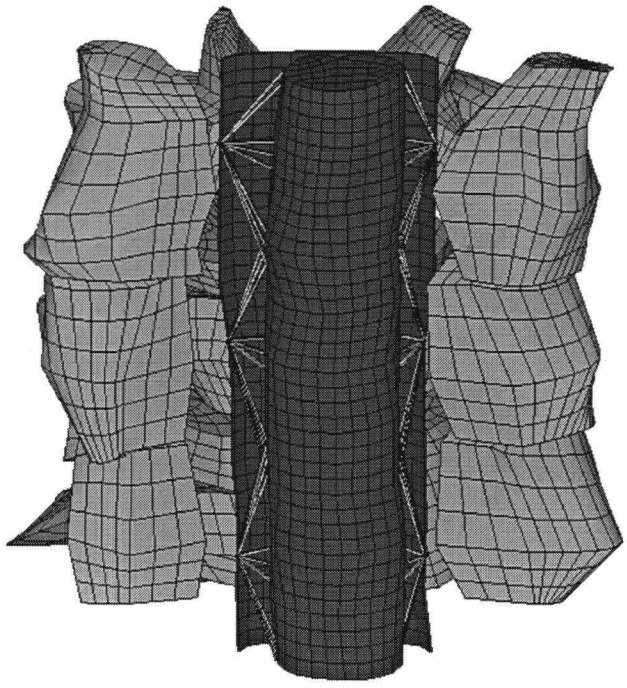

Figure 2.18: Posterior view of C4-6 (with posterior elements removed), spinal cord, anterior dura mater, and denticulate ligaments

2.1.7 Dural Attachments

The dura mater is attached to the vertebral canal by fibrous tissue. This tissue is referred to as dural attachments or ligaments (Spencer, Irwin et al. 1983), Hoffman's ligaments (Wiltse, Fonseca et al. 1993), epidural ligaments (Shinomiya, Sato et al. 1995), meningovertebral ligaments (Scapinelli 1990), or simply as extensions of the superficial layer of the PLL (Hayashi, Yabuki et al. 1977; Kubo, Waga et al. 1994). These minor anatomical structures are often ignored in neurosurgical and orthopaedic publications (Scapinelli 1990) and are most studied in the lumbar region, since medications are commonly injected into the lumbar epidural space. These dural attachments are membranous formations which connect the dura mater to the PLL and other structures in the spinal canal, and may vary from loose tissue to individualised ligaments and from mid-sagittal to lateral arrangements (Scapinelli 1990).

The most commonly described fibrous tissue connecting the dural sac to the spinal canal is that which is contained in the anterior region. These attachments are stronger than those located in the dorsal region (Parkin and Harrison 1985). They are consistently

found in the cervical region but are more predominant in the lumbosacral region (Scapinelli 1990) and serve to hold the dura forward against the anterior side of the spinal canal. Segmental fibers attach the outer surface of the dura mater to the PLL (Spencer, Irwin et al. 1983), however some fibres pass through the PLL to terminate on the IV discs and the vertebrae (Scapinelli 1990). Wiltse and Fonseca (Wiltse, Fonseca et al. 1993) found high variability in the number of ligaments, but generally found two at each spinal level (left and right), joining the superficial layer of PLL to the ventral dura. Midline attachments have been found from the anterior dura to the PLL as well as lateral attachments from anterolateral dura to the lateral extent of the PLL (Spencer, Irwin et al. 1983).

Dural attachments in the FE model were created based on a detailed study of the lumbosacral meningovertebral ligaments (Scapinelli 1990). This study reported ligaments arranged sagittally in a median, or paramedian line in the ventral epidural space. Bands of 1-1.5 mm thickness were observed to attach to the PLL at disc and vertebral body levels with a length of 3-6 mm. This study suggested that fibres may be represented by two or more paramedian bands in the transverse plane. Similar ligaments have been reported in the lower cervical spine (Figure 2.21) (Hayashi, Yabuki et al. 1977).

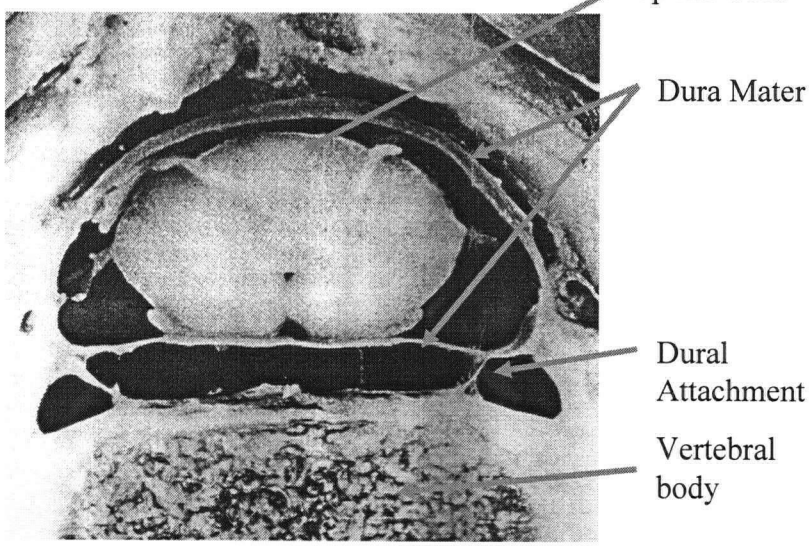

Figure 2.19: Transverse section through the spinal canal illustrating the dural attachements (Figure modified from Hayashi, Yabuki et al. 1977)

Dural attachments between the anterior dura mater and the posterior vertebral bodies were modelled using 24 first order link elements with 2 nodes and linear shape functions, LINK10, located at mid-vertebral body height (Figures 2.20 and 2.21). Since the link elements are tension-only elements, they have a nonlinear response.

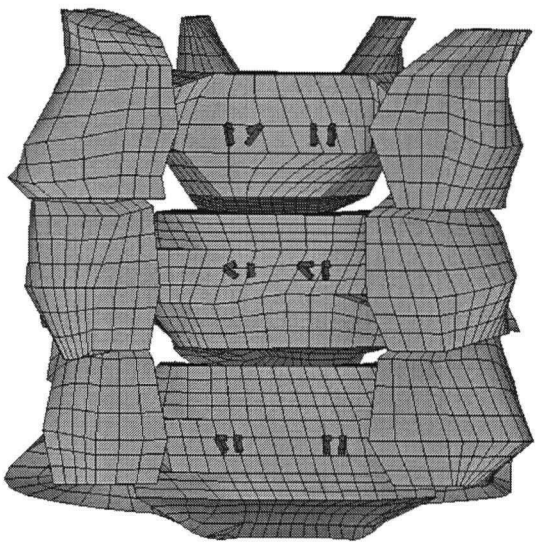

Figure 2.20: Posterior view of C4-6 (posterior elements removed) showing connections to the dura mater

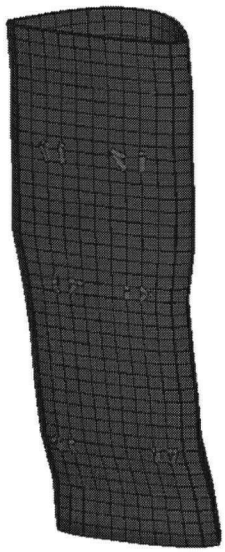

Figure 2.21: Dura mater with connections to the vertebrae

2.2 Material Properties

Material properties for the various components of the model were selected or calculated based on experimental data in the literature.

All components, except for those modelled by LINK10 elements, were assumed to behave as linear elastic. The tension behaviour of those components modelled by LINK10 element is also assumed to behave as linear elastic. The compression behaviour of these elements is automatically assigned a very low stiffness by the program.

2.2.1 Vertebrae

Vertebrae consist of a core of cancellous (or spongy) bone with a shell of cortical (or compact) bone. Mechanical properties of bone vary with drying of the tissue, rate of loading, direction of loading, variations in bone mineral content, and density (Park and

Lakes 1992). In general, the elastic modulus of cancellous bone is 100 MPa, while that of cortical bone is 10 GPa (Yamada 1970; Evans 1973). Poisson's ratio of bone is an average of 0.29 (Yamada 1970; Evans 1973).

Elements of the vertebrae were assigned material properties of cortical bone (Yamada 1970; Evans 1973). An elastic modulus of 10,000 MPa and a Poisson's ratio of 0.29 were assigned, which have been used in previous finite element models of cervical vertebrae (Kumaresan, Yoganandan et al. 1999; Ng and Teo 2001). Bone was assumed to behave as linear elastic.

2.2.2 Spinal Cord

The behaviour of the spinal cord in response to mechanical loading is not well understood. The earliest in vitro test of cadaver spinal cord tissue was performed by Brieg who found that it elongated under its own weight when suspended (Breig 1960). Load deformation data was provided which corresponded to an elastic modulus of 1.7 MPa for strain under 2%, and 5 MPa for strain above 3% (Breig 1960). Following in vitro studies of canine spinal cord tissue found the cord exhibited a primarily viscous response (Tunturi 1978); the elastic modulus of the spinal cord was 0.02 MPa for loads less than 0.34 N. Both of these early studies used primitive testing methods which elicit uncertainty in the validity and use of the results. Uniaxial tension tests of the spinal cord were later performed in vivo on cats and puppies (Chang, Hung et al. 1981; Hung and Chang 1981; Hung, Chang et al. 1981; Hung, Chang et al. 1981; Chang, Hung et al. 1988). The stress-strain relationship of the spinal cord was linear up to 3 or 5% strain with mean Young's modulii between 0.23 and 0.4 MPa (Figure 2.22). For these experiments, the tension in the cord in its natural state was applied as a pre-tension (0.04 to 0.06 N). Viscoelastic models were fit to the relaxation data from these experiments. Furthermore, uniaxial loading of in vitro rat spinal cord tissue exhibited elastic modulii between 0.6 and 1.3 MPa (Fiford and Bilston 1998). The use of surface markers indicated that the distribution of strain throughout the length of the spinal cord was not uniform (Fiford and Bilston 1998).

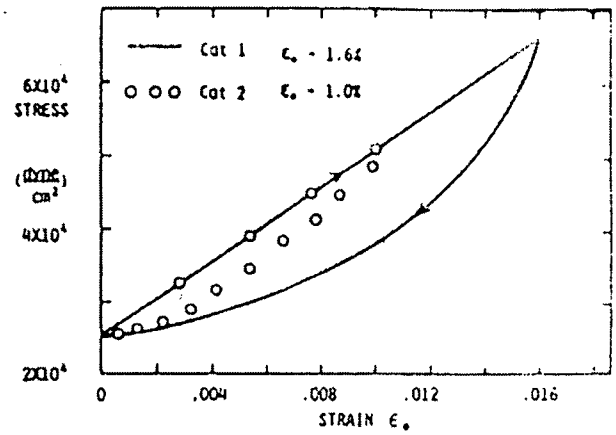

Figure 2.22: Linear stress-strain response for loading in uniaxial tension of in vivo spinal cord tissue up to small strains (Figure from Hung, Chang et al. 1981)

Bilston researched the response of the human spinal cord to uniaxial loading under a range of strain rates (Figure 2.23) (Bilston 1994; Bilston and Thibault 1996). The mechanical behaviour of the human spinal cord under uniaxial tension was characterized by a highly nonlinear elastic response and significant relaxation. Average modulii increased with an increase in strain rate, ranging from 1.02 to 1.37 MPa. These data were fit to three constitutive models: quasilinear viscoelastic, hyperelastic, and four element linear viscoelastic models. Uniaxial tension tests of spinal cord tissue (without the dura mater) are summarized in Table 2.2. Death and fixation of nervous (brain) tissue has been found to increase its elastic modulus (Metz, McElhaney et al. 1970), which may partially account for the increased elastic modulii of spinal cord tissue obtained through in vitro testing.

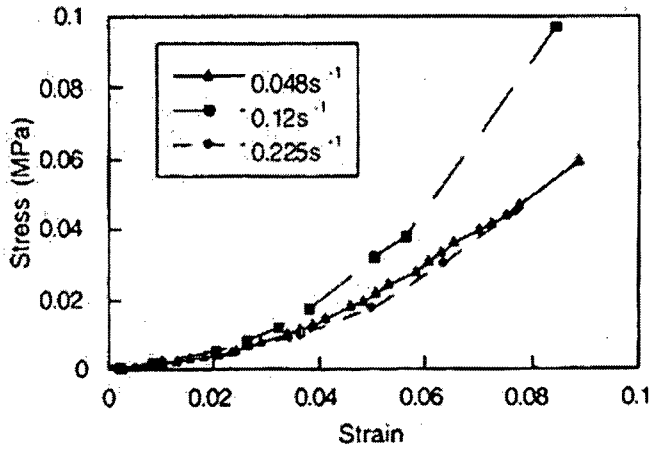

Figure 2.23: Sample stress-strain responses of human spinal cord tissue in uniaxial tension at various loading rates (Figure from Bilston and Thibault 1996)

Table 2.2: Summary of uniaxial tension tests of spinal cord tissue

Reference	Species	In vitro / In vivo	Strain rate (/s)	Max strain (%)	Elastic Modulus (MPa)
(Breig 1960)	Human	in vitro	incremental	2.0 3.0	1.7 5.0
(Tunturi 1978)	Dogs	not defined	incremental	5.0	0.02
(Hung, Chang et al. 1981)	Cats	in vivo	0.0003 (QS)	5.0	0.4
(Hung, Chang et al. 1981)	Cats	in vivo	0.002 (QS)	5.0	0.26
(Chang, Hung et al. 1981)	Dogs	in vivo	0.002 (QS)	5.0	0.265
(Hung and Chang 1981)	Dogs	in vivo	0.003 (QS)	3.0	0.265
(Chang, Hung et al. 1988)	Cats	in vivo	(QS)	0.6	0.23
(Bilston 1994; Bilston and Thibault 1996)	Human	in vitro	0.068 0.14 0.21	9.0	1.02 1.17 1.37
(Fiford and Bilston 1998)	Rats	in vitro	0.002	5.0	0.9

QS: quasi-static

The nonlinear elastic response of spinal cord tissue has recently been characterised as hyperelastic (Bilston 1994; Bilston and Thibault 1996; Bilston 1998). Brain tissue, which has a similar composition to spinal cord tissue, has also been described using hyperelastic material models (Sahay, Mehrotra et al. 1992; Mendis, Stalnaker et al. 1995; Miller 1999; Miller, Chinzei et al. 2000; Bilston, Liu et al. 2001; Miller and Chinzei 2002). Typically, hyperelastic materials have a bulk modulus that is several orders of magnitude larger than the shear modulus, and they tend to deform in an incompressible manner. Materials that undergo large elastic deformations are often characterized as hyperelastic; the classical example is rubber (Mooney 1940).

The state of strain at a point may be fully represented by the principal strain components (ε_1, ε_2, ε_3). If the material is homogeneous and isotropic, an element oriented in the

principal direction will not be subjected to shear strains. Furthermore, the state of strain may also be represented by the principal stretch ratios (λ_1, λ_2, λ_3)

$$\lambda_1 = \varepsilon_1 + 1$$
$$\lambda_2 = \varepsilon_2 + 1$$
$$\lambda_3 = \varepsilon_3 + 1$$

Hyperelastic materials are defined by a strain energy function (U), which indirectly relates stresses and strains. The strain energy is the internal energy stored in a material due to external loading. For a hyperelastic material, the strain energy function may be defined in terms of the principal stretch ratios or the strain invariants. Several forms of the strain energy function have been employed in spinal cord modelling. One simple form for the strain energy function is the Ogden model:

$$U = \frac{2\mu}{\alpha^2}(\lambda_1^\alpha + \lambda_2^\alpha + \lambda_3^\alpha - 3) + \frac{1}{d}(J_{elastic} - 1)^2$$

where μ, α, and d are material constants, λ_1, λ_2, and λ_3 are principal stretch ratios, and $J_{elastic}$ is the elastic volumetric strain. Total volumetric strain (J) is the change in volume per unit volume and is a function of the elastic and thermal volumetric strains ($J_{elastic}$ and $J_{thermal}$).

$$J = \varepsilon_x + \varepsilon_y + \varepsilon_z$$

$$J = J_{elastic} J_{thermal}$$

$$J_{thermal} = (1 + \varepsilon_{thermal})^2$$

where $\varepsilon_{thermal}$ is the linear thermal expansion which is a function of the temperature gradient and the coefficient of thermal expansion. This model assumes that the material is isotropic and incompressible, or nearly incompressible. The parameter, d, defines the

compressibility of the material and is set to zero for full incompressibility (d = 0). Furthermore, for full incompressibility, the volumetric strains are equal to one ($J_{elastic} = 1$) so that the final term in the Ogden strain energy function becomes zero.

The initial slope of the shear stress-shear strain curve is called the initial shear modulus (μ_o) and it is defined by:

$$\mu_o = \mu$$

The initial bulk modulus (K_o) is defined by:

$$K_o = \frac{2}{d}$$

With the parameter, d, set to zero, the initial bulk modulus is infinite. This form of the strain energy function has been used in finite element models of the spinal cord (Bilston and Thibault 1996; Bilston 1998).

Since the spinal cord was the tissue of interest for this study, two constitutive models were examined. First, a linear elastic material model was utilized for loading of the model in compression, distraction, and dislocation. This model was selected for simplicity and for general use in the development of the FE model. Parameters for the spinal cord behaviour were selected based on experimental work of Hung and Chang (Chang, Hung et al. 1981; Hung and Chang 1981; Hung, Chang et al. 1981; Chang, Hung et al. 1988) since the finite element model applied static loading and these tests were performed at quasistatic rates. Furthermore, in vivo experimental models were used for validation of the compression and distraction injury mechanisms; therefore it was reasonable to use material property data obtained from in vivo experiments. Elements of the spinal cord were assigned an elastic modulus of 0.26 MPa. The Poisson's ratio was set to 0.49, since spinal cord tissue may be considered to be incompressible and this value has been used in previous FE models of the spinal cord (Hosey and Liu 1982; Bilston 1994; Bilston 1998).

Second, a hyperelastic material model was applied for distraction of the cord alone, to investigate the effect of using a more accurate, nonlinear elastic model. A hyperelastic model (Ogden form) was fit to experimental data on human spinal cords in tension (Bilston and Thibault 1996). Parameters were found using a least-squares fit in Microsoft Excel and were found to be $\mu = 0.09$ and $\alpha = 29.52$. Details of this analysis are contained in Appendix B. Parameters from this fit were assigned to elements of the spinal cord.

The nonlinear stress-strain response of spinal cord tissue (Bilston and Thibault 1996) and the response of the linear elastic and hyperelastic model are illustrated in Figure 2.24.

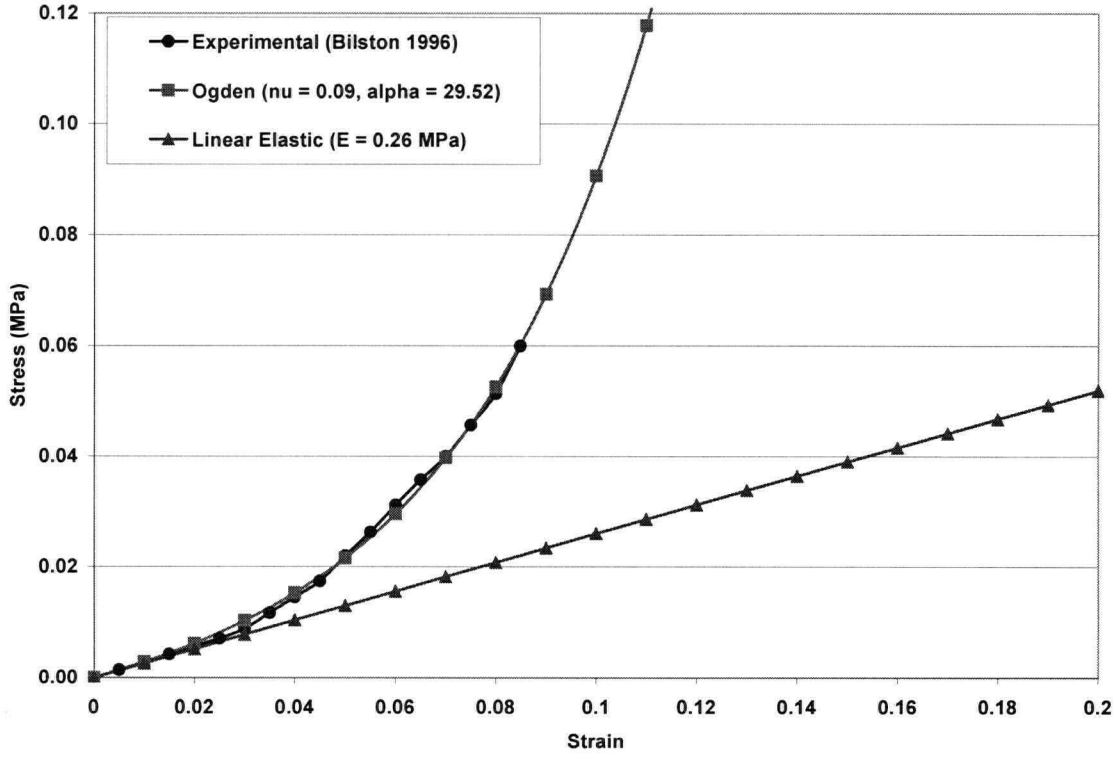

Figure 2.24: Spinal cord material modelling: experimental data of the human cervical spinal cord in tension (Bilston and Thibault 1996), linear elastic fit, and Ogden hyperelastic fit.

2.2.3 Dura Mater

The dura mater is dense connective tissue made up of collagen fibres (high tensile strength, low ultimate elongation) and elastin fibres (low tensile strength, high ultimate elongation). An early study of the material characteristics of canine dura mater found

that for loads less than 0.5 N, the elastic modulus was 0.4 MPa (Tunturi 1977), which is comparable to that of elastin fibres (Park and Lakes 1992). For loads between 0.5 and 1.5 N, the elastic modulus was 50 MPa (Tunturi 1977), which is comparable to that of collagen fibres (Park and Lakes 1992). This nonlinear elastic response, which is characteristic of biological materials, was also found for cadaveric dura mater removed from donors shortly after death (Figure 2.25) (van Noort, Black et al. 1981). The elastic modulus for small strains (less than 5%) was 5 MPa, and the average incremental elasticity (from 5 to 10% strain) was 29 MPa (van Noort, Black et al. 1981). This low strain response was similar to that obtained by testing cat dura mater in situ (Chang, Hung et al. 1988). The elastic modulus was 2 MPa for strains less than 6% (Figure 2.25). The elastic modulus of dura mater strained to failure is much larger, since the tissue becomes stiffer at higher strains. Tencer et. al. reported a modulus of elasticity in the cervical region of 129 MPa for loading to failure (Tencer, Allen et al. 1985).

Orientation effects may be significant in human spinal dura mater as several studies have found dura to be stiffer in the longitudinal direction (Patin, Eckstein et al. 1993; Runza, Pietrabissa et al. 1999), while another found specimens to be stiffer in the circumferential direction (Wilcox, Bilston et al. 2003). This difference is suggested to be attributed to variations in the maximum strain for each test (Wilcox, Bilston et al. 2003). Dynamic analyses of cranial dura mater found strain rate effects to be significant (McElhaney, Melvin et al. 1973). Human spinal dura mater is highly viscoelastic in both longitudinal and circumferential directions (Wilcox, Bilston et al. 2003). Recent studies have modelled the time dependent behaviour of dura mater as quasilinear using a relaxation function that can be separated into a reduced relaxation function and an elastic response, which is a function of the strain alone (Wilcox, Bilston et al. 2003).

The dura mater was to be strained up to approximately 5% in the FE model. Therefore, elements of the dura mater were assigned an elastic modulus representing the strain range of interest (5 MPa). A Poisson's ratio of 0.45 was assigned to elements of the dura mater. This value has been used in previous FE models of the dura mater (Ward, Nikravesh et al. 1978; Hosey and Liu 1982; Kumaresan and Radhakrishnan 1996). Dura mater was assumed to behave as linear elastic.

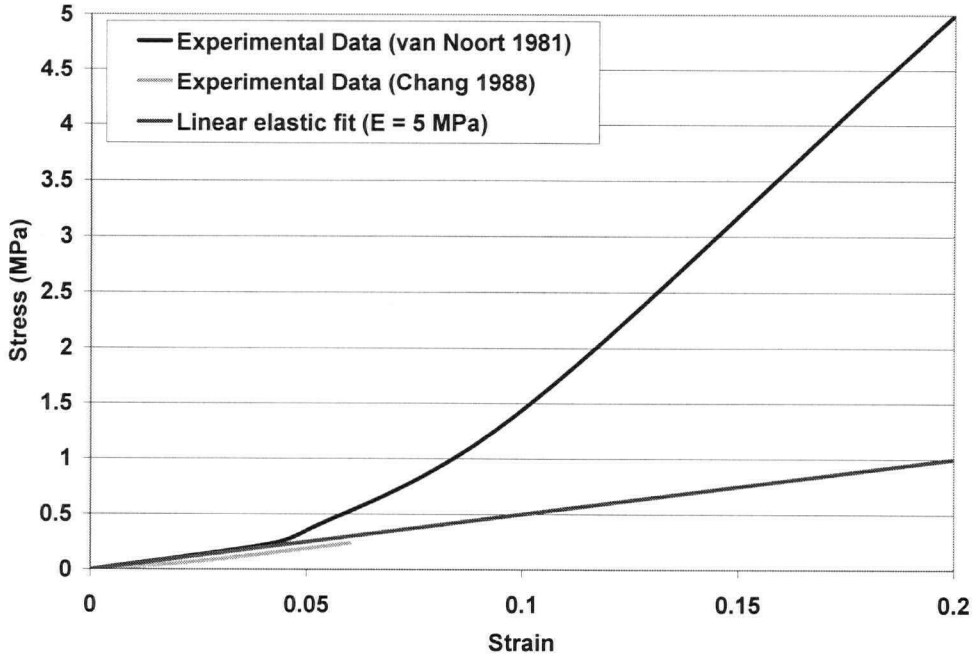

Figure 2.25: Stress-strain response of dura mater (van Noort, Black et al. 1981; Chang, Hung et al. 1988)

2.2.4 Spinal Ligaments

Spinal ligaments consist of collagen and elastin fibres and have a nonlinear stress-strain response typical of biological tissues. The initial region has a low slope, representing alignment of fibres in the direction of stress. The steep rise in slope represents the majority of fibres stretched along their long axes. Experimental tests have determined elastic modulii of spinal ligaments based on the linear portions of their stress-strain curves (Nachemson and Evans 1968; Chazal, Tanguy et al. 1985; Goel and Njus 1986; Yoganandan, Pintar et al. 1989; Pintar, Yoganandan et al. 1992; Przybylski, Carlin et al. 1996; Yoganandan, Kumaresan et al. 2000). Variations in the material properties exist between spinal ligaments and between spinal levels (Myklebust, Pintar et al. 1988). Figures 2.26 and 2.27 illustrate the various elastic modulii found for lumbar and cervical spinal ligaments, respectively. Variability exists between published values due to variations in techniques for fixing the ends of the ligaments, applied loading rates, and techniques for measuring strain. Furthermore biological variability exists between subjects since the mechanical properties of ligaments vary with bone mineral density

(Neumann, Keller et al. 1994). It may be noted that on average, elastic modulii of lumbar ligaments are greater than those of the cervical region, except for the ALL.

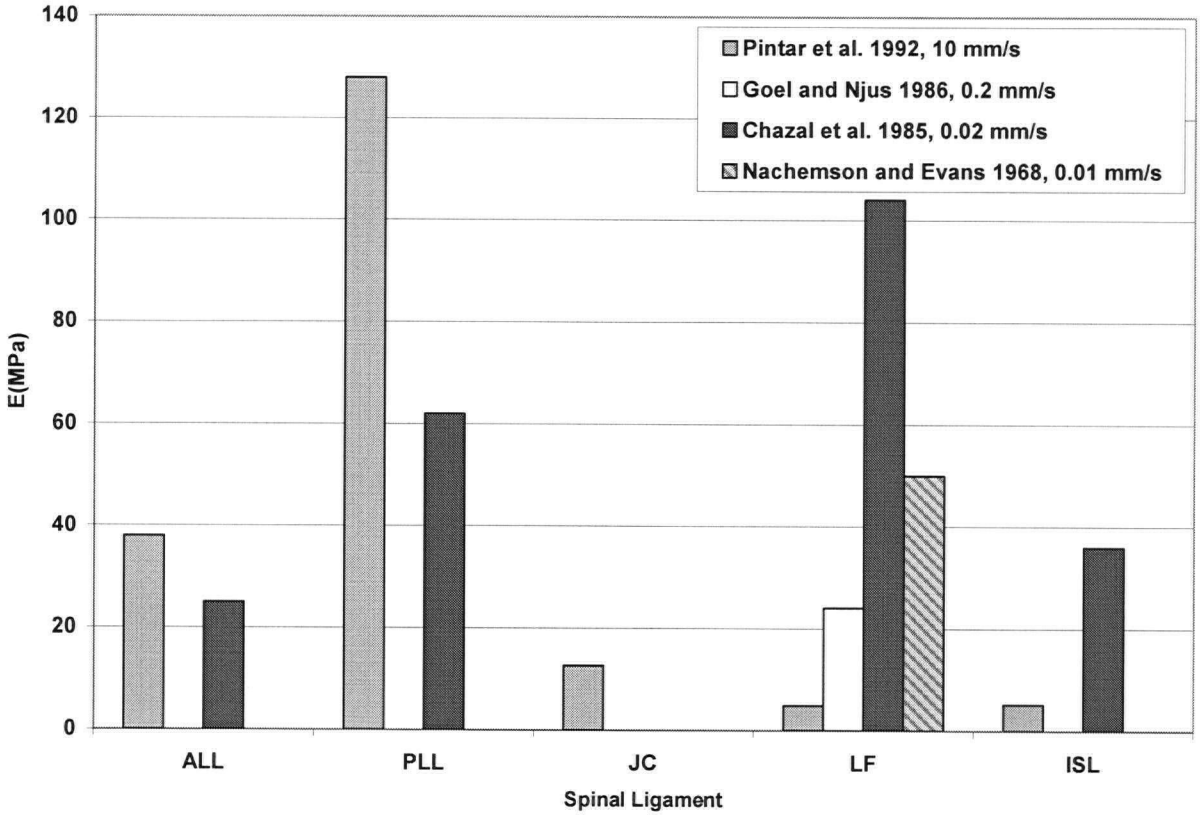

Figure 2.26: Elastic modulii of lumbar spinal ligaments (Nachemson and Evans 1968; Chazal, Tanguy et al. 1985; Goel and Njus 1986; Pintar, Yoganandan et al. 1992). References and loading rates are indicated in the legend.

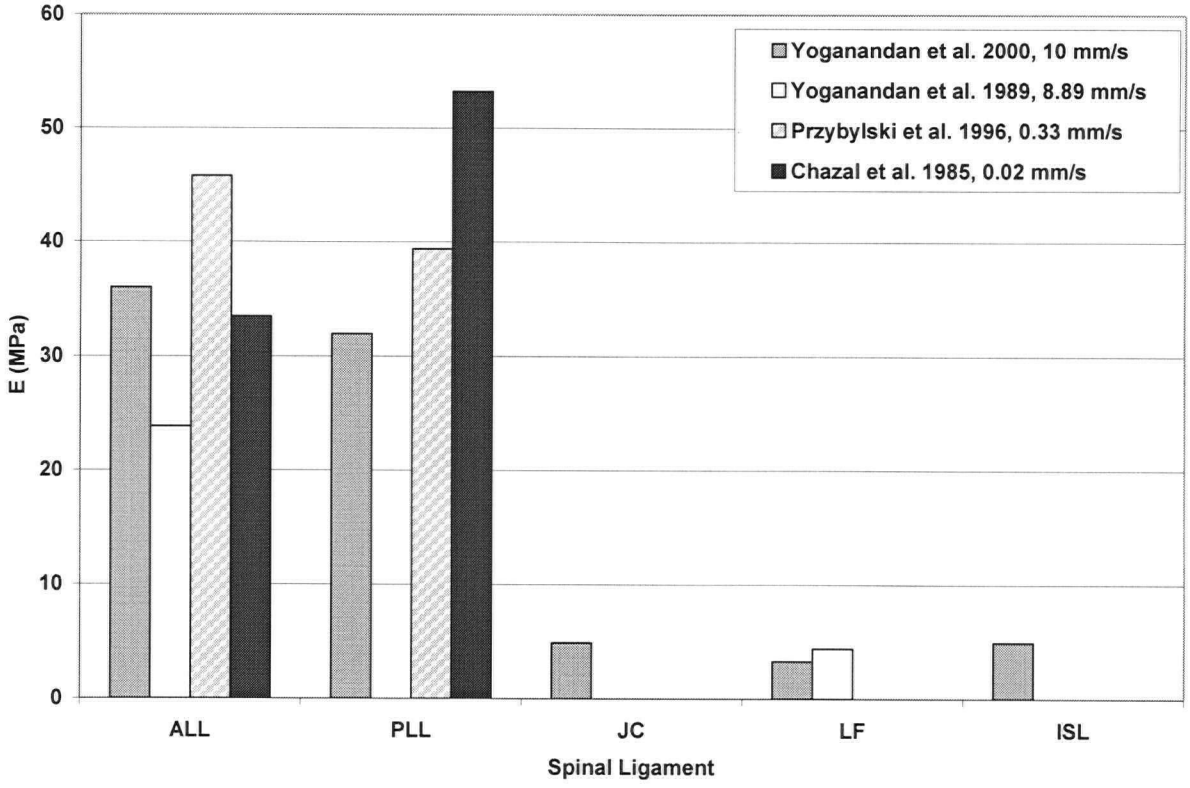

Figure 2.27: Elastic modulii of cervical spinal ligaments (Chazal, Tanguy et al. 1985; Yoganandan, Pintar et al. 1989; Przybylski, Carlin et al. 1996; Yoganandan, Kumaresan et al. 2000). References and loading rates are indicated in the legend.

Elastic modulii for the spinal ligaments were assigned average values from three studies which measured the in-situ behaviour of cervical spinal ligaments in tension (Yoganandan, Pintar et al. 1989; Przybylski, Carlin et al. 1996; Yoganandan, Kumaresan et al. 2000). The elastic modulii were assigned values of 35, 36, 5, 4, and 5 MPa for the ALL, PLL, JC, LF, and ISL, respectively.

2.2.5 IV Disc

Mechanical properties of the IV disc show large biological variability, as well as variations due to the experimental techniques (Moroney, Schultz et al. 1988). The stress-strain response of the IV disc demonstrates the typical nonlinear response of biological tissues (Figure 2.28). The stiffness of the IV disc or the annulus fibrosus is more often reported than the elastic modulus. An equivalent or effective elastic modulus [MPa] may be calculated from the stiffness [N/mm] by dividing the stiffness by the initial cross

sectional area [mm^2], and multiplying by the initial length [mm]. Using assumed geometry for the disc, elastic modulii in tension have been reported between 0.95 and 19.3 MPa (Table 2.3). The wide range of reported values is due to variability in testing methods, maximum strains applied during testing, spinal level tested, and inherent biological variability between specimens. Furthermore, cervical IV discs have more recently been found to differ significantly in structure from lumbar IV discs, which are more commonly examined in the literature (Mercer and Bogduk 1999). Similarly, elastic modulii in compression have been reported between 1 and 44 MPa (Brown, Hansen et al. 1957; Yamada 1970; Markolf 1972; Lin, Liu et al. 1978; Panjabi, Summers et al. 1986; Moroney, Schultz et al. 1988), with higher stiffnesses generally corresponding to greater maximum strains. Yamada provided stress vs. strain graphs for the behaviour of the disc in tension and compression (Figure 2.28) which illustrate the substantial nonlinear behaviour of the disc in compression, while in tension, the disc behaves almost linearly up to strains of 60% (Yamada 1970). This partially explains the large range of stiffness reported in Table 2.3; the final stiffness differs substantially from the initial stiffness. The elastic modulus of the disc calculated from this graph is 5 MPa for compressive strains less than 10% and 2.5 MPa for tensile strains less than 40%.

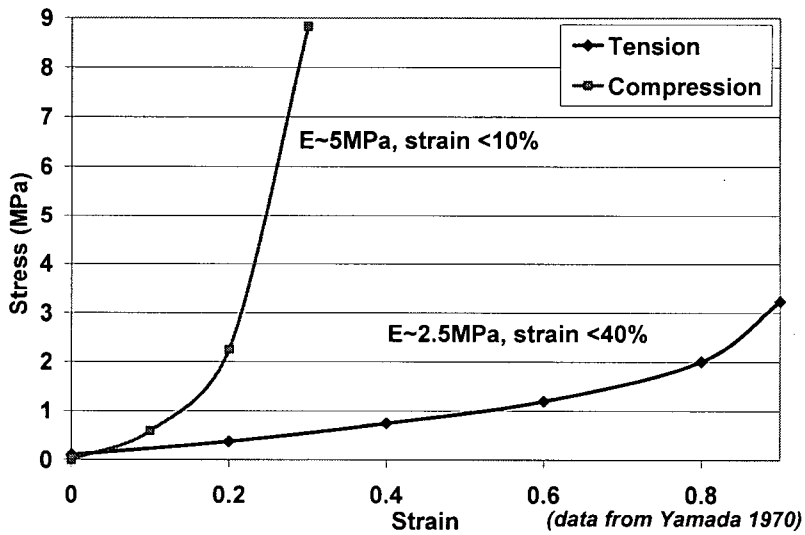

Figure 2.28: Stress-strain response of IV disc in tension and compression

Table 2.3: Stiffness and elastic modulus of IV discs

Reference	Level	Tension		Compression	
		N/mm	MPa	N/mm	MPa
(Brown, Hansen et al. 1957)	Lumbar	5.8 - 21.9	1.81*	83 - 1445, 2102 - 3504	1 – 18*, 26 - 44*
(Yamada 1970)	Cervical (tension)/ Lumbar (compression)		2.5		5 - 66
(Markolf 1972)	Thoracic/ Lumbar	700-1580	8.5 - 19.3*	1230 - 3320	15 - 40*
(Lin, Liu et al. 1978)	Lumbar			3400	14.8*
(Panjabi, Summers et al. 1986)	Cervical	53	0.95	140	2.53
(Moroney, Schultz et al. 1988)	Cervical			57 - 2060	5.52

**geometry was assumed from other studies to calculate the elastic modulus*

Complex FE studies of IV discs have modelled the disc as poroelastic (Lee, Kim et al. 2000), however it was considered appropriate for this study to model the IV discs as series of truss elements with linear response to loading. The disc modelled in this study was not meant to accurately model the kinematics of the spinal column. The elastic modulus was assigned a value of 3.4 MPa, which was in the range of published experimental values (Brown, Hansen et al. 1957; Yamada 1970; Markolf 1972; Lin, Liu et al. 1978; Panjabi, Summers et al. 1986; Moroney, Schultz et al. 1988). Furthermore, this value has been used in previous FE models of the spine (Yoganandan, Kumaresan et al. 1996; Voo, Kumaresan et al. 1997; Kumaresan, Yoganandan et al. 1999; Ng and Teo 2001).

2.2.6 Denticulate Ligaments

Denticulate ligaments are made up of pia-arachnoid tissue and are in the form of a ribbon. Microscopically, the ligaments consist of a rhomboid mesh of fibres (Breig 1960). The

denticulate ligament is a central bundle of collagen fibres wrapped with fine elastin fibres running principally parallel with the collagen fibres (Tunturi 1978). Similar to the dura mater, the elasticity of the dentate ligament for small loads is due to elastin fibres, whereas for large loads it is due to the central core of collagen fibres (Tunturi 1978).

The mechanical response of the denticulate ligament is not well known. One study reported the load-elongation response of the tissue loaded in increments by hanging weights (Tunturi 1978). Using this data and assuming a cross sectional area of 3 mm^2, the stress-strain response of the denticulate ligament was calculated (Figure 2.29). The elastic modulus of the modelled denticulate ligament was set at 5.8 MPa, which best represented the linear portion of the stress-strain curve.

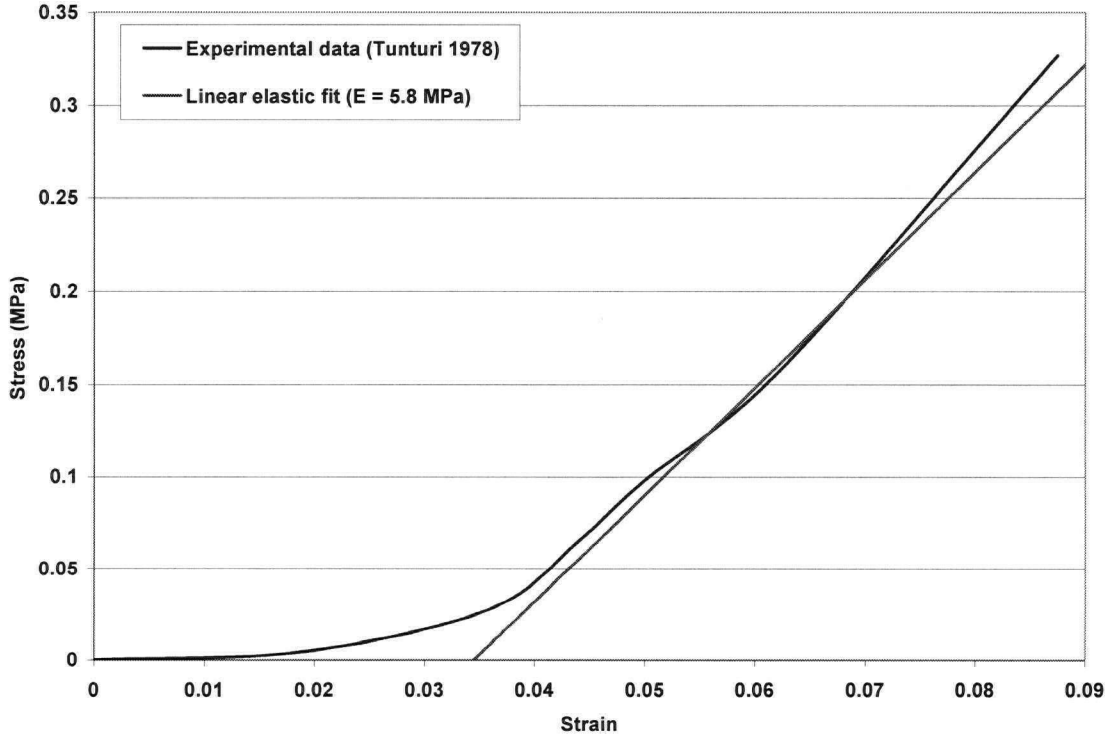

Figure 2.29: Stress-strain response of the denticulate ligament

2.2.7 Dural Attachments

Fibrous connections between the dura mater and the vertebral bodies have been described as extensions of the posterior longitudinal ligament (Hayashi, Yabuki et al. 1977; Kubo, Waga et al. 1994). Therefore, the elastic modulus of the dural attachments was assigned

a value equal to that of the PLL (36 MPa). No experimental studies of the mechanical behaviour of these attachments were found in the literature.

2.2.8 Summary

Material properties used in the model and references for these parameters are listed in Table 2.4.

Table 2.4: Mechanical properties of model components

Component	E (MPa)	ν	References
Vertebrae	10,000	0.29	(Yamada 1970; Evans 1973)
Spinal Cord	0.26	0.49	(Chang, Hung et al. 1981; Hung and Chang 1981; Hung, Chang et al. 1981; Hung, Chang et al. 1981; Chang, Hung et al. 1988)
Dura Mater	5	0.45	(van Noort, Black et al. 1981; Chang, Hung et al. 1988)
ALL	35.2	n/a	(Chazal, Tanguy et al. 1985; Przybylski, Carlin et al. 1996; Yoganandan, Kumaresan et al. 2000)
PLL	35.7	n/a	
JC	4.9	n/a	
LF	3.8	n/a	
ISL	5.0	n/a	
IV Disc	3.4	n/a	(Brown, Hansen et al. 1957; Markolf 1972; Lin, Liu et al. 1978; Panjabi, Summers et al. 1986; Moroney, Schultz et al. 1988)
Denticulate Ligament	5.8	n/a	(Tunturi 1978)
Dural Attachments	35.7	n/a	(Chazal, Tanguy et al. 1985; Przybylski, Carlin et al. 1996; Yoganandan, Kumaresan et al. 2000)

2.3 Loading and boundary conditions

2.3.1 Compression

A static compression experiment was simulated based on experimental work by Hung et al. (Hung, Lin et al. 1982). This experiment was performed on cats in the thoracic spine; however, the finite element model was of a human cervical spine. The elements, loading, and boundary conditions of the model are illustrated in Figure 2.30. The elements on the lamina and spinous process of the middle vertebrae (C5) were deleted, to simulate the effect of laminectomy (removal of the lamina) performed in the experiment. Furthermore, the interspinous ligament and ligamentum flavum were not included, since the lamina of C5 was removed. The nodes of the spinous processes of C4 and C6 were fixed in space (u_x, u_y, $u_z = 0$), since the upper and lower spinous processes were rigidly clamped in the experimental procedure as is typical in contusion experiments. A flat ended cylinder of diameter 12.1mm (100% of the spinal cord diameter) was created and placed posterior to the spinal cord and dura mater at the level of C5. This represented the indentor used in the experimental procedure, which was 100% of the cat spinal cord diameter. The indentor was meshed with brick elements (SOLID45) and was assigned material properties of polymethylmethacrylate (PMMA): Young's Modulus 2,800 MPa (Park and Lakes 1992), Poisson's ratio 0.35. Although the material of the indentor was not described for the validation experiment, others have reported using PMMA (Bresnahan, Beattie et al. 1987; Noyes 1987; Behrmann, Bresnahan et al. 1992). The indentor was rotated 10^0 in the sagittal plane to be aligned with the edge of the spinal cord at the C5 level. This angle was due to the lordotic curvature of the spine at this level. A local co-ordinate system was also set up to describe forces and displacements in terms of this orientation.

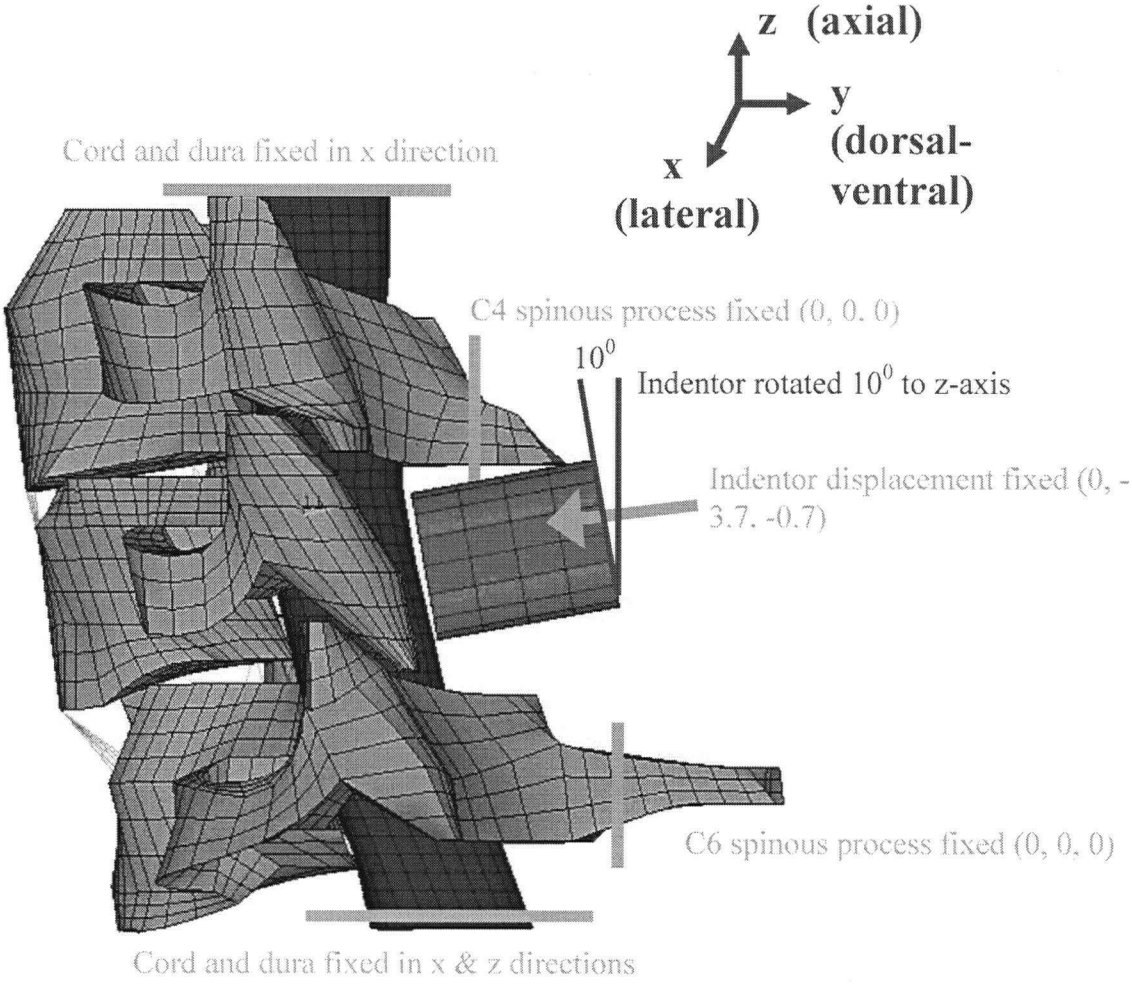

Figure 2.30: Spinal cord compression loading and boundary conditions

Three-dimensional contact elements were created for several groups of contacting structures (Table 2.5). These contact and target elements overlaid the solid elements describing the boundary of the contact set. For each group of contacting surfaces, a target and a contact surface were required. The shell elements were set to be the contact elements and included shell thickness effects. For the contact elements, a normal stiffness was set to account for the effect of fat and CSF in the connecting spaces. The normal stiffness was set at 0.02 (relative to the stiffness of the underlying element). The effect created was that the contacted element started to move before contact was achieved with the target element. Furthermore, an allowable penetration tolerance of 0.08 (relative to the size of the underlying element) was set for the calculation.

Table 2.5: Ansys contact element sets for compressive injury model

Contact Element Set	Target Elements (TARGE170)	Contact Elements (CONTA173)
1	Anterior indentor	Posterior dura mater
2	Posterior spinal cord	Posterior dura mater
3	Anterior spinal cord	Anterior dura mater
4	Posterior vertebral bodies	Anterior dura mater

All nodes of the indentor were set to displace anteriorly, along the local co-ordinate system, so that the cord was compressed perpendicular to its axial direction at the level of compression. A static displacement of 3.8 mm was set for the indentor. This value was selected in order to result in compression of the spinal cord and to reproduce the experimental data available in the literature (Figure 2.31) (Hung, Lin et al. 1982). Although a 1.1 mm compression was desired for the human cord (12% of the anterior-posterior dimension of the cord), a 3.8 mm displacement was set for the indentor to account for spaces between the contacting elements. The nodes at the inferior end of the spinal cord and dura mater were also fixed in space in the lateral and inferior-superior directions (u_x, $u_z = 0$) to prevent rigid body motion in the model. The nodes at the superior end of the spinal cord and dura mater were fixed in space in the lateral direction ($u_x = 0$) to prevent sideways slipping of the spinal cord in the canal.

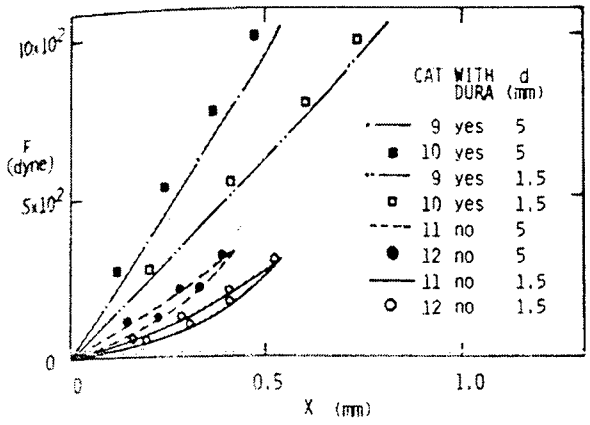

Figure 2.31: Force vs. deformation relationships for static compression of cat spinal cords (Figure from Hung, Lin et al. 1982). Comparison of elastic behaviour of cord with and without dura mater intact (d: diameter of indentor).

The parameter for validation was the reaction force at the indentor, which was measured in a previous experimental study (Hung, Lin et al. 1982) and corresponded to other reports of cord compression (Hung, Lin et al. 1979).

The size of the indentor, spinal cord compression depth, and reaction force at the indentor were scaled to represent an experimental spinal cord compression in a human model. The size of the indentor was scaled to the lateral dimension of the spinal cord at the level of compression. The indentor diameter used for the animal study was 5 mm (Cat 9 and 10 in Figure 2.31), which was also the lateral dimension of the cat spinal cord. Therefore, the size of the indentor for the human FE model was set to 12 mm (the lateral dimension of the human cord at the cervical level).

The compression depth was scaled to the anterior-posterior dimension of the spinal cord; therefore the compression represented an equal amount of strain in the anterior-posterior direction. The compression depth was scaled as follows:

$$\frac{\Delta d_{cat}}{D_{cat}} = \frac{\Delta d_{human}}{D_{human}}$$

where

Δd_{cat} is the displacement of the cat indentor (0.5 mm: cat 9 and 10 in Figure 2.31)

D_{cat} is the antero-posterior dimension of the cat cord at T10 (4.0 mm)

D_{human} is the antero-posterior dimension of the human cord at the C5 level (8.6 mm)

Δd_{human} is the displacement of the human indentor = 1.1 mm

The reaction force was scaled to the area of the indentor tip; therefore the compression represented an equal amount of stress in the anterior-posterior direction. The reaction force was scaled as follows:

$$\frac{F_{cat}}{A_{cat}} = \frac{F_{human}}{A_{human}}$$

where

F_{cat} is the reaction force at the cat indentor tip (0.0094 N: cat 9 and 10 in Figure 2.31)

A_{cat} is the area of the cat indentor tip (19.6 mm^2)

A_{human} is the area of the human indentor tip (113.1 mm^2)

F_{human} is the reaction force at the human indentor tip = 0.054 N

The experimental and scaled data are summarized in Table 2.6.

Table 2.6: In vivo validation data for compression injury mechanism

Cat (experimental)		Human (scaled from experimental)	
Force (N)	Displacement (mm)	Force (N)	Displacement (mm)
0.0094	0.5	0.054	1.1

A second experimental study (Tencer, Allen et al. 1985) provided validation data for an in vitro study of compression on human cadaver specimens. In this study, a tube mounted into the dura was filled with water to simulate the effect of CSF pressure, and forces were measured using a load cell. Although the FE model was not loaded to simulate this experiment, the results provide further insight into the mechanics of cord-column interactions in the human anatomy. This study demonstrated the relationship between contact force and percent canal occlusion for anterior compression tests (Figure 2.32).

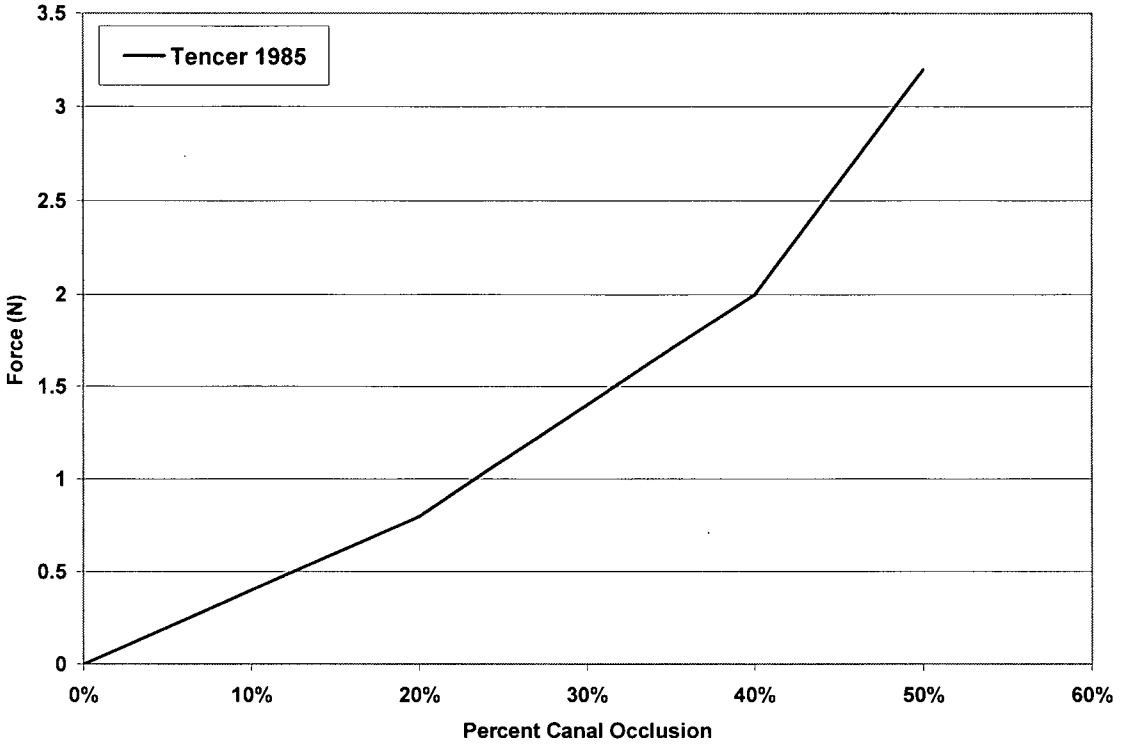

Figure 2.32: In vitro validation data for compression injury mechanism (Tencer, Allen et al. 1985)

2.3.2 Distraction

A static distraction experiment was simulated based on experimental work by Maiman et al. (Maiman, Coats et al. 1989). Nodes of the C4 vertebra, the top of the cord, and the top of the dura mater were fixed in space (u_x, u_y, $u_z = 0$), while inferior displacements were set on the nodes of the C6 vertebra, the bottom of the cord, and the bottom of the dura mater (Figure 2.33). The inferior displacements acted along the axial direction of the spinal cord at the bottom of the model, which had a angle of 21.5^0 to the z-axis. The values of the inferior displacements were based on the previous experimental work.

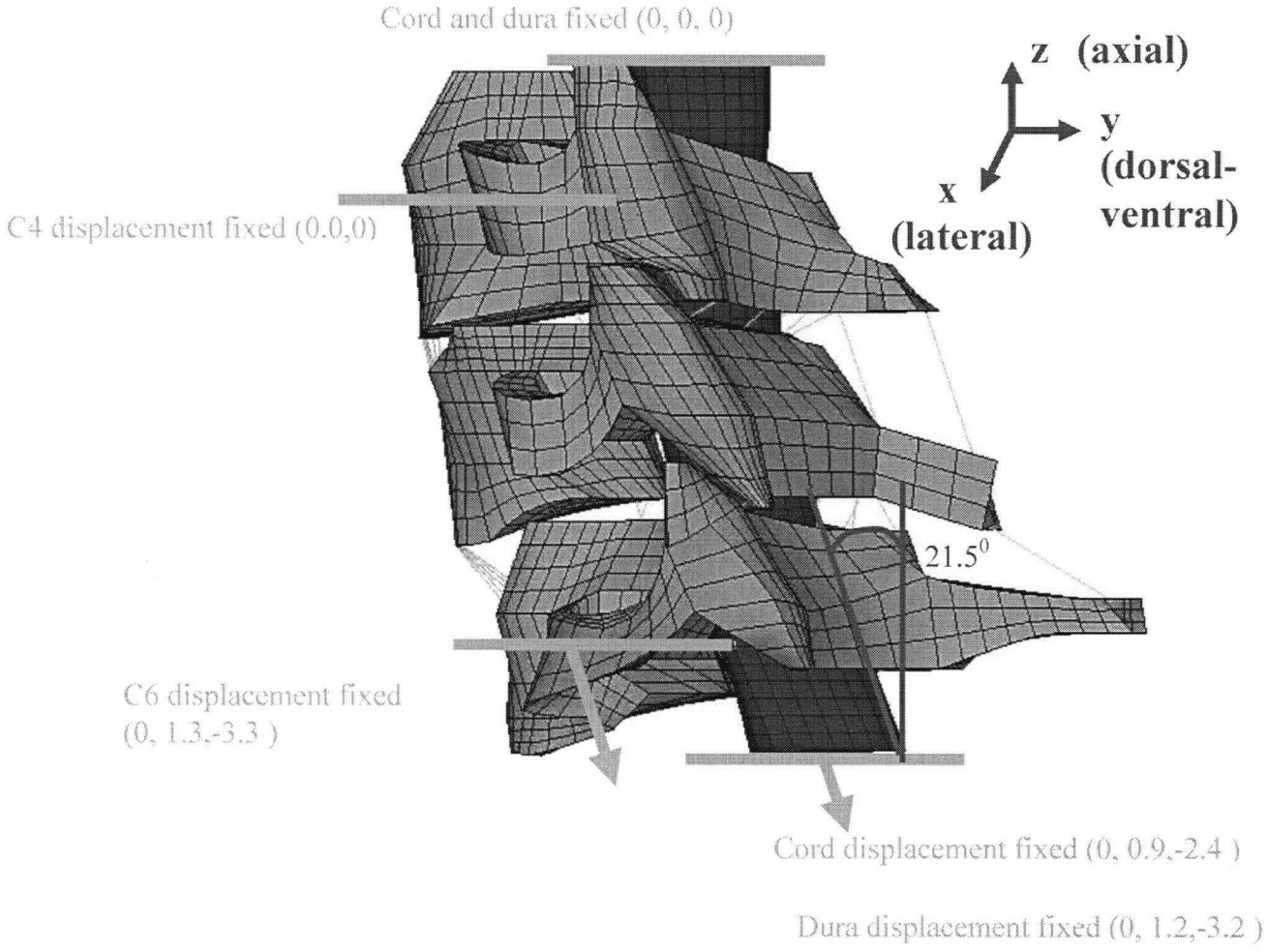

Figure 2.33: Spinal cord distraction loading and boundary conditions

The modelled distraction injury simulated experiments previously performed on cats and reported by Maiman et al. (Maiman, Coats et al. 1989). The experiment involved fixing the head and applying traction to the pelvis, thus distracting the spinal cord through the skin and vertebral column. This was the only published experimental work to report displacements of the vertebrae and spinal cord (measured by radiopaque markers) in traction. Forces were also listed, however these forces were applied to the surface of the animal, not the vertebrae; therefore they were not useful in the validation of this model. In the animal model of distraction, C4, C5, and C6 each displaced downwards; however, since only three vertebrae were included in the model, one side of the model was fixed while the other was set to displace inferiorly.

The translation of experimental distractions to model boundary conditions are illustrated in Figure 2.34. This was necessary since the experiment distracted the entire spinal

column; all three modelled vertebrae were displaced experimentally. For loading and boundary conditions of a finite element model, some components must remain fixed. The inferior displacement of C6 was set as the summation of the experimental displacements of segments C45 and C56 (3.6 mm). The inferior displacement of the spinal cord was set as the summation of the experimental displacements of cord segments C45 and C56 as well as half of the displacements of C34 and C67 (2.6 mm). The addition of half the C34 and C67 displacements was because, presumably, cord displacements were measured from vertebral body centre to vertebral body centre. Superiorly, the finite element model included the spinal cord above the vertebral body of C4, approximately halfway to the vertebral body centre of C3. Inferiorly, the model included the spinal cord below the vertebral body of C6, approximately halfway to the vertebral body centre of C7. Therefore, half of the adjoining spinal cord displacements were added to the displacement boundary condition at the bottom end of the spinal cord. The model was validated by comparing the C5 vertebral body displacement, as well as C45 and C56 spinal cord displacements.

Validation of the distraction injury mechanism was not scaled from the animal model, since relative displacements of the vertebrae and spinal cord were compared. It was therefore assumed that cats and humans have similar connecting ligaments between the vertebrae, dura mater, and spinal cord.

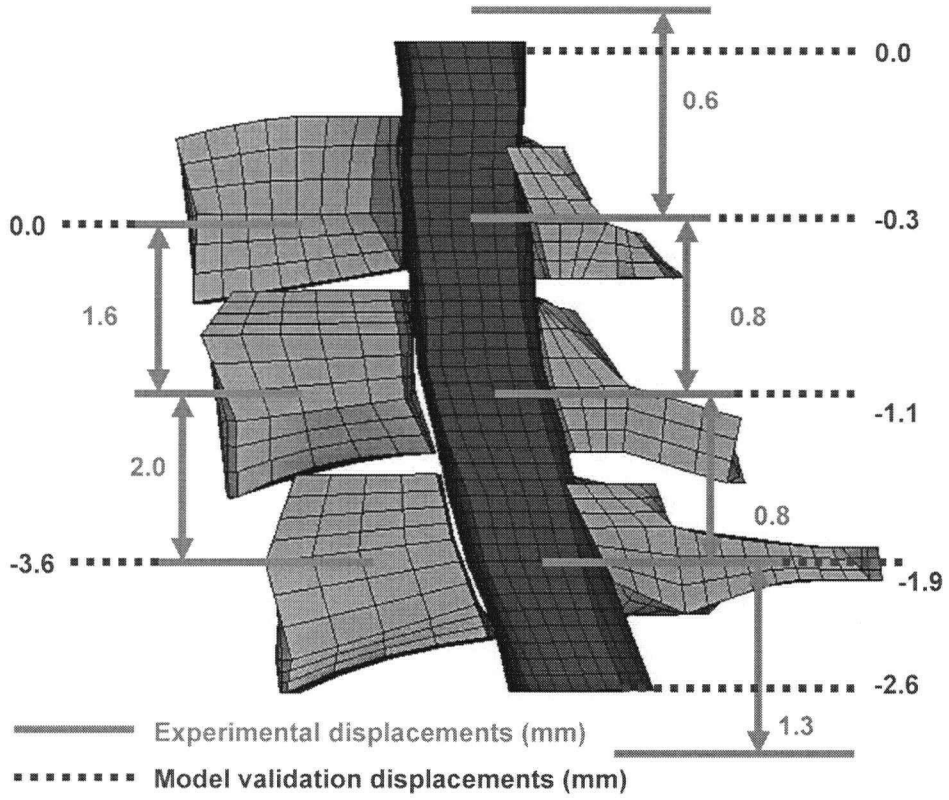

Figure 2.34: Spinal cord distraction - experimental and model validation displacements (Maiman, Coats et al. 1989)

Contact element sets were assigned in the distraction model, similar to those in the compression model (Table 2.7).

Table 2.7: Ansys contact element sets for distractive injury model

Contact Element Set	Target Elements (TARGE170)	Contact Elements (CONTA173)
1	Anterior Lamina & spinous processes	Posterior dura mater
2	Posterior spinal cord	Posterior dura mater
3	Anterior spinal cord	Anterior dura mater
4	Posterior vertebral bodies	Anterior dura mater

2.3.3 Dislocation

There is currently no validation data available in the literature for dislocation of the vertebral canal, containing the spinal cord. For ease of modelling, elements of the superior facets of the C6 vertebrae were deleted, since this contact would add substantial computational time (Figure 2.35). The nodes of the C6 vertebrae were fixed in space (u_x, u_y, $u_z = 0$) while those of the C5 vertebrae were set to displace 4 mm in the anterior direction. This displacement was set arbitrarily to evaluate the strain distribution in the spinal cord for a dislocation injury. The bottom nodes of the spinal cord and dura mater were fixed in space (u_x, u_y, $u_z = 0$) to prevent rigid body motion in the model. Contact elements sets in this simulation were the same as for the distraction model (Table 2.7).

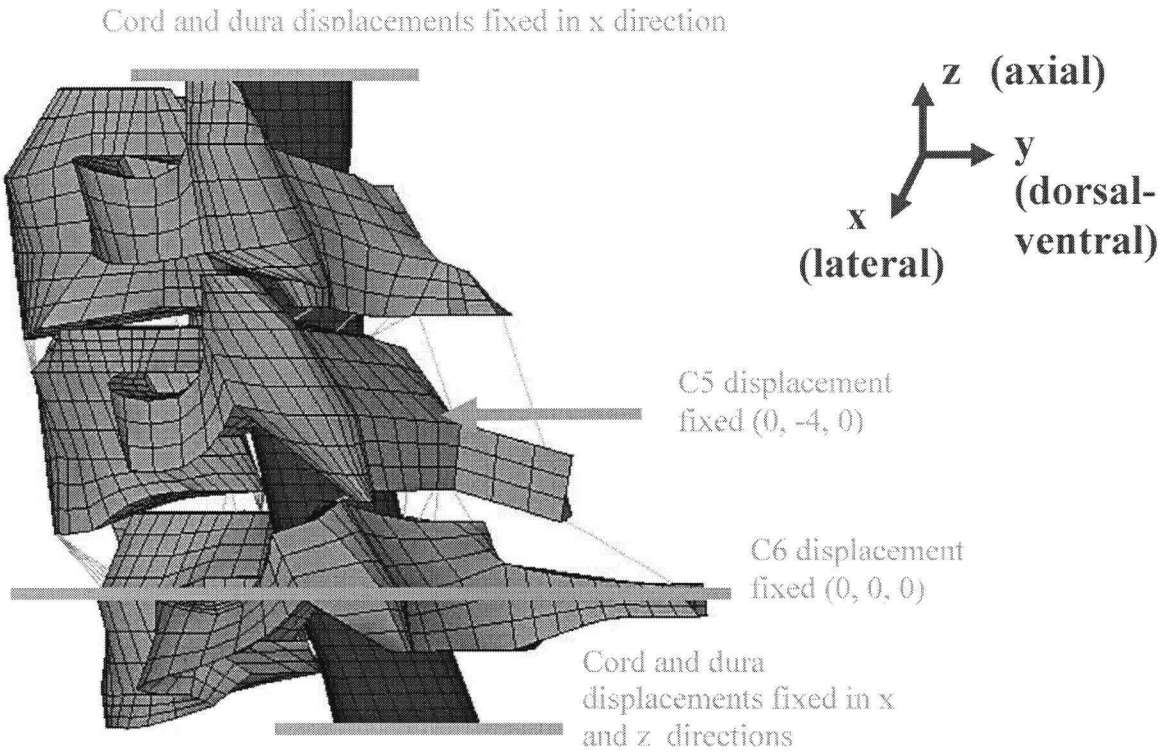

Figure 2.35: Spinal cord dislocation – model loading and boundary conditions

2.3.4 *Hyperelastic Material Modelling*

In order to investigate the effect of constitutive model on the strain distribution throughout the spinal cord, simple distraction of the cord alone was modelled. Due to the simplicity of this case, no contact elements were required. Sample loading and boundary conditions for one of the loading cases are illustrated in Figure 2.36 .

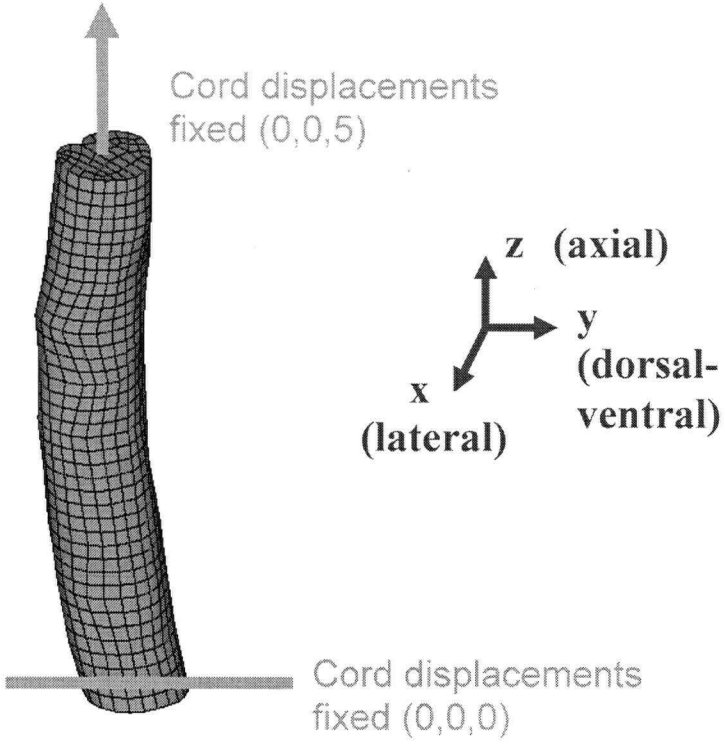

Figure 2.36: Loading and boundary conditions for hyperelastic material modelling

Four loading scenarios were applied to the cord and are listed in Table 2.8. The first level of distraction (2.6 mm) was selected to represent that applied in the linear elastic model with the vertebrae, dura mater, and connecting ligaments. The subsequent distraction levels (5, 10, and 20 mm) were selected to represent a continuum of strains in order to determine the effect of constitutive model for varying strains. Since the spinal cord segment was 60 mm in length, these distraction levels corresponded to mean axial strains of 4 to 33%.

Table 2.8: Loading scenario summary for constitutive model comparison

Material Model	Distraction (mm)			
Linear Elastic	2.6	5	10	20
Hyperelastic	2.6	5	10	20

2.4 Model Summary

The number of elements and degrees of freedom (DOF) in the model are given in Table 2.9. The compression model had the most degrees of freedom, since most of the vertebrae were free to move.

Table 2.9: Summary of elements in the finite element model

Component	# Elements		
	Compression	Distraction	Dislocation
C4-6	5,199	5,496	5,271
Contact Elements	2,573	2,388	3,364
Spinal Cord	1,920	1,920	1,920
Dura Mater	1,120	1,120	1,120
Indentor	132	n/a	n/a
Denticulate Ligament	50	50	50
Spinal Ligaments	28	44	44
Dural Attachments	24	24	24
IV Discs	8	8	8
Total	11,054	11,050	11,801
DOF	36,279	22,395	34,914

2.5 Organization of Results

2.5.1 Mean Column Strains

In order to compare strain distributions in the spinal cord for the three injury mechanisms, the nodes were arranged into four columns: dorsal, ventral, central, left lateral and right lateral (Figure 2.37). This allowed four mean strains to be computed at each caudal-cranial level of the spinal cord. To calculate these mean strains, two Matlab programs

were written. The first program used nodal x, y, z data at each axial level (exported from Ansys) to divide the cord into the four columns. The second program sorted strain results calculated by Ansys into the various columns by using the nodal numbers. These programs are provided in Appendix C. Clinically, tracts of neurons in the spinal cord are described as being in one of these columns. Furthermore, results of animal models may describe damage as being in one of these columns.

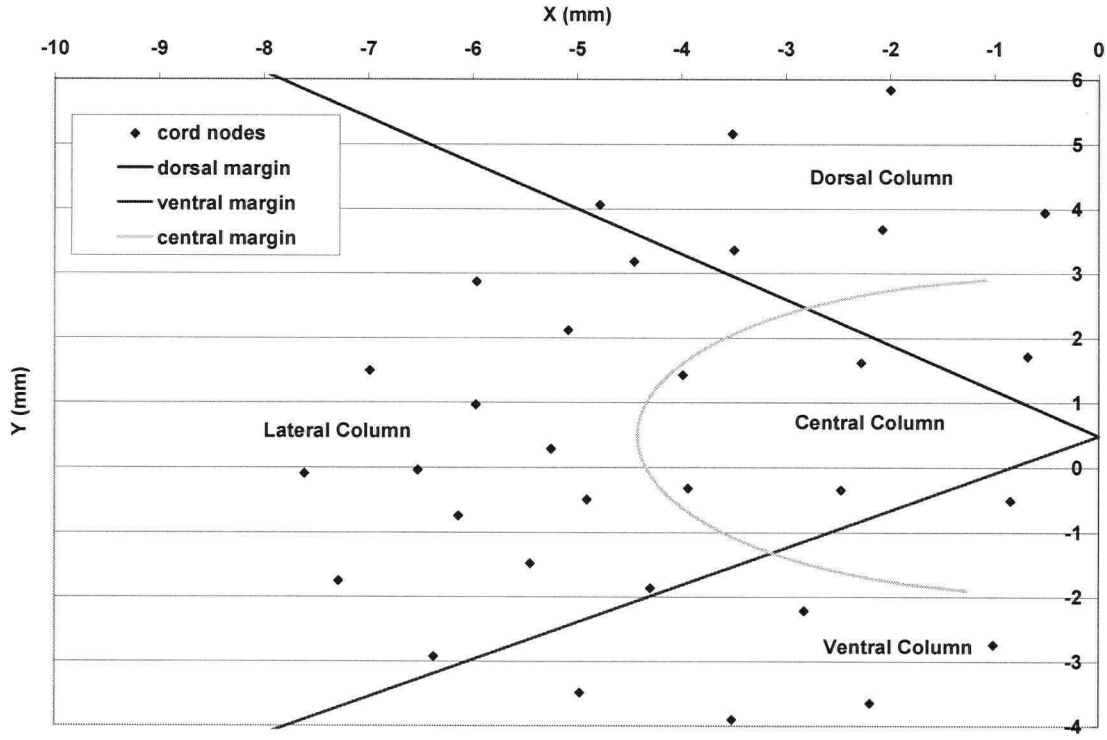

Figure 2.37: Transverse section of cord nodes on the left side showing the arrangement of nodal results into mean column strains

2.5.2 Strains Examined

Due to the longitudinal nature of axons, it is of primary interest to compare the components of strain. Strain components described were: lateral (x-direction), anteroposterior (y-direction), axial (z-direction), transverse shear (xy-plane), sagittal shear strain (yz-plane), and coronal shear strain (xz-plane) (Figure 2.38). For compression, a local axis was set with the y-direction along the indenting direction (Figure 2.38). For distraction, a local axis was set with the z-direction along the inferior

edge of the spinal cord to set the inferior distraction displacement along this direction (Figure 2.38). No local axes were set for dislocation; the global axis was used to describe strain results in dislocation. Strain results were described in terms the local axes for compression and distraction.

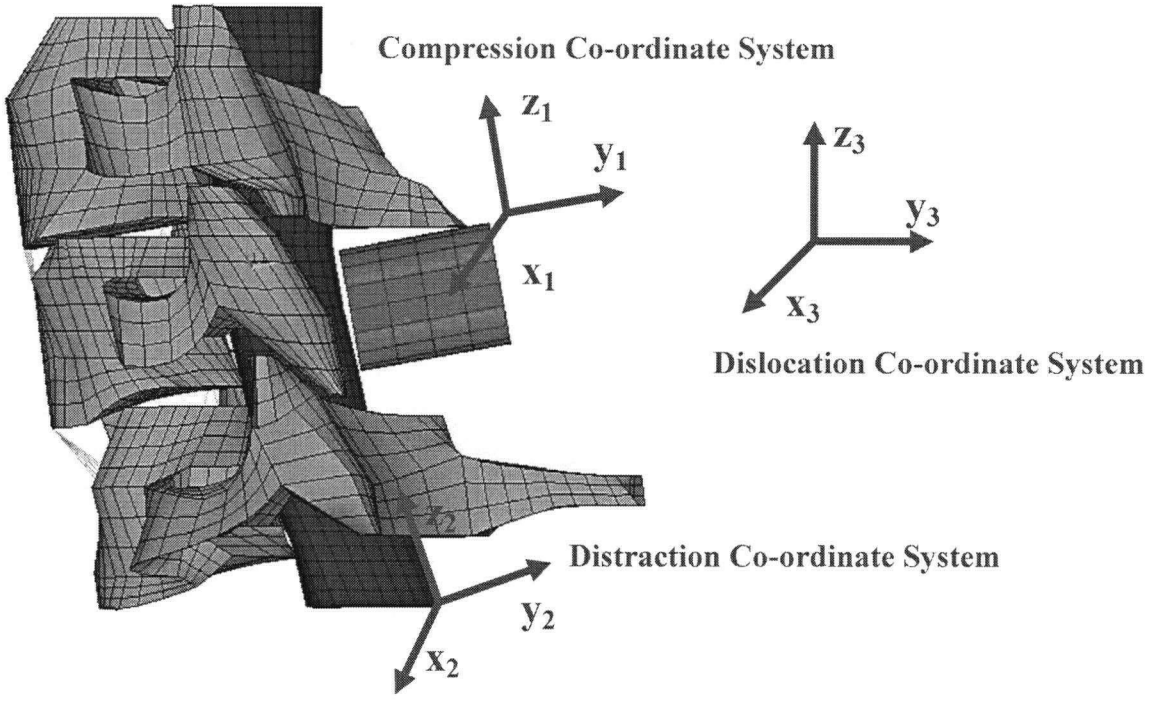

Figure 2.38: Local axes used in FE model

The von-Mises criterion, also known as maximum distortion energy theory defines failure in terms of the principal stresses (σ_1, σ_2, σ_3) and a yield stress determined from a simple tension test (σ_{yp}). Failure is defined as

$$(\sigma_1 - \sigma_2)^2 + (\sigma_2 - \sigma_3)^2 + (\sigma_3 - \sigma_1)^2 = 2\sigma_{yp}^2$$

or, alternatively,

$$\left(\frac{\sigma_1}{\sigma_{yp}}\right)^2 + \left(\frac{\sigma_2}{\sigma_{yp}}\right)^2 + \left(\frac{\sigma_3}{\sigma_{yp}}\right)^2 - \left(\frac{\sigma_1}{\sigma_{yp}}\right)\left(\frac{\sigma_2}{\sigma_{yp}}\right) - \left(\frac{\sigma_2}{\sigma_{yp}}\right)\left(\frac{\sigma_3}{\sigma_{yp}}\right) - \left(\frac{\sigma_3}{\sigma_{yp}}\right)\left(\frac{\sigma_1}{\sigma_{yp}}\right) = 1$$

The equivalent von-Mises stress may be defined therefore as

$$\sigma_e = \sigma_{yp} = \sqrt{\frac{(\sigma_1 - \sigma_2)^2 + (\sigma_2 - \sigma_3)^2 + (\sigma_3 - \sigma_1)^2}{2}}$$

This failure criteria is useful in situations involving ductile materials and plane stress; consequently, it is commonly used in design (Ugural and Fenster 1995). In biomechanics, the von-Mises strain criterion has accurately predicted in vitro failure data of cortical bone (Lotz, Cheal et al. 1991). For this finite element study, equivalent von-Mises strains were compared between the loading cases.

3 Results

A finite element model of the spinal cord and the surrounding structures was developed and validated based on experimental data. Strain distributions in the spinal cord were compared for three injury mechanisms: compression, distraction, and dislocation.

3.1 Validation of Finite Element Model

3.1.1 Compression

An experimentally produced compression injury to the spinal cord was simulated through finite element modelling. The anterior displacement of the indentor in the FE model caused the dura mater and the spinal cord to displace anteriorly, until contact was achieved with the posterior aspect of the C5 vertebral body. Displacement of the C5 vertebral body was less than 0.02 mm in the anterior direction (Figure 3.1).

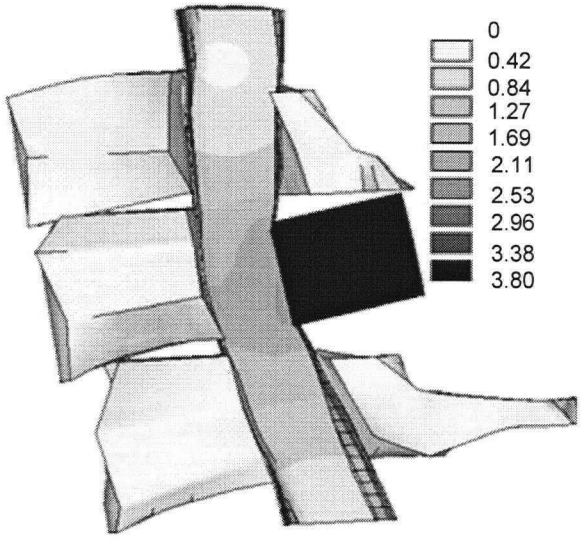

Figure 3.1: Mid-sagittal view of the total displacement in spinal cord compression [mm]

Although the indentor displacement was set at 3.8 mm, the spinal cord was compressed less than this distance due to spaces between the vertebral canal, dura mater, and the spinal cord. The indentor displaced 3.8 mm anteriorly, which resulted in a maximum displacement of 3.6 mm of the posterior aspect of the dura mater (due to an initial space between the two surfaces). The amount of spinal cord compression varied along the length of the spinal cord under the indentor, due to variations in the profile of the posterior aspect of the C5 vertebral body. Although the posterior aspect of the spinal cord displaced a maximum of 2.1 mm, the anterior aspect of the spinal cord displaced between 0.5 and 1.6 mm (Figure 3.2). The average spinal cord compression at the level of the indentor was 1.0 mm.

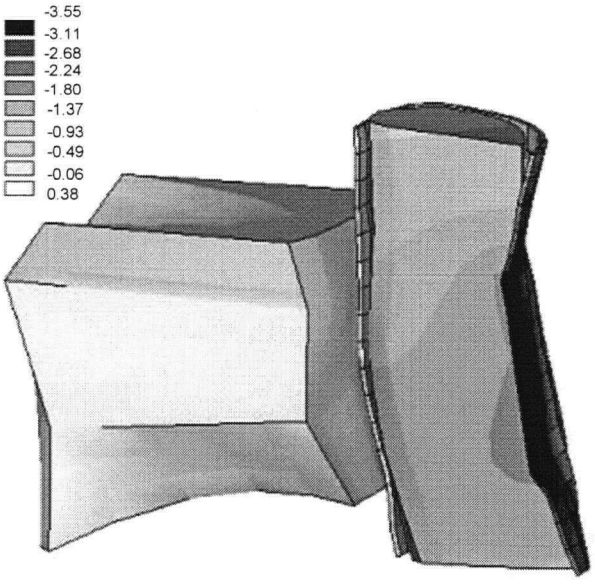

Figure 3.2: Displacement in the local anterior-posterior direction in spinal cord contusion [mm]

Although nodes of the spinal cord at the inferior and superior ends of the model were fixed in the lateral direction (u_x = 0), the spinal cord at the level of compression displaced 0.75 mm to one side. This was because symmetry was not assumed in the replication of anatomy or in constraints on the motion of the cord.

The FE model was validated by comparison of the reaction force at the indentor tip to experimental results. The model produced higher forces than those expected from the animal in vivo experimental results (Table 3.1).

Table 3.1: Comparison of reaction force at the indentor tip for a compression injury: FE results and an in vivo model

Source		**Dura displacement (mm)**	**Cord compression (mm)**	**Force (N)**
(Hung, Lin et al. 1982)			1.1	0.054
FE Results	Simulation 2	0.3	0	8 e -4
	Simulation 3	1.3	0	0.01
	Simulation 4	2.6	0.45	0.3
	Simulation 1	3.6	1.0	2.1

The force from simulation 1 was expected to correspond to the experimental force; however it was two orders of magnitude greater than the experimental force. Several other indentor displacements were simulated to investigate this difference (simulations 2-4). Although the experimental model of injury included the dura mater, it was not clear how cord compressions were measured or calculated from the dura displacements. It is possible that dura displacements were assumed to equal the cord compressions. If the

reported cord compressions were assumed to be equal to the dura displacements, the results from the additional FE simulations corresponded to experimental results (Figure 3.3). The reaction force calculated by the FE model was nonlinear with an increase in dura displacement because several stages of loading occurred. First, the dura contacted the indentor and moved as a solid body before coming into contact with the anterior aspect of the canal. Second, the dura became compressed which caused rigid body motion of the cord in the canal. Third, once the cord contacted the anterior aspect of the canal, spinal cord compression began.

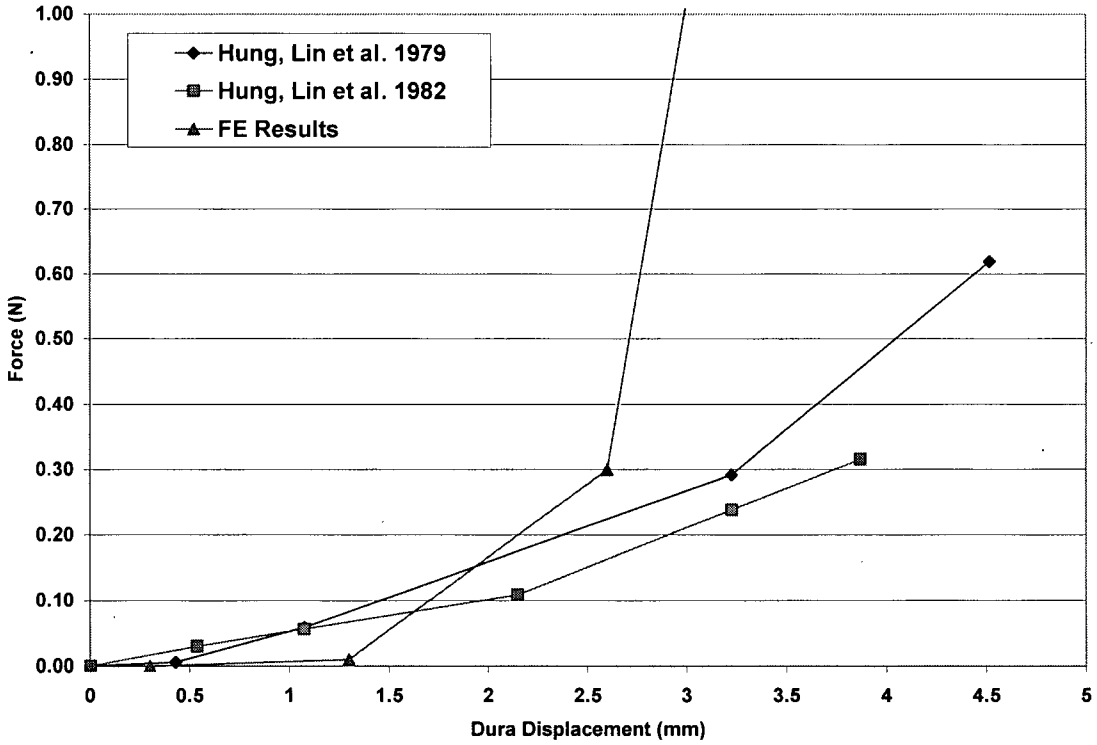

Figure 3.3: Comparison of reaction force at indentor tip for compression injury: FE results and in vivo models - Assumed the experimental cord compression equals the dura displacement

The first simulation, which compressed the cord 1.0 mm, corresponded to a 33% canal occlusion. The calculated reaction force at this level of compression correlated well to experimental results from the human in vitro study (Figure 3.4). Reaction forces for the other simulations were slightly low, but within the range of forces presented for the cadaver study (Tencer, Allen et al. 1985).

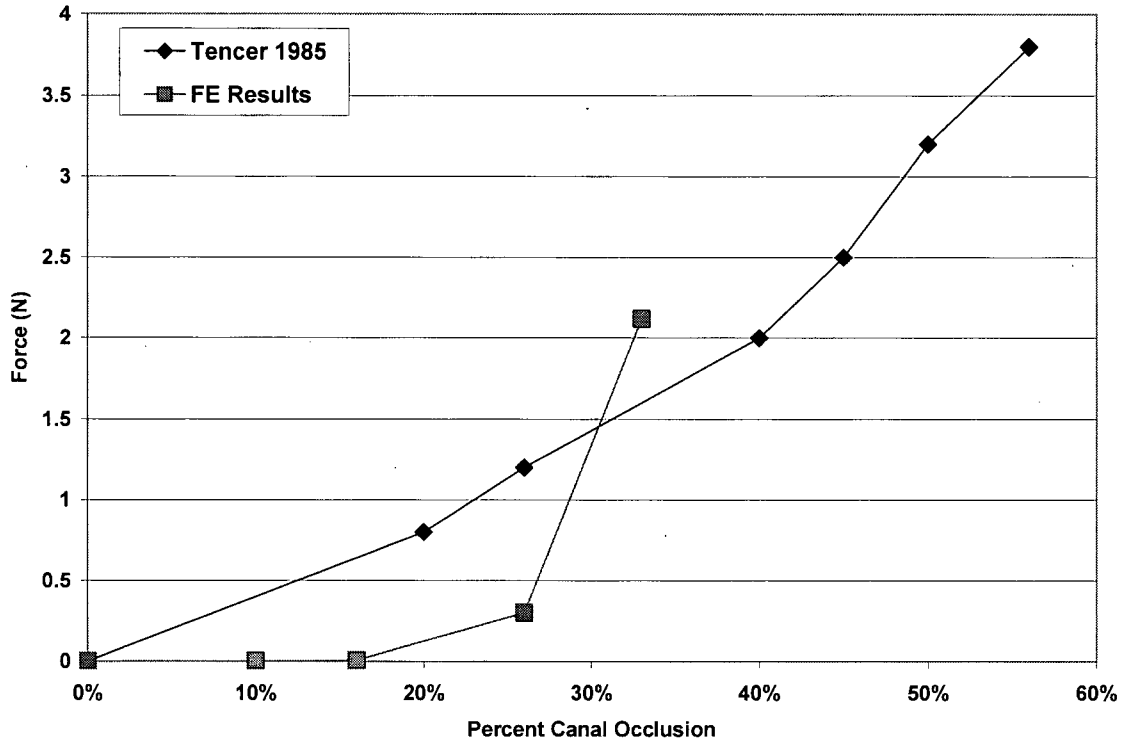

Figure 3.4: Comparison of reaction force at indentor tip for compression injury: FE results and an in vitro model (Tencer, Allen et al. 1985)

3.1.2 Distraction

An experimentally produced distraction injury to the spinal cord was simulated through finite element modelling. The inferior displacement of the C6 vertebra, along the angle made by the inferior aspect of the spinal cord, caused the C5 vertebra to displace inferiorly and the intervertebral spaces to open; the spinous process of C5 displaced more than the vertebral body (Figure 3.5). The spinal cord and dura mater were stretched and pulled out of the lordotic curvature of the spinal canal (Figure 3.6).

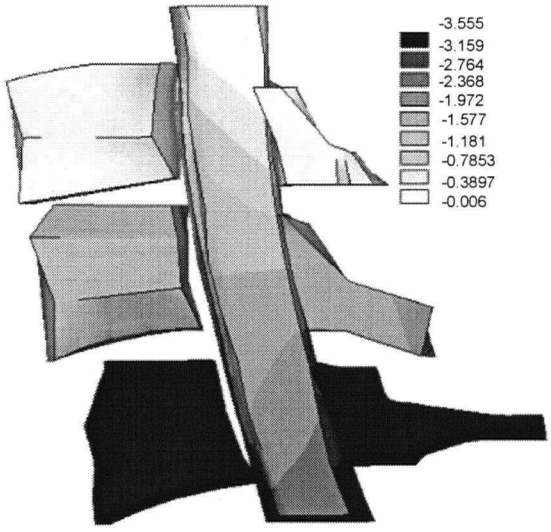

Figure 3.5: Inferior displacements (local axis) in a spinal cord injury produced by distraction [mm]

The displacements of the C5 vertebral body and the spinal cord calculated from the model correlated well to those from the experimental study (Table 3.2). The C4 and C6 vertebral displacements were imposed as nodal displacements. The C5 vertebral displacement was 0.15 mm less than the experimental displacement, which represents a 10% error. The spinal cord displacements at the superior edge of C4 and the inferior edge of C6 (the boundaries of the model) were imposed as nodal displacements. The intermediate spinal cord displacements at the centres of the C4, 5, and 6 vertebral bodies correlated well to those found experimentally (Figure 3.7). The spinal cord displacements were closest to the experimental values near the boundaries of the model (Figure 3.7), with the greatest difference at the centre of C5 (0.40 mm). Overall, the displacements were within an acceptable range.

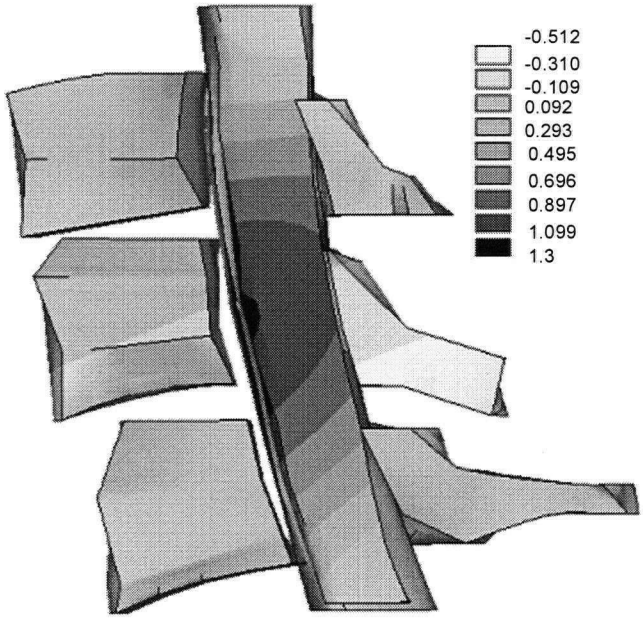

Figure 3.6: Anterior-posterior displacements (local axis) in a spinal cord injury produced by distraction [mm]

Table 3.2: Experimental and calculated vertebral and spinal cord displacements (Maiman, Coats et al. 1989)

Axial Location	Vertebral Displacements (mm)		Spinal Cord Displacements (mm)	
	Experimental	Model	Experimental	Model
C4 superior edge			0	0
C4 centre	0	0	-0.31	-0.56
C5 centre	-1.55	-1.4	-1.08	-1.48
C6 centre	-3.55	-3.55	-1.92	-2.12
C6 inferior edge			-2.55	-2.55

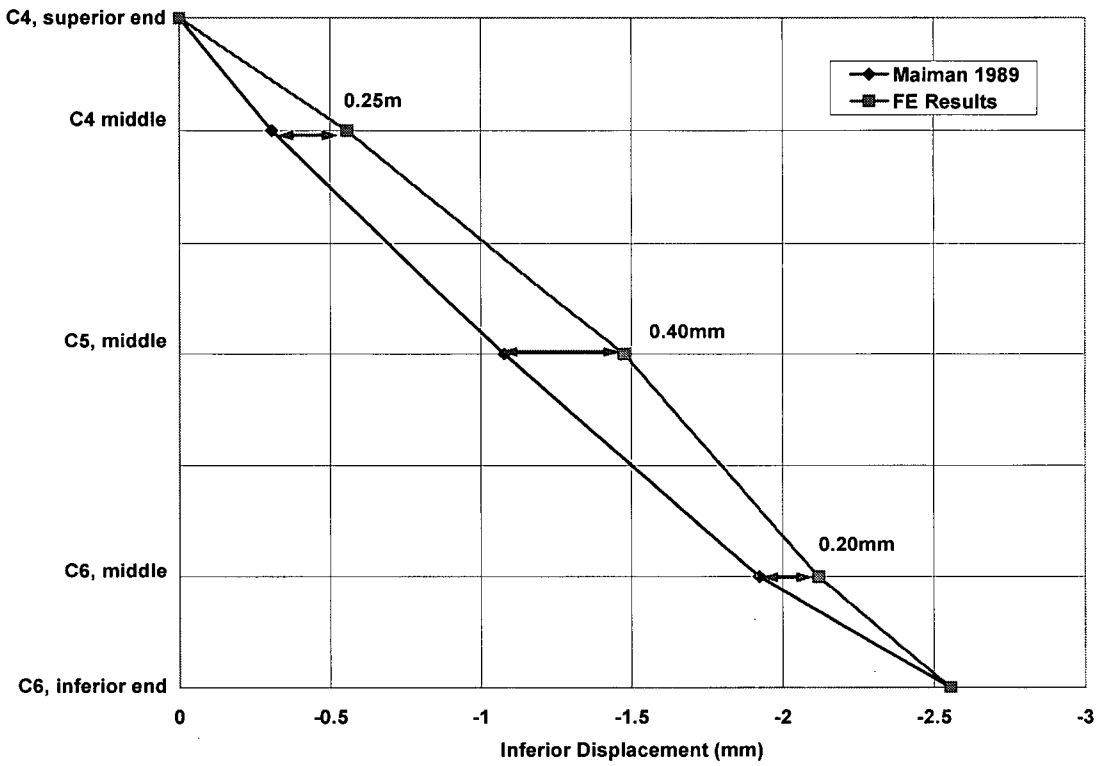

Figure 3.7: Comparison of experimental and simulated spinal cord displacements

3.1.3 Dislocation

An experimentally produced dislocation injury to the spinal cord was simulated through finite element modelling. The anterior displacement of the C5 vertebra caused the lamina of C5 and the vertebral body of C6 to contact the dura mater and compress the spinal cord (Figure 3.8). The C4 vertebra displaced with C5, since its motion was not restricted.

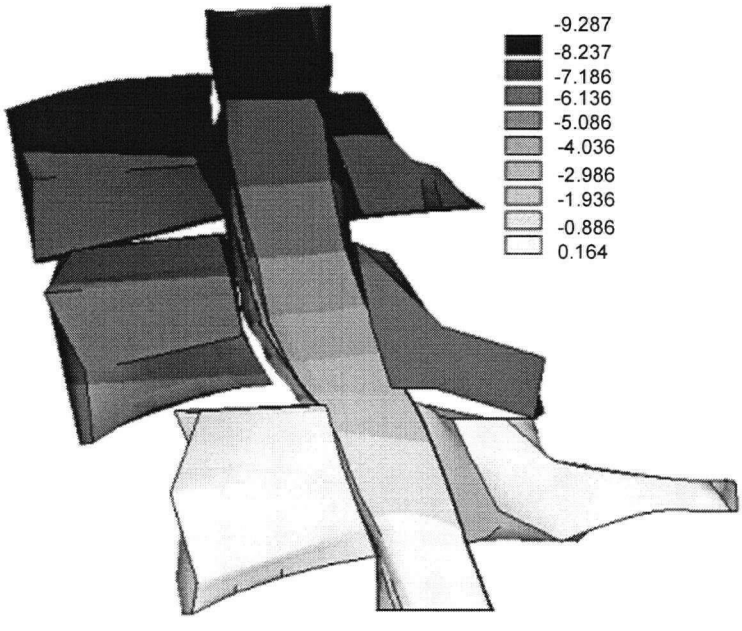

Figure 3.8: Mid-sagittal view of anterior-posterior displacements for a dislocation injury [mm]

There was no validation data available for the dislocation injury mode, as this method of producing spinal cord injuries is not currently in practice.

3.2 Comparison of Strain Distributions

Mean and maximum absolute strains for the five columns (ventral, dorsal, central, left lateral, and right lateral) at each axial level were calculated. The mean strains show the general distribution of strain, while maximum absolute strains provide critical points in the model.

3.2.1 Dorsal-Ventral Strain

Critical points for dorsal-ventral strain in the modelled compression injury were the dorsal column at the cranial edge of the indentor, and the ventral column at the caudal edge of the C5 vertebral body (Figure 3.9). The maximum mean and absolute strains in the dorsal-ventral direction for the modelled compression injury were 10 and 22%, respectively, in the dorsal columns at the cranial tip of the indentor (Figure 3.10). The strains at the caudal 10 mm of the cord were not included since boundary conditions at this end resulted in artefact strains. The two peaks in dorsal-ventral compressive strains resulted from two distinct compression points in the cord: between the cranial and caudal edges of the indentor and the C5 vertebral body. The central and ventral columns were also compressed at the level of the indentor with maximum mean dorsal-ventral strains of 9 and 8%, respectively. The lateral columns had the lowest peak mean dorsal-ventral compressive strains, which were 2 and 3%. The right lateral column was more compressed than the left lateral column due to the asymmetry of the compression injury.

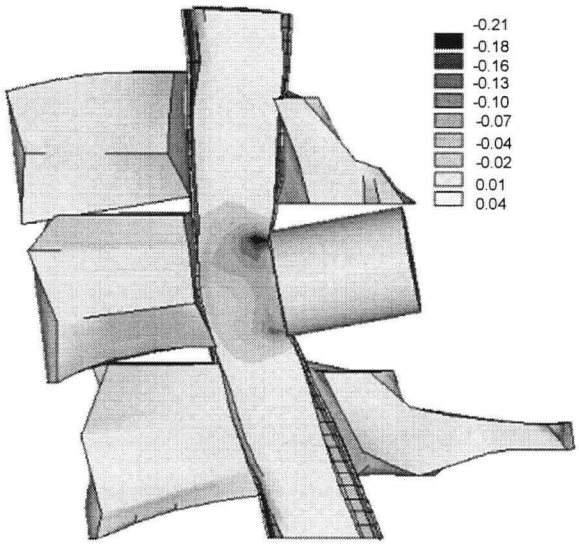

Figure 3.9: Mid-sagittal view of the dorsal-ventral strain for a compression injury

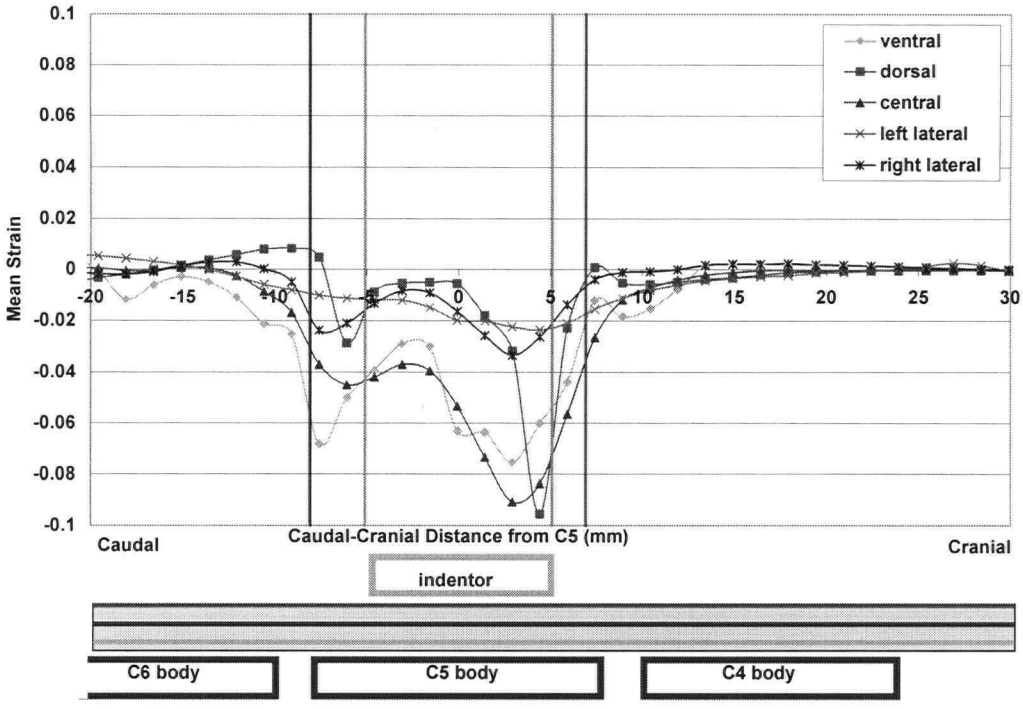

Figure 3.10: Mean dorsal-ventral strain as a function of axial distance from C5 (mm) for a compression injury

The critical region for dorsal-ventral strain in the modelled distraction injury was in the dorsal column at the level of C5, where the peak mean dorsal-ventral compressive strain was 3% (Figures 3.11 and 3.12). The dorsal column was on the concave aspect of the initial curvature of the cord, which was reduced by distraction. The strains at the ends of the model (caudal and cranial 10 mm of the model) were not included since they represent artefacts due to the boundary conditions applied at the ends of the spinal cord. The peak mean strains in the other columns were between 1.6 and 2.0%; dorsal-ventral strains were evenly distributed between columns in distraction injury.

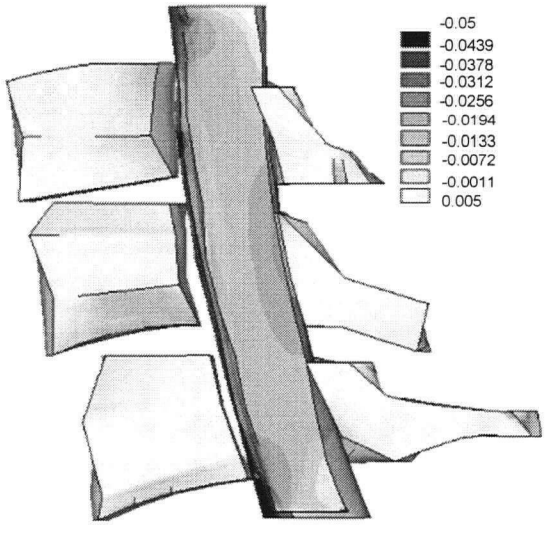

Figure 3.11: Mid-sagittal view of the dorsal-ventral strain for a distraction injury

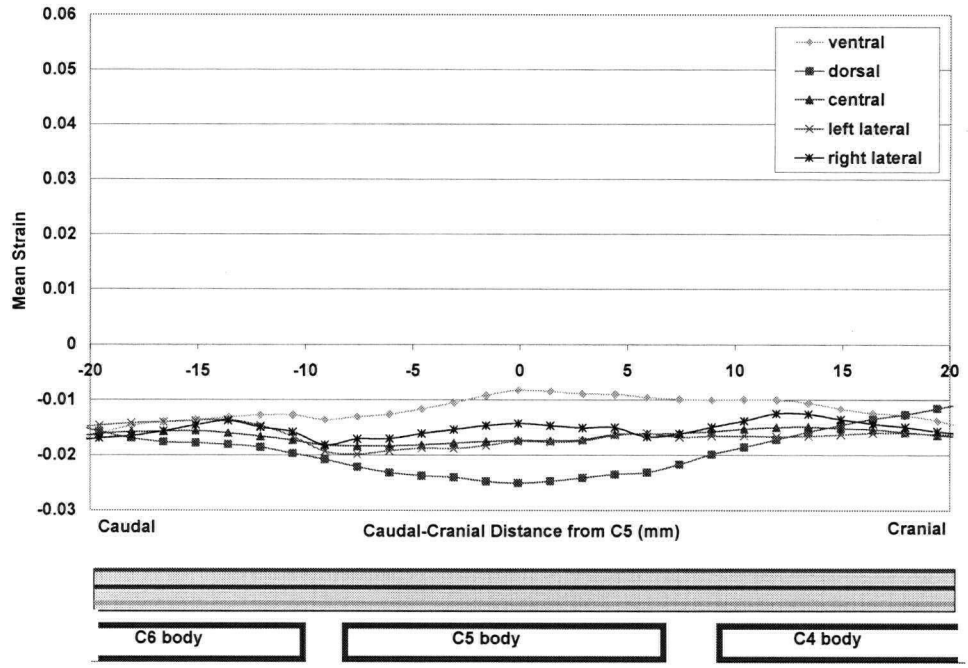

Figure 3.12: Mean dorsal-ventral strain as a function of axial distance from C5 (mm) for a distractive injury

The maximum dorsal-ventral strains for the dislocation injury were between the two contacting surfaces: the cranial edge of the C6 vertebral body and the caudal edge of the C5 vertebral arch (Figure 3.13). The maximum mean and absolute dorsal-ventral compressive strains for the modelled dislocation injury were 12% and 20%, respectively, in the ventral column (Figure 3.14). The strains at the caudal end of the model (10 mm) were not included since they represented artefacts due to the boundary conditions applied at the end of the cord. The lateral columns had the lowest mean peak dorsal-ventral compressive strains, which were 4 and 6%.

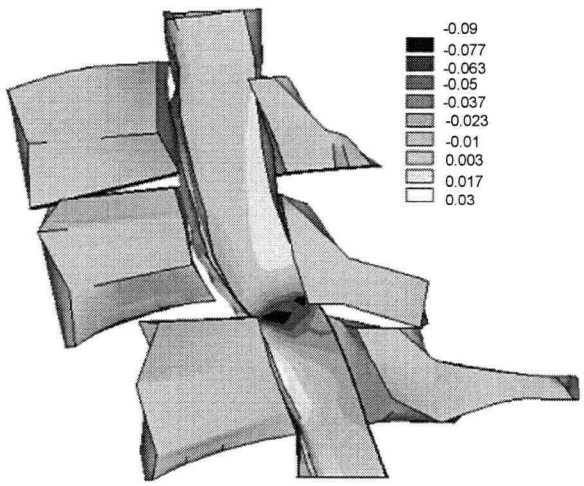

Figure 3.13: Mid-sagittal view of the dorsal-ventral strain for a dislocation injury

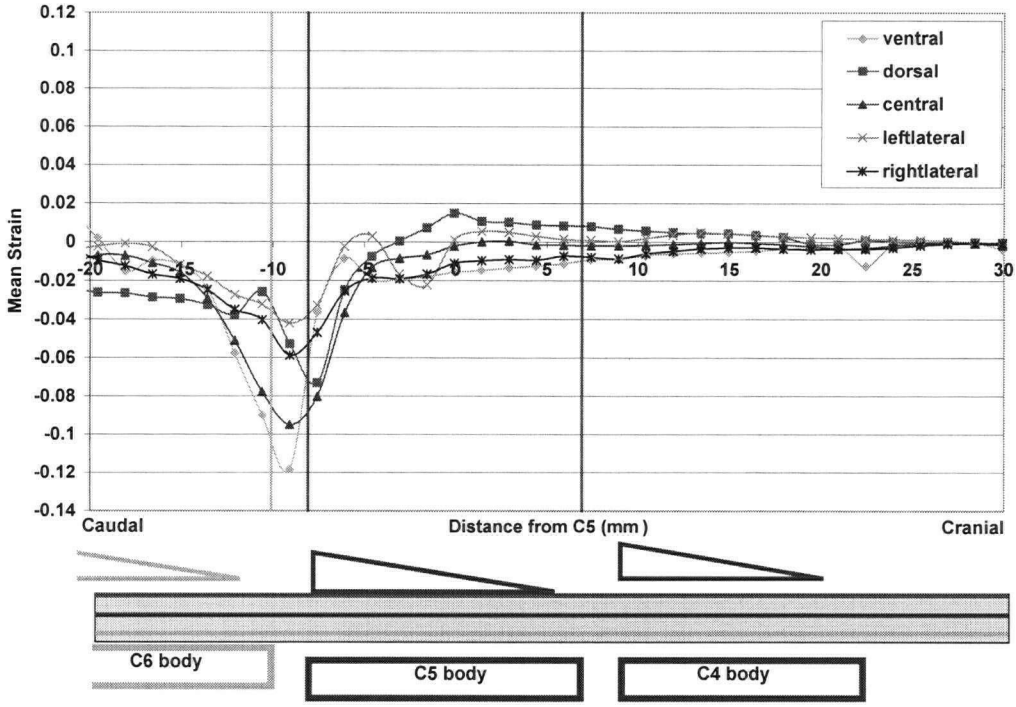

Figure 3.14: Mean dorsal-ventral strain as a function of axial distance from C5 (mm) for a dislocation injury

3.2.2 Axial Strain

Critical points for axial strain in the modelled compression injury were the dorsal column at the cranial tip of the indentor, and the ventral column at the caudal edge of the contacting vertebral body. The compression injury mechanism resulted in tensile strains in the axial direction under the indentor, and particularly at the critical points (Figure 3.15). Axial compressive strains at the caudal end of the indentor resulted from the irregular surface of the C5 vertebra. The cranial tip of the vertebra was flat while the caudal tip of the vertebra curved into the canal (Figure 3.16). This induced some local bending of the spinal cord. The peak mean and absolute axial tensile strains were 6.5 and 11% in the dorsal column at the cranial tip of the indentor. The peak mean strains for the remaining columns were between 2 and 5%.

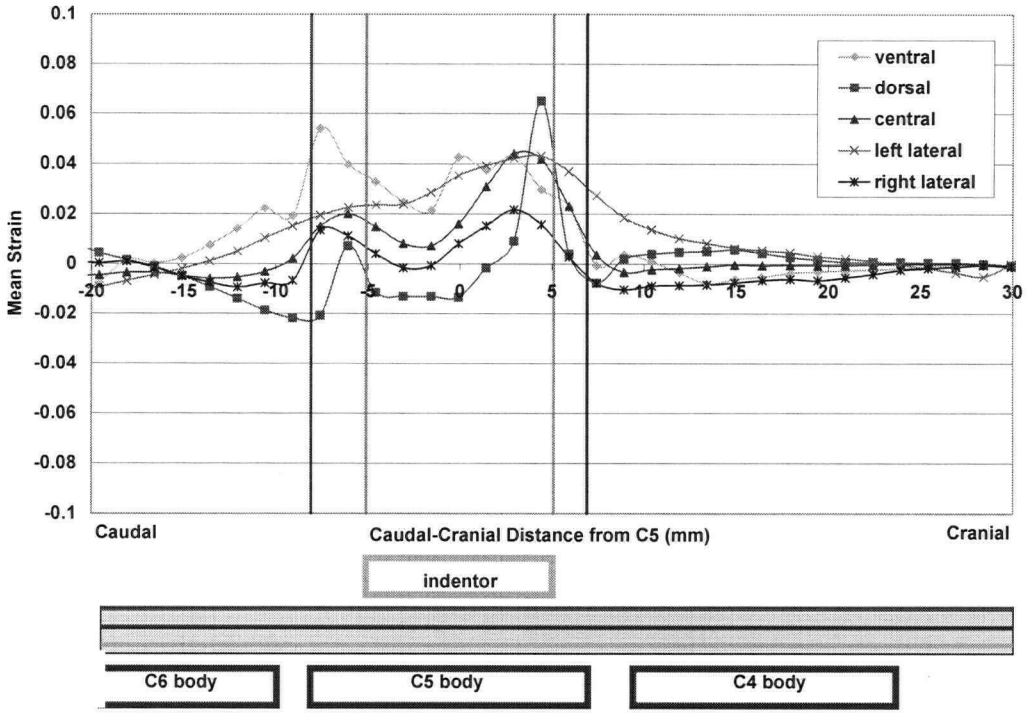

Figure 3.15: Mean axial strain as a function of the axial distance from C5 (mm) for a compressive injury

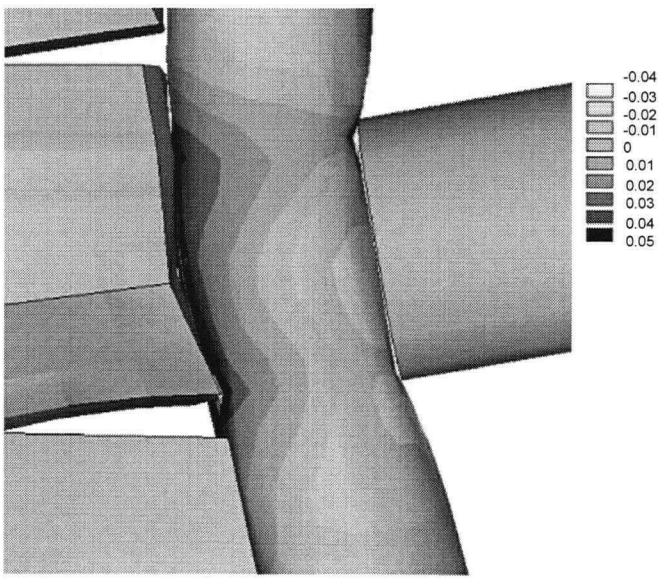

Figure 3.16: Lateral view of the axial strain in the spinal cord at the level of the indentor

The peak mean tensile strain in the axial direction for a distraction injury was 5.4%, in the dorsal column (Figure 3.17). For the remaining columns, the peak mean strains were between 3.6 and 4.1%.

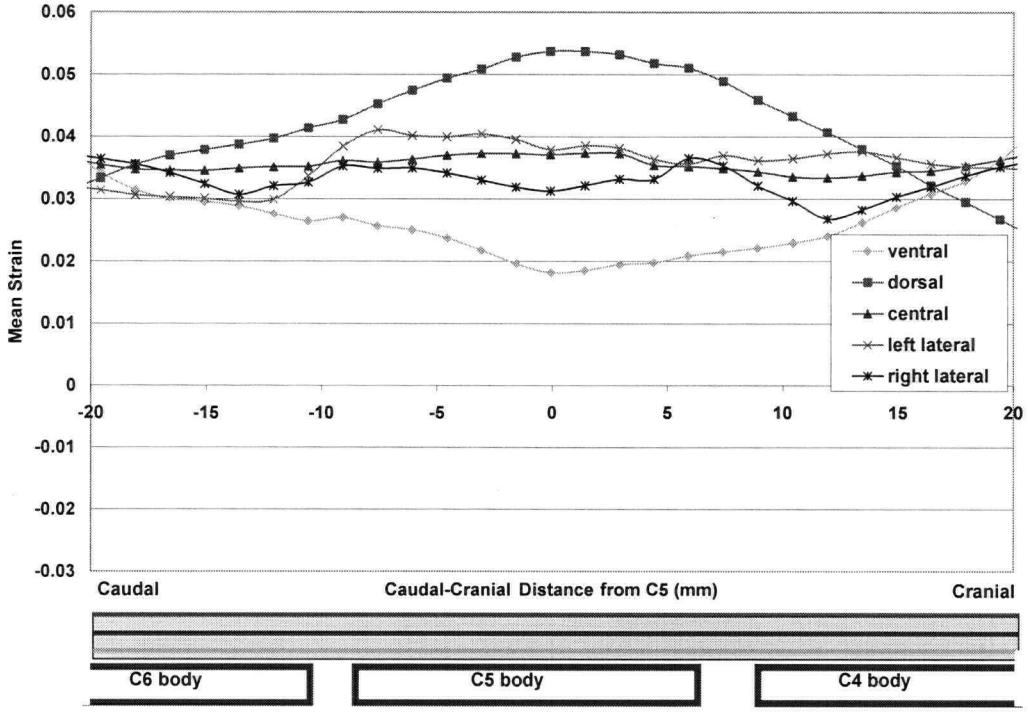

Figure 3.17: Mean axial strain as a function of the axial distance from C5 (mm) for a distractive injury

The maximum mean and absolute strains in the axial direction for a dislocation injury were 11 and 13%, respectively, in the dorsal column, at the level where the caudal end of the C5 vertebral arch contacted the dorsal surface of the cord. The peak mean strains in the remaining columns were between 5 and 6% (Figure 3.18).

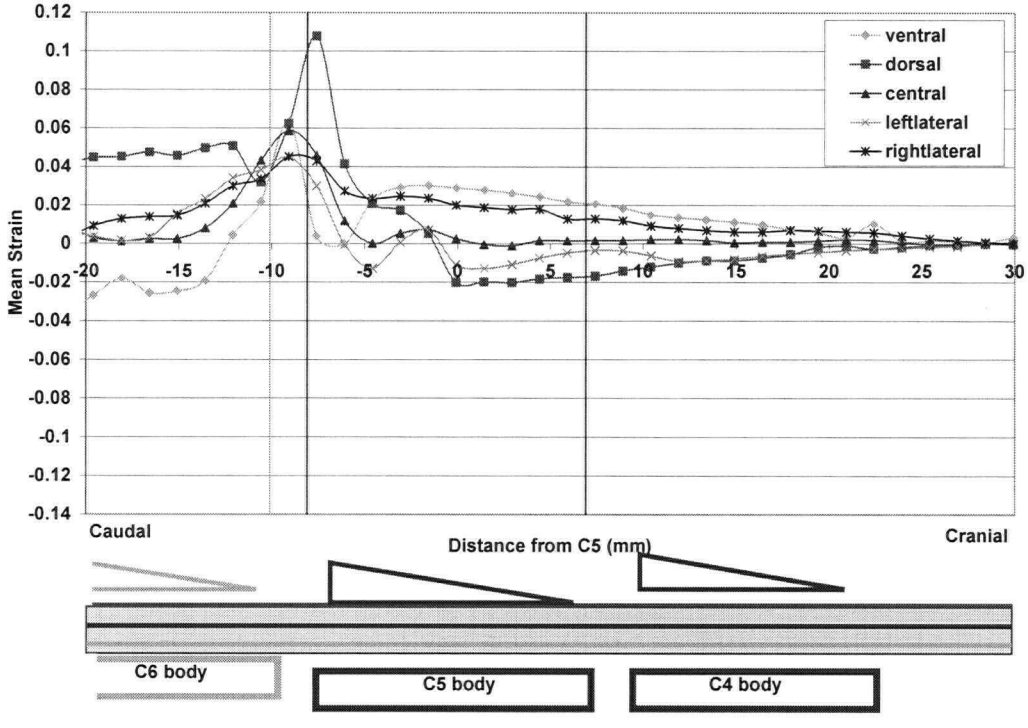

Figure 3.18: Mean axial strain as a function of the axial distance from C5 (mm) for a dislocation injury

3.2.3 Lateral Strain

Since the spinal cord was compressed asymmetrically in the compression injury mechanism, all columns of the cord experienced lateral tension except for the left lateral column which experienced lateral compression (Figure 3.19). The peak mean lateral strain was 4.5% in the central region, while the peak absolute lateral strain was 11% in the dorsal column near the cranial tip of the indentor.

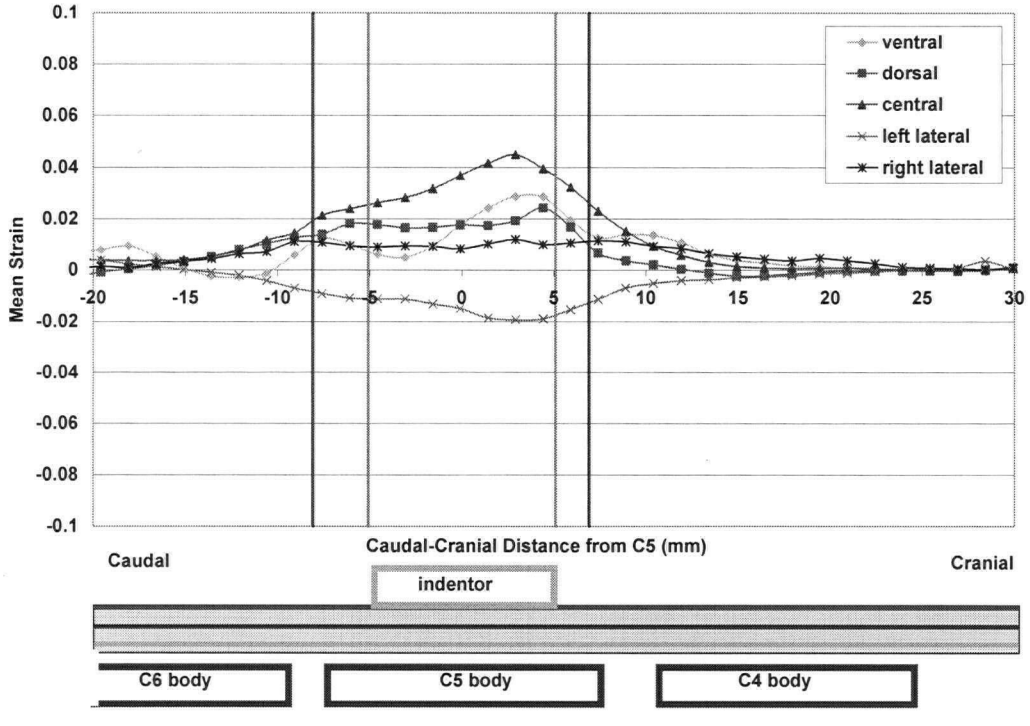

Figure 3.19: Mean lateral strain as a function of the axial distance from C5 (mm) for a compression injury

In the modelled distraction injury, all columns of the cord experienced lateral compressive strain, with a maximum mean of 2.8% in the dorsal column (Figure 3.20).

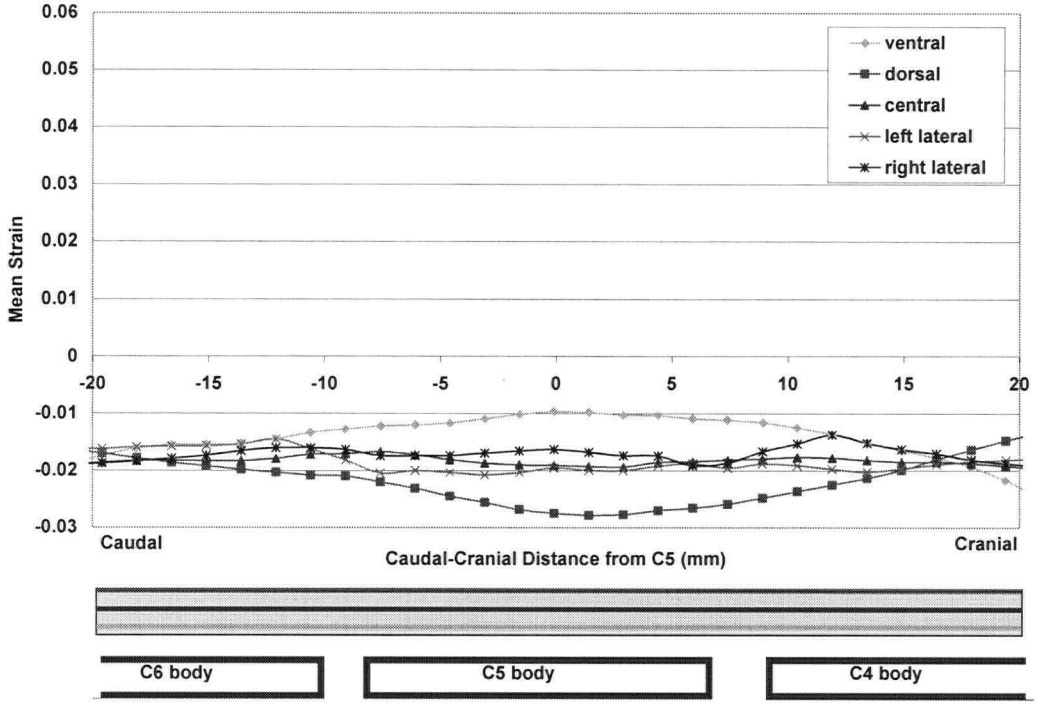

Figure 3.20: Mean lateral strain as a function of the axial distance from C5 (mm) for a distraction injury

In the dislocation injury, all columns experienced lateral tensile strain except the dorsal column, which was compressed between the two sides of the vertebral arch of C5 (Figure 3.21). This resulted in mean and absolute peak compressive strains of 4 and 9%, respectively. The maximum mean and absolute lateral strains were 6 and 10%, respectively, in the ventral column at the cranial tip of the C6 vertebral body.

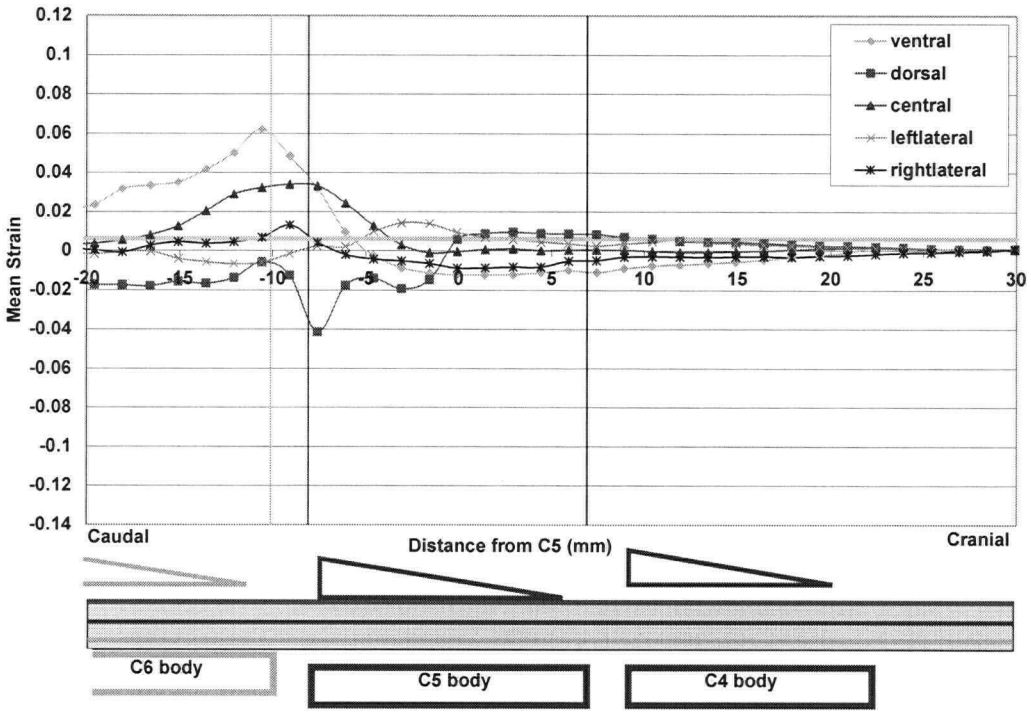

Figure 3.21: Mean lateral strain as a function of the axial distance from C5 (mm) for a dislocation injury

3.2.4 Transverse Shear Strain

Transverse shear strains in compression ranged from -14% to 14%. The mean nodal transverse shear strains were small (between -2% and 2%), due to the averaging procedure; transverse shear strains changed sign across the mid-sagittal plane (Figure 3.22). Mean absolute strains were calculated to examine the distribution of transverse shear strains.

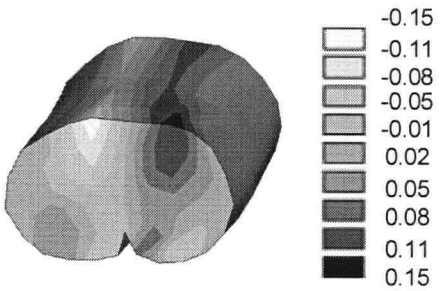

Transverse shear strains were greatest at the points of contact (dorsal and ventral at the edges of the indentor and the contacting vertebral body) (Figures 3.22 and 3.23).

Figure 3.22: Transverse shear strain for a compression injury at the level of the indentor

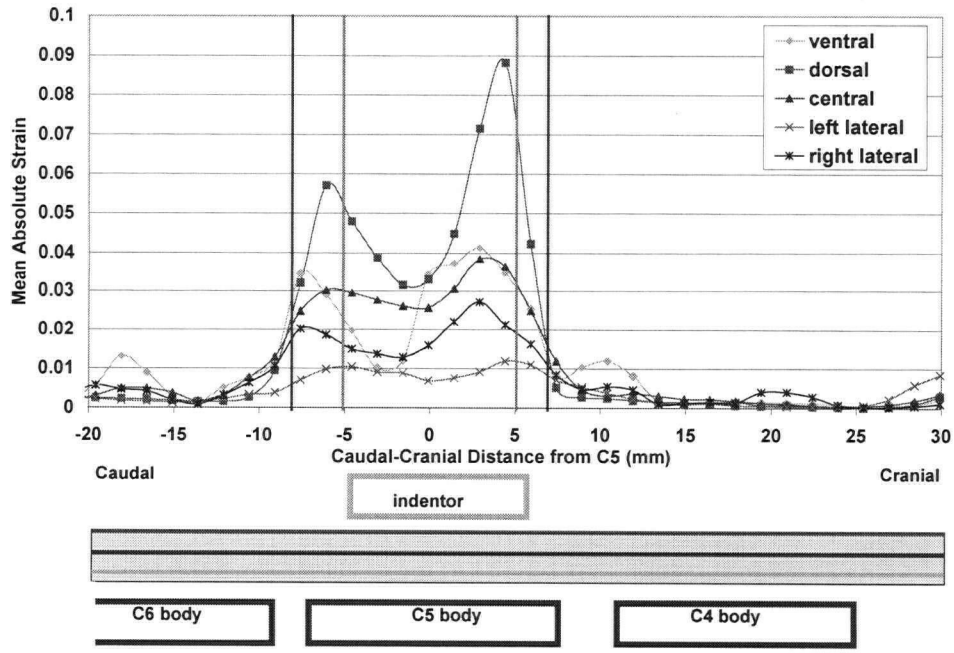

Figure 3.23: Mean absolute transverse shear strain as a function of the axial distance from C5 (mm) for a compression injury

Transverse shear strains for a distraction injury ranged from -1 to 2%.

Transverse shear strains for a dislocation injury ranged from -18% to 13%. The mean absolute transverse shear strains were greatest at the points of contact (5% in the ventral column at the cranial tip of the C6 vertebral body and 8% in the dorsal column at the caudal tip of the C5 lamina) (Figure 3.24). Mean transverse shear strains in the dorsal column were 4% at the mid-vertebral body level of C5.

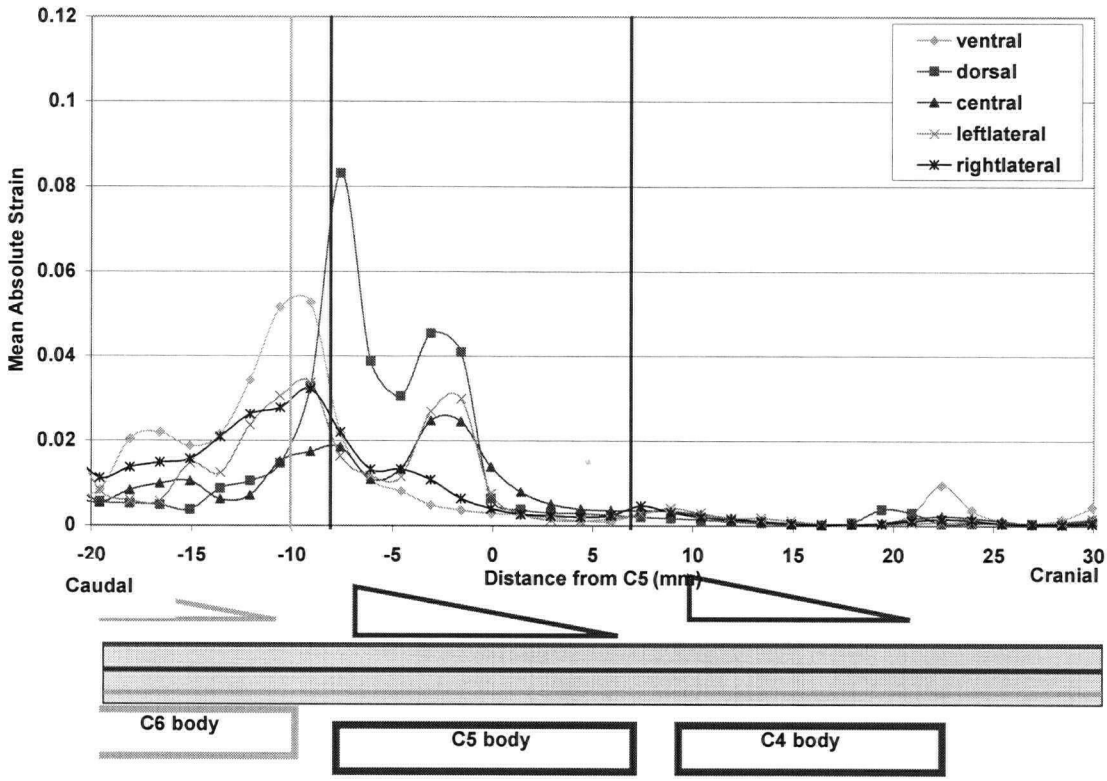

Figure 3.24: Absolute maximum transverse shear strain as a function of the axial distance from C5 (mm) for a dislocation injury

3.2.5 Sagittal Shear Strain

As previously described, the compression injury model demonstrated two distinct contact points due to the irregular surface of the C5 vertebral body. In the modelled compression injury, sagittal plane shear strains were negative at the caudal contact point, and positive at the cranial contact point (Figure 3.25). The maximum mean and absolute sagittal shear strains were 8 and 15%, respectively, in the dorsal column at the cranial tip of the indentor. The dorsal column also had a minimum absolute sagittal shear strain of 16% at the caudal end of the indentor.

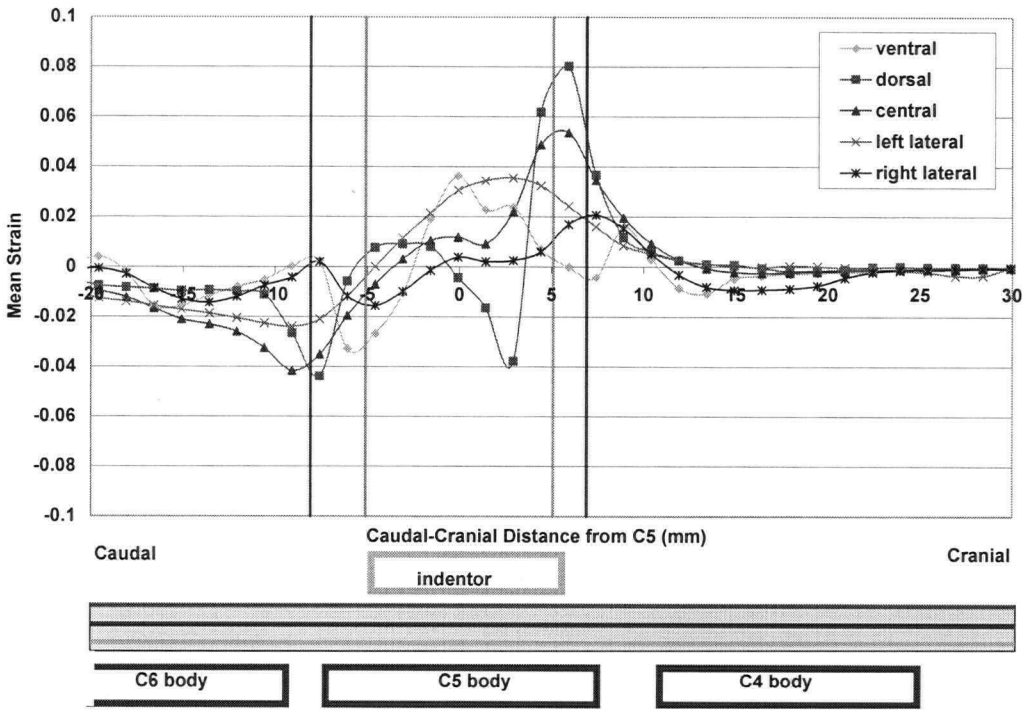

Figure 3.25: Mean sagittal shear strain as a function of the axial distance from C5 (mm) for a compression injury

The maximum mean and absolute sagittal shear strains in distraction were 4 and 5%, respectively, in the dorsal column (Figure 3.26). The peak mean strains in the other columns were between 2.8 and 4.0%.

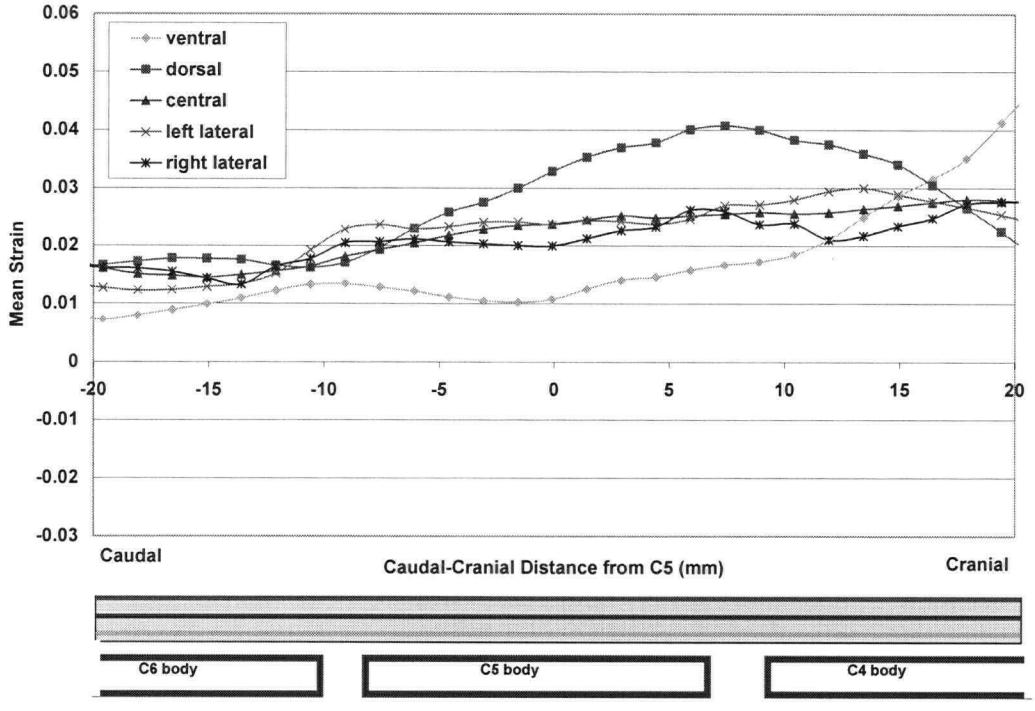

Figure 3.26: Mean sagittal shear strain as a function of the axial distance from C5 (mm) for a distraction injury

The sagittal shear strains for the dislocation injury mechanism were a minimum at the injury centre, between the caudal edge of the C5 vertebral arch and the cranial edge of the C6 vertebral body (Figure 3.27). The maximum mean and absolute sagittal shear strains were 14 and 20%, respectively, in the ventral column. Peak sagittal shear strains were similar in all columns, as the peak mean strains in the remaining columns were between 11 and 13%.

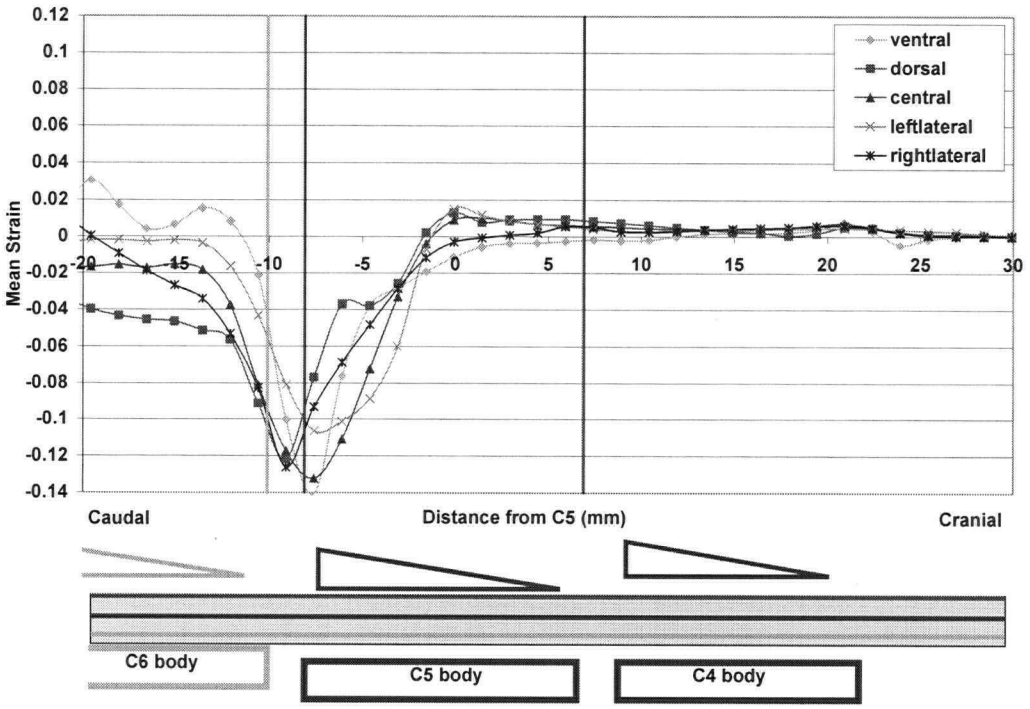

Figure 3.27: Mean sagittal shear strain as a function of the axial distance from C5 (mm) for a dislocation injury

3.2.6 Coronal Shear Strain

For the compression and dislocation injury mechanisms, the smallest range of strains was for the coronal shear strain. For compression, coronal shear strains were between -6% and 7%, while for dislocation they were between -7% and 8%.

For the distraction injury mechanism, the coronal shear strains were between -6% and 7%, and these maximum points were due to concentrations around the denticulate ligament attachment points (Figure 3.28). This was likely an artefact of the FE model.

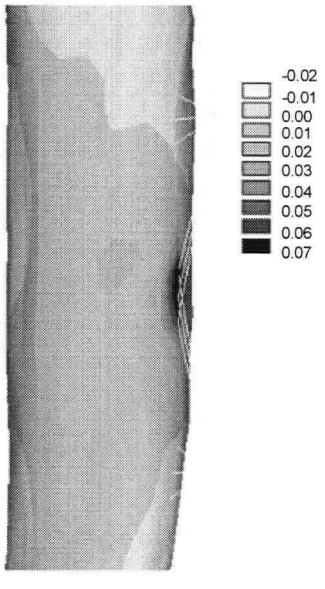

Figure 3.28: Posterolateral view of the coronal shear strain in the spinal cord during distraction with denticulate ligaments shown

3.2.7 Von Mises Strain

In the modelled compression injury, the maximum mean and absolute von Mises strains were 18 and 34%, respectively, in the dorsal column, at the cranial tip of the indentor (Figure 3.29). The lateral columns had the lowest peak von Mises strains. The distribution was similar to that of dorsal-ventral strains.

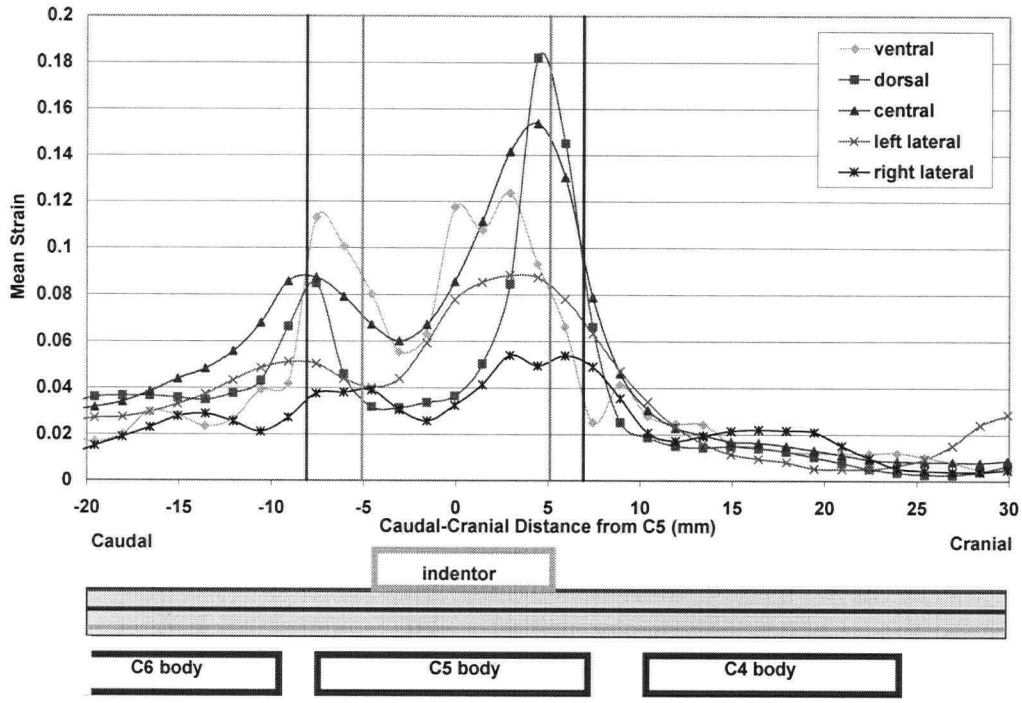

Figure 3.29: Mean von Mises strain as a function of the axial distance from C5 (mm) for a compression injury

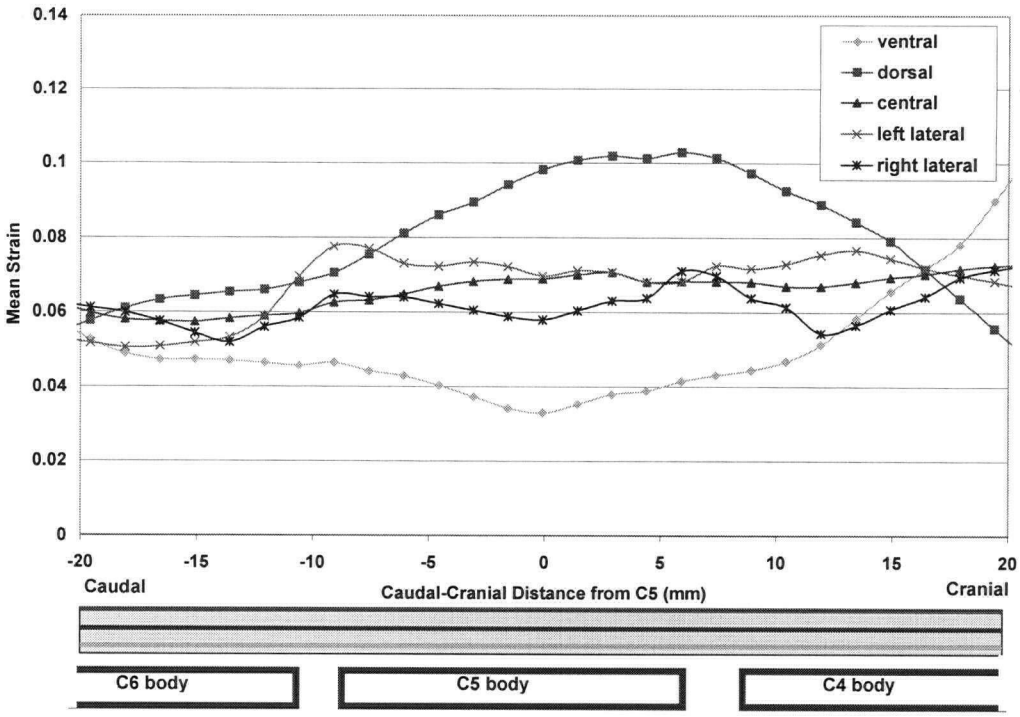

Figure 3.30: Mean von Mises strain as a function of the axial distance from C5 (mm) for a distraction injury

In the modelled distraction injury, the peak mean von Mises strains were similar in all columns (between 7 and 10%) (Figure 3.30). The absolute maximum von Mises strain was 16% in the lateral column, due to a concentration at the attachment point of the denticulate ligaments.

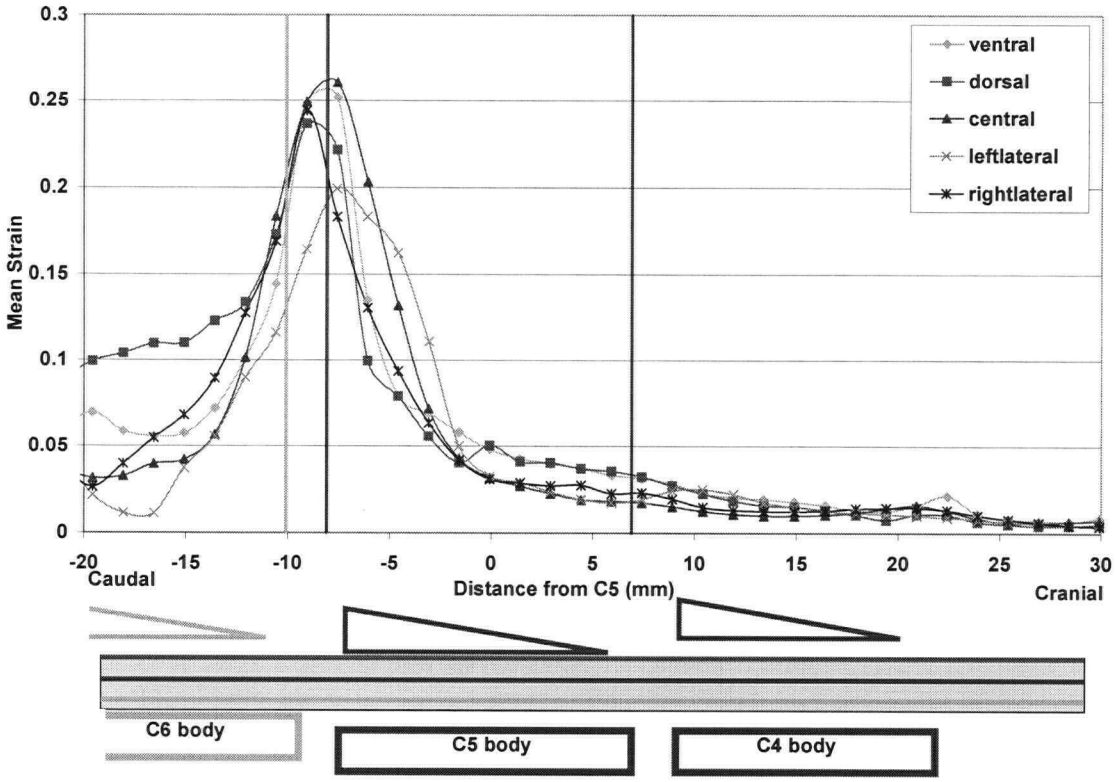

Figure 3.31: Mean von Mises strain as a function of the axial distance from C5 (mm) for a dislocation injury

In the modelled dislocation injury, the maximum mean von Mises strain was 26%, however peak mean von Mises strains were between 20 and 26% in all columns (Figure 3.31). Similarly, maximum absolute von Mises strains were between 32 and 38% in all columns. The distribution of von Mises strains was similar to that of sagittal shear strains.

3.2.8 Summary

The modelled injury mechanisms differed in the strain components with the largest mean values (Figure 3.32). For compression injury, the strain component with the greatest mean absolute value was dorsal-ventral strain, followed by transverse and sagittal shear strains, respectively. For distraction injury, the strain component with the greatest mean absolute value was axial strain, followed by sagittal shear strain and lateral strain, respectively. For dislocation injury, the strain component with the greatest mean absolute value was sagittal shear strain, followed by dorsal-ventral and axial strains. These strain components may be considered as characteristic of their respective injury mechanisms.

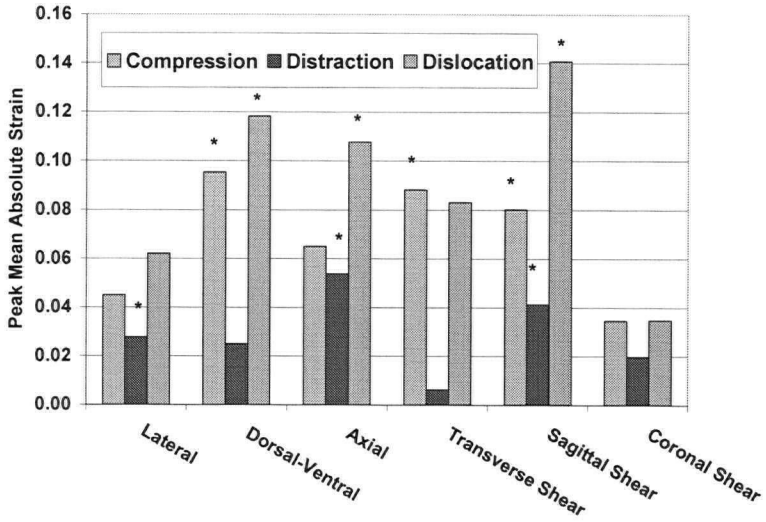

Figure 3.32: Maximum mean absolute strains for compression, distraction, and dislocation injury mechanisms. The top three values for each injury mechanism are indicated with asterisks.

In order to allow further comparisons, mean absolute strains were normalized to the maximum strain of the corresponding component in the corresponding injury mechanism. Normalized peak mean strains (NPM) were between 0 and 100%. 100% indicated the maximum peak mean absolute strain (Figures 3.33 and 3.34).

Regions of peak strains were different between injury mechanisms (Figures 3.33 and 3.34). By comparing distributions of their characteristic strain components, injury mechanisms may be contrasted.

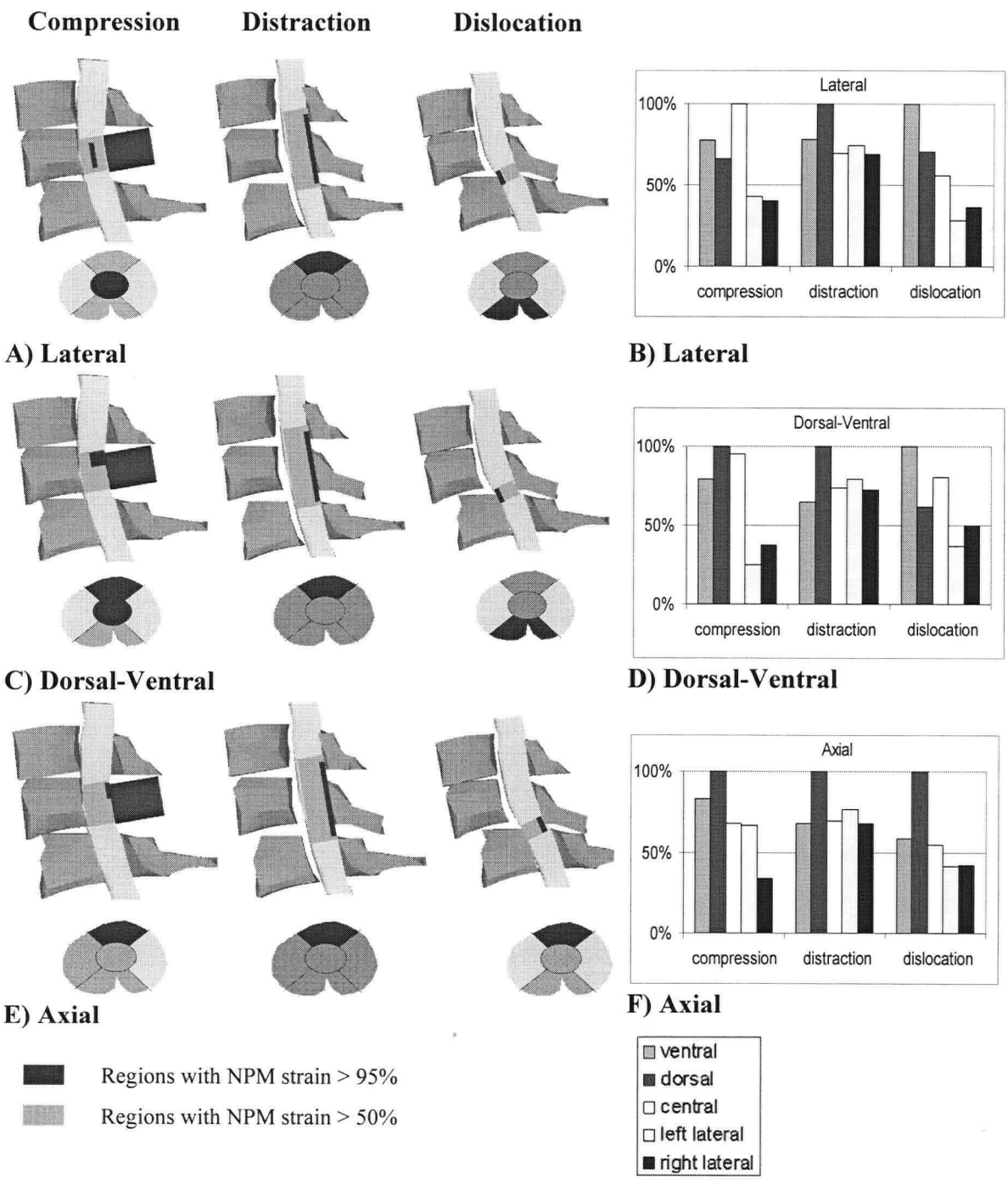

Figure 3.33: A,C,E) Mid-sagittal and transverse views of critical regions of normal strains in compression, distraction, and dislocation injury mechanisms. (A-lateral, C-dorsal-ventral, E-axial). B, D, F) Normalized peak mean (NPM) strains (B-lateral, D-dorsal-ventral, F-axial).

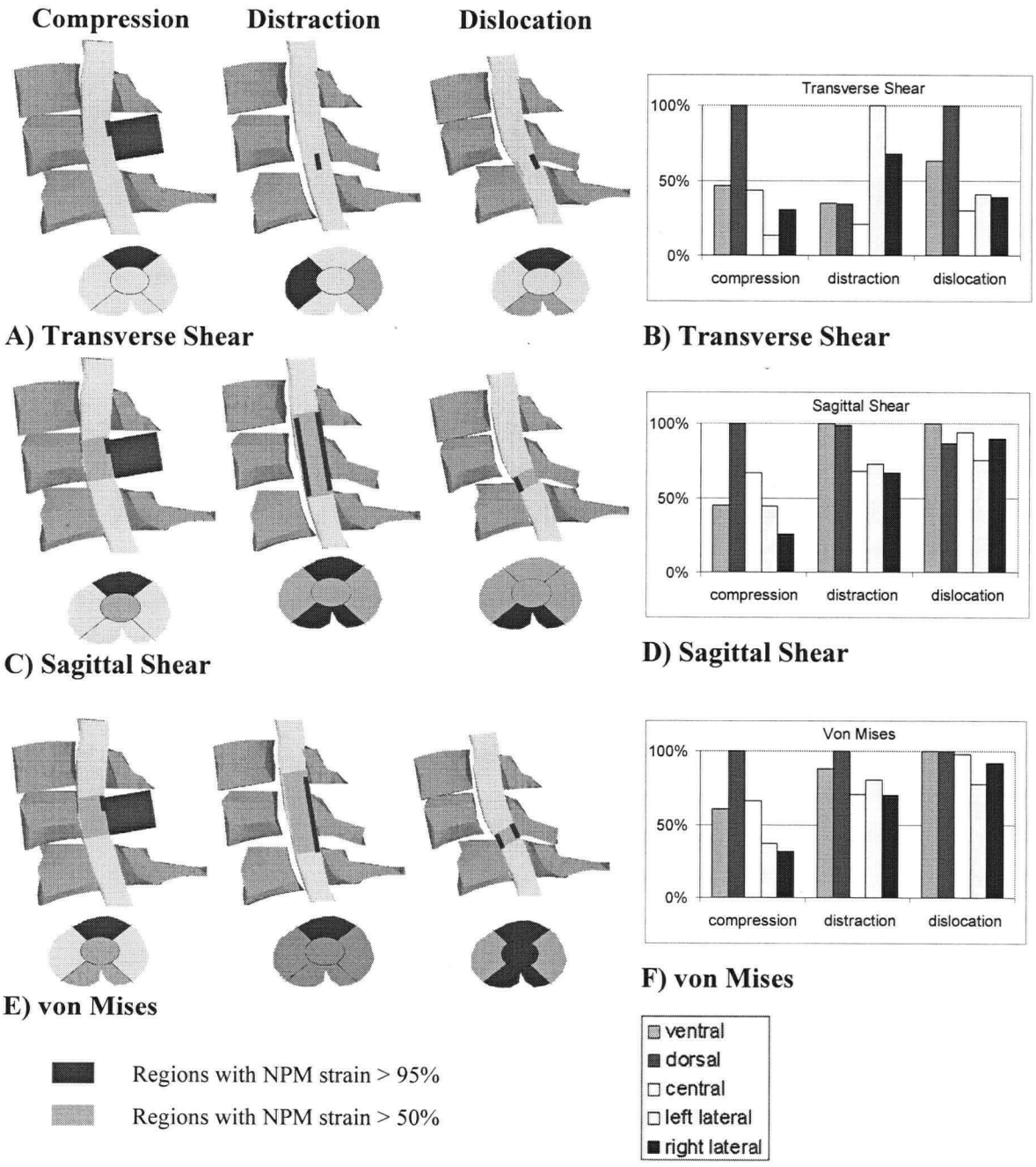

Figure 3.34: A,C,E) Mid-sagittal and transverse views of critical regions of strains in compression, distraction, and dislocation injury mechanisms (A-transverse shear, C-sagittal shear, E-von Mises). B, D, F) Normalized peak mean (NPM) strains (B-transverse shear, D-sagittal shear, F-von Mises).

In compression, the dorsal, central, and ventral columns had NPM dorsal-ventral strains greater than 50% and the lateral columns had NPM normal strains less than 50% (Figure 3.33). NPM shear strains were greater than 95% in the dorsal column and the central column had NPM sagittal shear strains greater than 50% (Figure 3.34). The NPM von Mises strain was greater than 95% in the dorsal column, with strains greater than 50% in the central and ventral columns (Figure 3.34). As a general summary, the compression injury mechanism targeted the dorsal, central, and ventral columns, while the lateral columns experienced less strain.

In distraction, the dorsal column had maximum NPM axial strains and all other columns had NPM axial strains greater than 50% (Figure 3.33). In sagittal shear strain, the NPM was greater than 95% in the dorsal and ventral columns and the remaining columns had NPM sagittal shear strains greater than 50% (Figure 3.34). The distribution of NPM lateral strains was similar to that of axial strains (Figure 3.33). The NPM von Mises strain was a maximum in the dorsal column and all other columns had strains greater than 50% (Figure 3.34). As a general summary, the distraction injury mechanism targeted the dorsal column, however all columns were similarly strained.

In dislocation, NPM sagittal shear strains were greater than 95% in the ventral column and greater than 50% in all columns (Figure 3.34). NPM dorsal-ventral and axial strains were greater than 50% in the dorsal, ventral, and central columns, while the lateral strains had NPM values less than 50% (Figure 3.33). NPM von Mises strains were greater than 95% in the dorsal, central, and ventral columns and they were greater than 50% in all columns (Figure 3.34). Although the dislocation injury mechanism targeted the ventral, dorsal, and central columns in normal strain, the most characteristic strain component, sagittal shear strain, was more uniformly distributed throughout the columns.

3.3 Material Property Sensitivity

Distraction of the 60 mm spinal cord segment was applied in four increments, for two constitutive models: linear elastic and hyperelastic. The distractions were applied as displacement constraints; therefore reaction forces were compared (Table 3.3).

Table 3.3: Reaction force at the top of the cord (N) required for various distractions

	2.6 mm (4% strain)	**5 mm (8% strain)**	**10 mm (17% strain)**	**20 mm (33% strain)**
Linear Elastic Model	1 N	2 N	4 N	6 N
Hyperelastic Model	2 N	6 N	51 N	2,465 N
Percent Error	39%	67%	93%	100%

Although the reaction force for the 2.6 mm displacement, linear elastic model had an error of 39%, the peak mean and maximum absolute strains for this model were within 1% strain of those for the hyperelastic model (Figure 3.35).

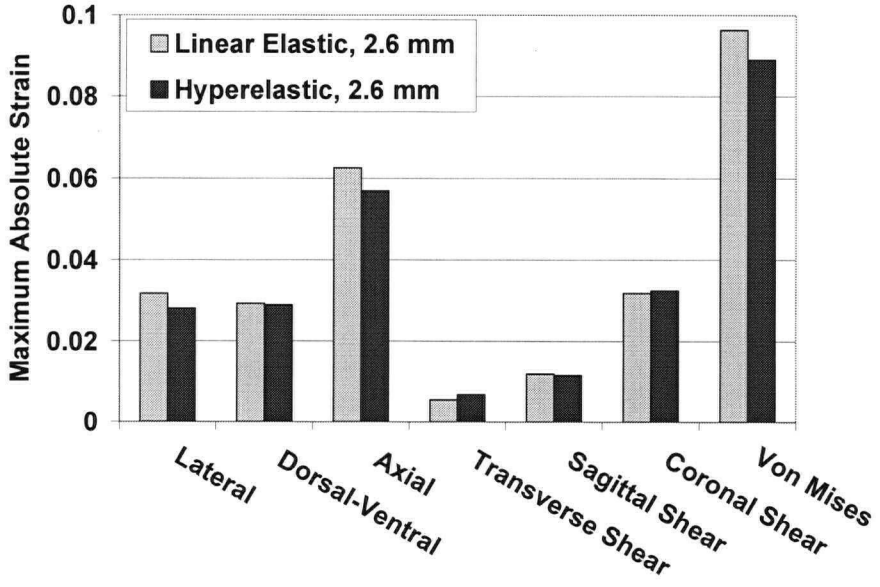

Figure 3.35: Maximum absolute strains for the 2.6 mm displacement group (4% strain)

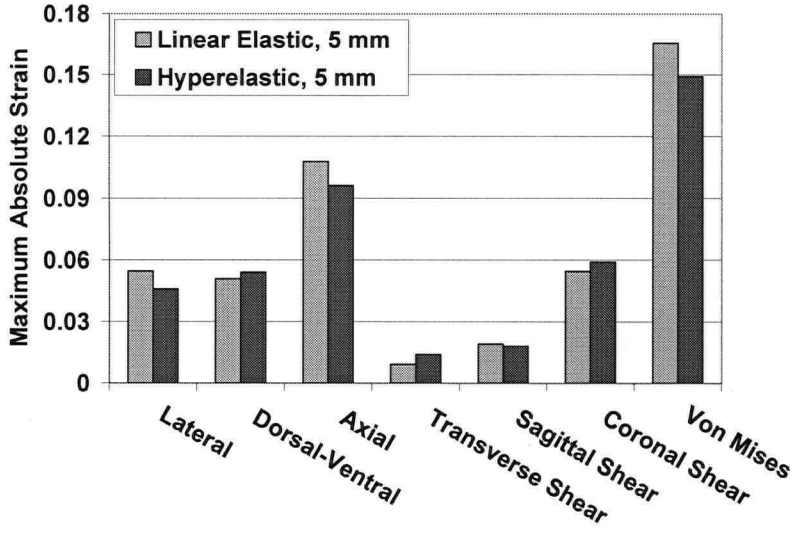

Similarly, the peak mean and maximum absolute strains for the 5 mm displacement, linear elastic model were within 1% strain of those for the hyperelastic model (Figure 3.36).

Figure 3.36: Maximum absolute strains for the 5 mm displacement group (8% strain)

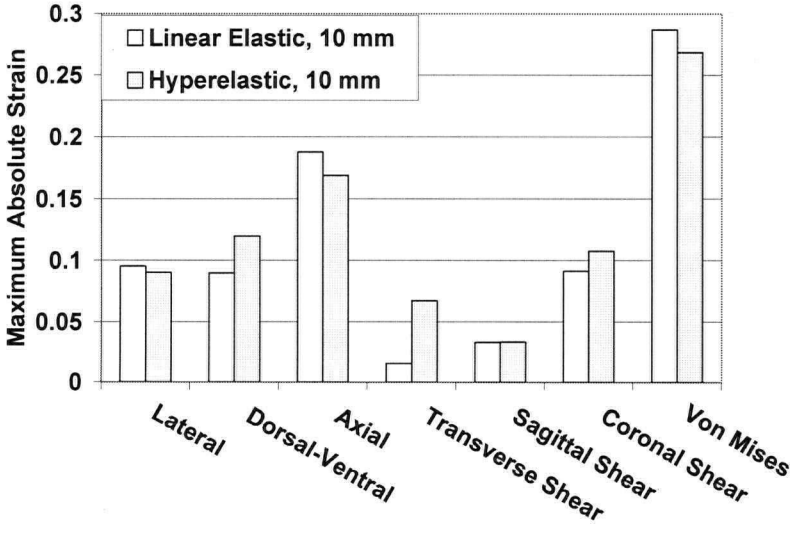

For the 10 mm displacement simulations, the hyperelastic model had greater maximum transverse shear strain (7 vs. 2%), greater maximum dorsal-ventral compressive strain (12 vs. 9%), and smaller maximum axial strain (17 vs. 19%) (Figure 3.37).

Figure 3.37: Maximum absolute strains for the 10 mm displacement group (17% strain)

For the 20 mm displacement simulations, the hyperelastic model had greater maximum transverse shear strain (21 vs. 3%), greater maximum dorsal-ventral compressive strain (23 vs. 16%), and smaller maximum axial strain (30 vs. 32%) (Figure 3.38).

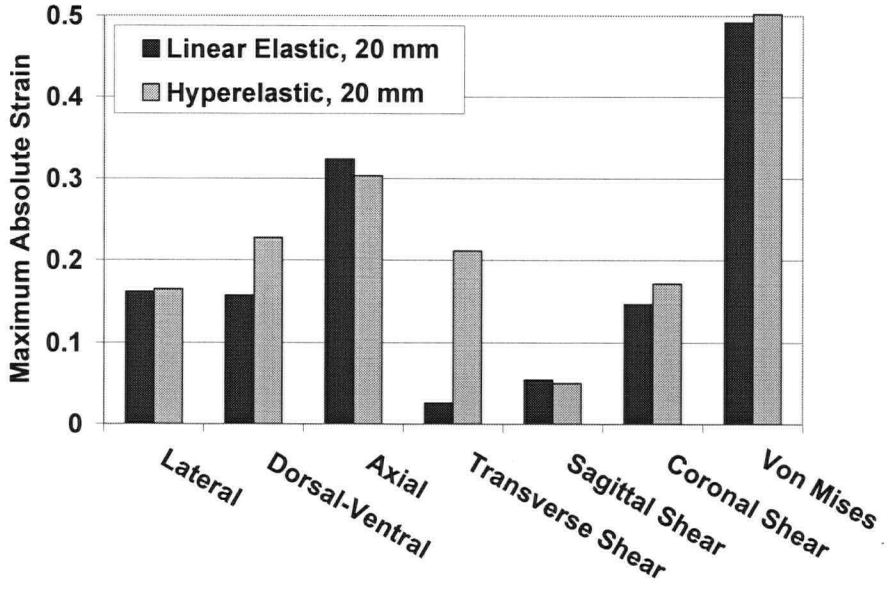

Figure 3.38: Maximum absolute strains for the 20 mm displacement group (33% strain)

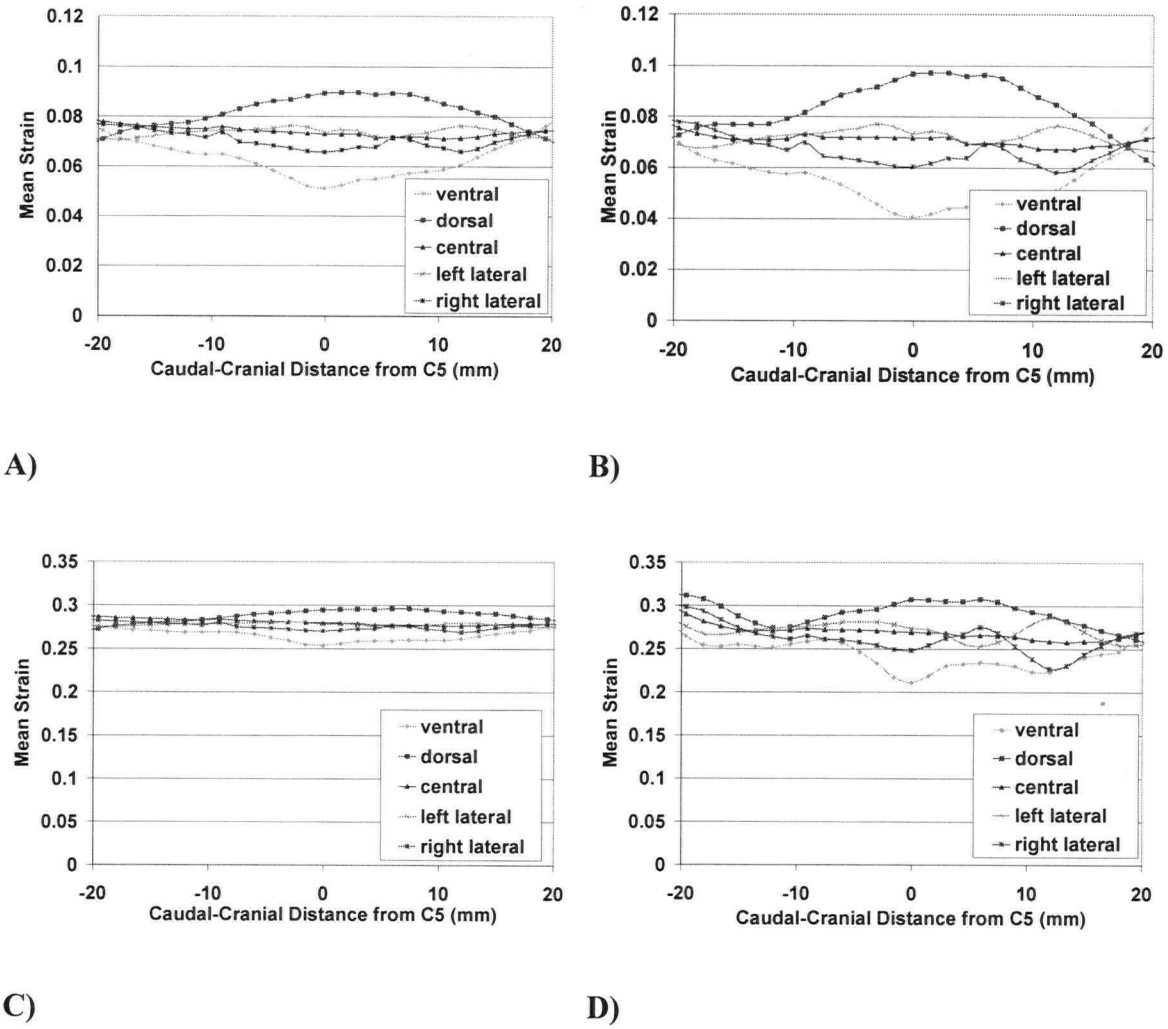

Figure 3.39: Mean axial strains as a function of the axial distance from C5 (mm) in a distraction injury (hyperelastic vs. linear elastic constitutive models). A) Hyperelastic, 5 mm distraction, B) Linear elastic, 5 mm distraction, C) Hyperelastic, 20 mm distraction, D) Linear elastic, 20 mm distraction.

The axial strains for each of the hyperelastic simulations were contained in a smaller range than those of the corresponding linear elastic model (Figure 3.39). The axial strains for the linear elastic models had ranges of 5, 8, 11, and 15% strain, while those of the hyperelastic models had ranges of 4, 5, 6, and 7% strain (for the 2.6, 5, 10, and 20 mm displacement simulations, respectively).

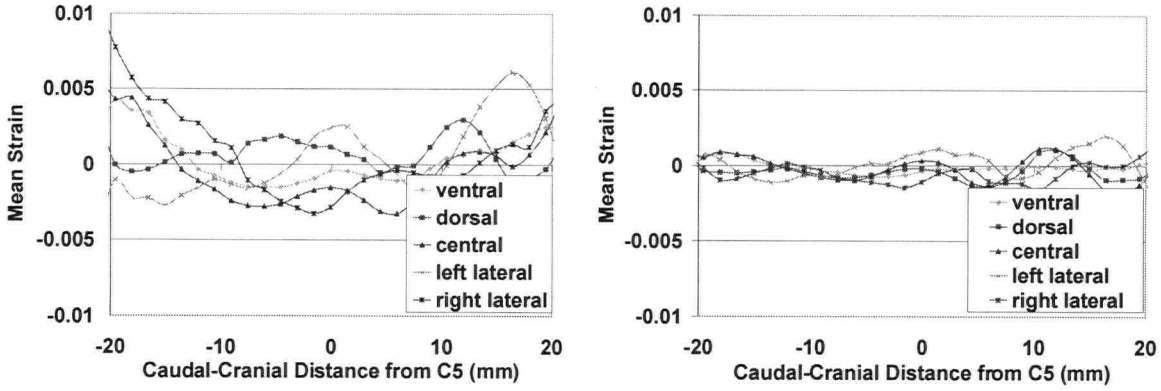

A)

B)

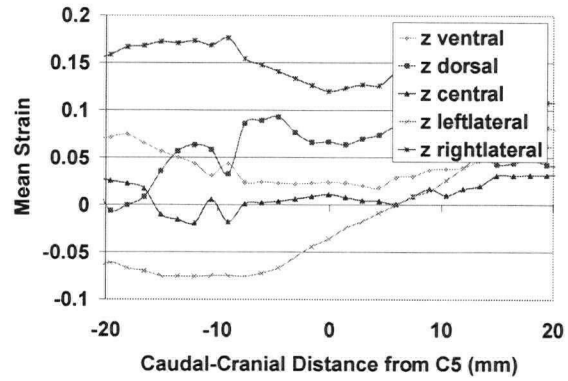

C)

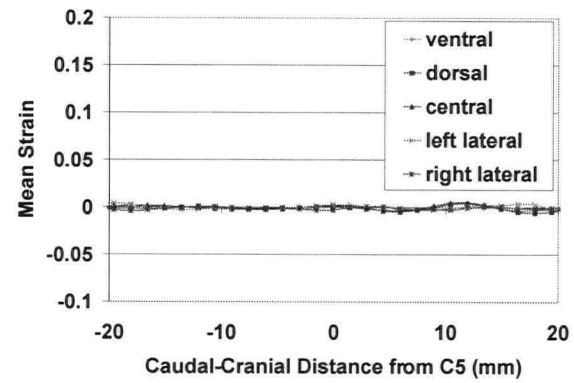

D)

Figure 3.40: Mean transverse shear strains as a function of the axial distance from C5 (mm) in a distraction injury (hyperelastic vs. linear elastic constitutive models). A) Hyperelastic, 5 mm distraction, B) Linear elastic, 5 mm distraction, C) Hyperelastic, 20 mm distraction, D) Linear elastic, 20 mm distraction.

In addition, the transverse shear strains for each of the hyperelastic simulations had a larger range than those of the corresponding linear elastic models (Figure 3.40). The transverse shear strains for the linear elastic models had ranges of 1, 2, 2, and 4% strain, while those of the hyperelastic models had ranges of 1, 3, 12, and 36% strain (for the 2.6, 5, 10, and 20 mm displacement simulations, respectively).

As a general summary, the hyperelastic model resulted in a more uniform distribution of axial strains, which resulted because of increased dorsal-ventral compression and transverse shear strains.

The root mean square error of maximum strains for all components (lateral, dorsal-ventral, axial, and transverse, sagittal, and coronal shear) increased with an increase in mean distraction strain (Figure 3.41).

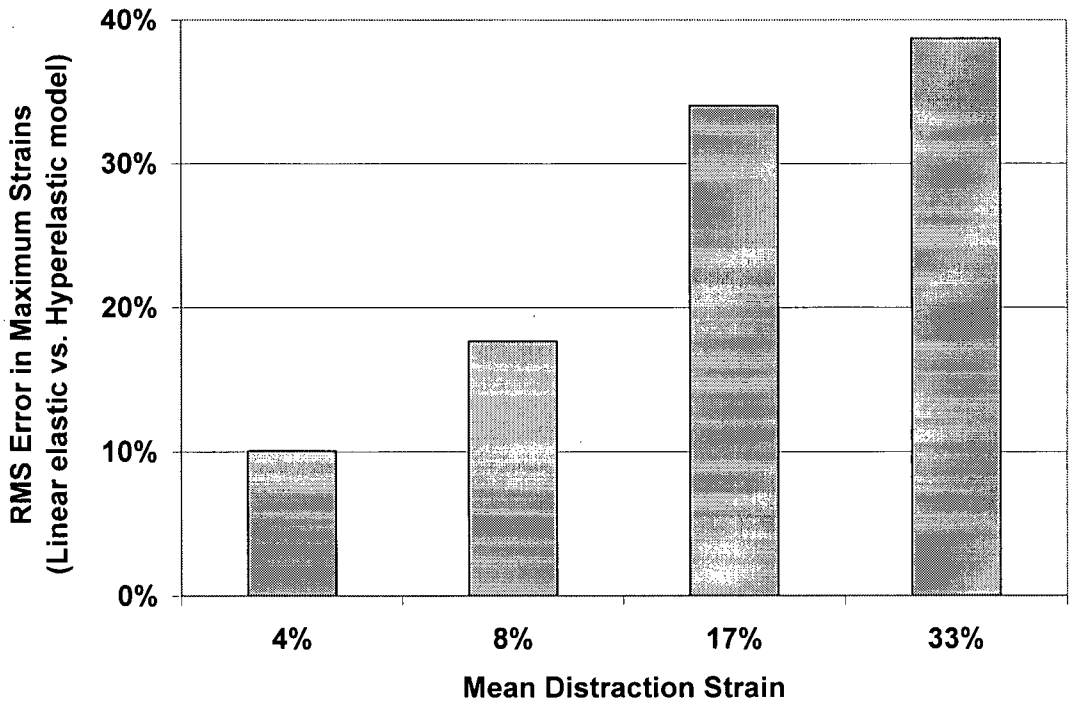

Figure 3.41: Root mean square error of maximum absolute strains (linear elastic vs. hyperelastic constitutive models)

4 Discussion

This study was motivated by a desire to understand the effect of mechanical loading on the spinal cord. A three dimensional, anatomically accurate FE model of the spinal cord and the surrounding structures was developed and validated. The model was subjected to three loading scenarios (compression, distraction, and dislocation), which were selected to represent three basic mechanisms of SCI. The FE model was validated with experimental data from the literature (Hung, Lin et al. 1982; Tencer, Allen et al. 1985; Maiman, Coats et al. 1989) for compression and distraction injury mechanisms. No experimental data was available for validation of the dislocation injury mechanism.

Different strain distributions were found for compression, distraction, and dislocation injury mechanisms. Three characteristic strain components were defined for each mechanism as those with the top three mean absolute strains. These components included sagittal shear strain for all injury mechanisms, dorsal-ventral strain for compression and dislocation mechanisms, and axial strain for distraction and dislocation mechanisms. Furthermore, transverse shear strain was characteristic of compression injury, while lateral strain was characteristic of distraction injury.

Further general conclusions were made based on the characteristic strain component distributions. The compression injury mechanism targeted the dorsal, central, and ventral columns, while the lateral columns experienced less strain. The distraction injury mechanism applied the most strain to the dorsal column, which was on the most concave aspect of the initial curvature, however all columns were similarly strained. Although the dislocation injury mechanism targeted the ventral, dorsal, and central columns in normal strain, the most characteristic strain component, sagittal shear strain, was more uniformly distributed throughout the columns.

The effect of constitutive model selection for the spinal cord was investigated by comparing the response of the linear elastic model to that of a hyperelastic model for three levels of distraction. At a low level of strain (for a displacement controlled simulation), the maximum strains were similar between both models, however the forces

were dissimilar. With increasing levels of strain, the RMS error of the linear elastic response increased (considering the hyperelastic response to be most accurate). At high levels of strain, although the maximum von Mises strains correlated well, the maximum transverse shear strain, dorsal-ventral strain, and axial strain patterns were different. In general, the hyperelastic model resulted in a more uniform distribution of axial strains, which resulted because of increased dorsal-ventral compression and transverse shear strains.

4.1 Limitations

Although biological tissues generally have a nonlinear stress-strain response, all components of the finite element model were assumed to behave according as linear elastic, with the exception of the spinal cord for the material sensitivity study. A previous FE study found the kinematics of the spinal column were most affected by the material property selection of the of the soft tissue structures (IV discs, ligaments and connective tissues) than that of the vertebrae (Kumaresan, Yoganandan et al. 1999). Furthermore, the elastic modulus of bone is considerably greater than that of the spinal cord (10,000 vs. 0.26 MPa); it is probable that the results of this study were the least sensitive to the material property of the vertebrae. Although the choice of material model for the soft tissues may have had an effect on the motion of the column and the stress distribution within these components, it is likely to have a negligible effect on the distribution of strains throughout the spinal cord, which was the main goal of this project. The choice of material model for the spinal cord tissue had the most important role in obtaining this goal.

Spinal column kinematics were not modelled or validated, as this was outside the scope of the current project. To accurately model spinal column behaviour, contact between the vertebrae at the facets would need to be included, and the intervertebral discs would need to be modelled to greater detail. In the current model, the discs were represented with a small number of link elements, which captured the tension-compression response, but did not include bending. Discs have been included in other FE studies by modelling the annulus and nucleus separately as brick elements with different material properties (Saito,

Yamamuro et al. 1991; Yoganandan, Kumaresan et al. 1996; Voo, Kumaresan et al. 1997; Goel and Clausen 1998; Kumaresan, Yoganandan et al. 1999; Ng and Teo 2001).

Spinal cord tissue is anisotropic. It consists of longitudinally running axons of varying dimensions as well as a central core of grey matter, which is more randomly oriented. Experimental testing of the mechanical properties of spinal cord tissue has focused on the composite structure of white and grey matter as a whole (Chang, Hung et al. 1981; Hung and Chang 1981; Hung, Chang et al. 1981; Hung, Chang et al. 1981; Chang, Hung et al. 1988; Bilston and Thibault 1996; Fiford and Bilston 1998). As previously mentioned, controversy exists as to whether or not there is a difference in elastic modulus between white and grey matter (Ichihara, Taguchi et al. 2001; Ozawa, Matsumoto et al. 2001) and evidence exists suggesting that that these two tissues have different tolerances to mechanical loading (Ichihara, Taguchi et al. 2001). Although varying material properties of white and grey matter would be of interest to include in a FE model of the cord, it was concluded that the experimental data available were insufficient to consider modelling these tissues with different properties. Furthermore, experimental testing has thus far been limited to uniaxial tension tests (Chang, Hung et al. 1981; Hung and Chang 1981; Hung, Chang et al. 1981; Hung, Chang et al. 1981; Chang, Hung et al. 1988; Bilston and Thibault 1996; Fiford and Bilston 1998). Spinal cord tissue may also have different properties in the radial direction, due to the longitudinal orientation of white matter. Some finite element studies have assumed an elastic modulus found in brain testing for the radial stiffness of spinal cord tissue (Bilston 1994; Bilston 1998), however the white matter in brain tissue is more randomly oriented; therefore this value may not be appropriate. Experimental data in the literature were insufficient to assume orthotropic material properties for the spinal cord in a finite element model.

Another limitation of this study is the lack of appropriate validation data in the literature. The dislocation injury mechanism could not be validated due to this deficiency. For the other two injury mechanisms, some validation data was found, however further issues must be considered in their use. First, experimental data from biological experiments have inherent variability. For example, for in vivo animal experiments, a 30% variation in force required to contuse spinal cords to a fixed displacement has been found

(Bresnahan, Beattie et al. 1987), presumably due to variations in spinal cord properties, tethering ligaments, and vasculature. Differences in the age of the animal, the injury device used, and anaesthetic and surgical procedures applied to the animals may affect the mechanical response of the test and the resulting injury (Young 2002). For validation of the compression injury mechanism, data from the experiments on cat spinal cords had the advantage of representing live tissue with perfusion; this most accurately represents clinical damage to nervous tissue. However, data from the cadaveric experiment (Tencer, Allen et al. 1985) translates well to the finite element model, since the geometry of human vertebrae more accurately represents that in the FE model. Presumably, the geometry of the boundary structures would affect the strain distribution throughout the spinal cord.

Furthermore, there are limitations in translating the mechanical response of an animal experimental model to a human finite element model. Human spinal cord tissue has only been tested in vitro; therefore it is not known if the cat and human spinal cords have the same elastic modulus. In addition, the geometry of the spinal cord and vertebrae are different between species. The compression data applied in this model was from an experiment performed in the thoracic level in a cat (Hung, Lin et al. 1982), while the model was of a segment of the human cervical spine. The spinal cord at the thoracic level is smaller and more round than that at the cervical level and there is more space in the vertebral canal, since the spinal cord is the largest at the lower cervical level. In addition, vertebrae are smaller in the cervical region. The distraction data applied in this model was from an experiment performed over the whole spine with results focused in the cervical region (Maiman, Coats et al. 1989). The curvature of the cat spinal column is different from that of the human, which may have an effect on the axial motion of the spinal cord inside the canal.

The FE model was developed from the anatomy of a human male who was 180 cm in stature with a mass of 90 kg. Ninety percent of males have masses between 55 and 92 kg and statures between 163 and 186 cm, as indicated by 5^{th} and 95^{th} percentile anthropometric data (O'Brien 1996). Therefore, the size of the replicated anatomy was on the upper end of the anthropometric spectrum. This overall difference in the size of

the anatomy would not have affected the results of this study, since relative distributions of strains were of interest. The most significant limitation of this geometry may have been the effect of freezing on the size of the spinal cord. The size of the spinal canal would have been the least affected by freezing; the thermal expansion of bone at freezing temperatures has been found to be half that of soft tissues (Rabin, Taylor et al. 1998). The spinal cord has been found to increase in volume by 4-6% whereas fat in the canal would have decreased by 5-6% (Pech, Bergstrom et al. 1987). This would account for a decrease of 0.6 and 0.4 mm in the anteroposterior and lateral dimensions of the cord, respectively. This effect explains the crowding in the spinal canal observed in the development of the model. At some levels, the dura mater was placed very close to the spinal cord and vertebrae, since there was no room in the canal for gaps.

Another limitation of the geometry selected for the model is the lack of nerve roots and rootlets in the model. The dura matter extends into the IV foramina as it ensheathes the dorsal and ventral roots. An early anatomical study by Reid found that a pull on the nerve roots transmitted its forces to the spinal cord through the dura matter and denticulate ligaments rather than by the rootlets (Reid 1960). It seems reasonable that ligaments, as opposed to nervous tissue, would be strongly loaded, since their functions generally involve resisting tensile loading and maintaining physiologic motion between anatomic components. As a future development of the model, the dura mater may be extended into the IV foramina and attached to the foramina with link elements. Since the mechanics of the spinal cord within the column are not well understood, the effect of including nerve roots in this FE model is not clear. It is hypothesized that nerve roots would provide another boundary condition for elements of the spinal cord and may create additional strain concentrations near their attachment points to the cord. They were not included at this stage of model development for simplicity.

Cerebrospinal fluid (CSF) was indirectly included in the model through the use of pure slip interfaces between the spinal cord and dura mater, as well as a normal stiffness that caused the spinal cord to displace before contact with the dura was achieved. These options were selected through the use of contact elements. It may have been more appropriate to model CSF in the canal with fluid elements, since parameters such as the

fluid pressure and viscosity are available (Ommaya 1968), whereas the normal stiffness of the contact elements had to be approximated. Contact elements were used for ease of modelling at the current stage of model development.

The selection of three vertebrae to be included in the model affected the results since boundary conditions at the edges of the model affected the strain distribution in the cord. Furthermore, the mesh density of the spinal cord may be considered a limitation of this study, since there were approximately five integration points along the dorsal-ventral axis and eight along the lateral axis. However this model is an advancement for the field of spinal cord research and well represents the anatomy, since most other FE models are two-dimensional. This model is the only three-dimensional FE model of the spinal cord that we know of to date, containing the surrounding structures with experimental validation of cord deformation.

4.2 Comparison with Validation Data

A uniaxial testing device (Instron Corp., Canton, MA) was used to obtain the in vivo compression validation data (Hung, Lin et al. 1982). Assuming that no further device was used to measure the spinal cord compression, it is likely that the Instron machine measured dura motion and not cord compression. The motion of the dura would be greater than the cord compression for several reasons. First, the spinal cord may not have been held firmly against the anterior aspect of the spinal canal since there is space in the canal and the cord and dura mater may have been held to the posterior aspect of the canal above and below the level of laminectomy due to posterior dural attachments. Measurement of the displacement of the Instron would not take this rigid motion of the cord and dura mater into account. Second, the space between the cord and dura mater is filled with CSF, which would have affected the resulting cord compression. Third, motion of the vertebrae would not have been accounted. Other studies that have measured spinal motion during dorsal impact have found no measurable spine motion, however these tests were performed at high rates (Maiman, Coats et al. 1989). Spinal ligaments are less stiff at slower speeds; therefore some motion of the vertebrae may have occurred during the quasistatic compression tests. The relationship between forces and

displacements observed during the quasistatic spinal cord compression experiments was consistent with that demonstrated previously by measuring the deformation of the dura mater (by a micropoint gage) due to the weight of an impounder resting on its surface (Hung, Lin et al. 1979). These earlier measurements did not control the rate of compression; an impounder was placed on the dorsal surface of the dura mater and the amount of time which passed before taking the displacement measurement is not clear. The contacting surface area was the same in both studies (19.6 mm^2).

In addition, further discrepancies between the in vivo experimental results and those of the FE model may be partially due to a difference in mechanical properties of the spinal cord in tension and compression. The constitutive model of the spinal cord for this model was based on uniaxial tension data. Due to the longitudinal nature of white matter axons, it is hypothesized that spinal cord tissue may be softer in radial compression than in axial tension. Brain tissue has been found to be softer in tension than in compression (Miller and Chinzei 2002), however axons in brain tissue have a more random orientation. This could partially explain the difference between the scaled reaction force measured in the in vivo experimental model (0.3 N) (Hung, Lin et al. 1979) and the FE model (2.1 N) at the highest level of strain. Furthermore, the indentor was modelled with a flat tip; however the in vivo experimental model did not specify the shape of the indentor tip (Hung, Lin et al. 1982). This could also account for differences between the model and the in vivo experimental results.

Furthermore, the selection of contact parameters (normal stiffness and penetration tolerance) may have affected the reaction force at the indentor tip. For example, a high normal stiffness would have resulted in an artificially high reaction force at the indentor tip. These parameters were set to minimize penetration of elements and to achieve model convergence. The normal stiffness was set at 0.02 (relative to the material properties of the underlying elements), which was designated to be at the lower end of appropriate values, since contact was assumed to be soft. Normal stiffness values between 0.01 and 10 are recommended (Ansys User's Manual version 7.1 2003). This normal stiffness was also selected to achieve convergence of the complicated contact model. The penetration tolerance was set at 0.08 (relative to the size of the underlying elements) and the cord

elements had an anteroposterior dimension of approximately 2 mm; therefore, the dura was permitted to penetrate 0.16 mm into the spinal cord.

The secondary source of compression validation data was from cadaver specimens which were compressed anteriorly (Tencer, Allen et al. 1985). This data provided further validation since the geometry of the vertebrae and spinal cord more accurately represent those in the finite element model. In this model of injury, the dura mater (complete with its attachments) was left intact and a tube was mounted into the dura though a hole drilled into the base of the skull to simulate the pressure of CSF. A load sensing probe coupled to a linear variable differential transformer was used to measure the contact force and position of the tip of the sensor in the canal. Compression was applied from the anterior side of the canal, through a hole drilled into a vertebral body, which was in the opposite direction from that simulated in the FE model. Furthermore, compression of the dural sac was applied at T12, whereas the FE model simulated compression at C5. These are limitations of the use of this experimental data in validating the FE model. The predicted contact load from the FE model at the highest level of strain had an error of approximately 30% in comparison to this source of validation data.

Validation of the distraction injury mechanism was not scaled from the animal model since relative displacements of the vertebrae and spinal cord were compared. It was therefore assumed that cats and humans have similar connecting ligaments between the vertebrae, dura mater, and spinal cord. Some of these connecting ligaments are minor anatomical structures and are often ignored in neurosurgical and orthopaedic publications (Scapinelli 1990). Differences between the experimental and the model results are likely due to limitations in modelling of these connective tissues and also to anatomical variations between species.

4.3 Effect of Constitutive Model of the Spinal Cord

For the comparison of injury mechanisms, the spinal cord was assumed to behave according to the linear elastic constitutive model because simplicity was desired for the initial development of the model. The effect of this choice, as compared to a hyperelastic material was investigated and found to be small, in terms of maximum strains, for low

levels of strain. Maximum strains for the linear elastic model were within 1% strain of those determined using the hyperelastic model for mean distractions of 4 and 8%, and root mean square (RMS) errors were 10 and 18%, respectively. At higher levels of strain, the difference between the linear elastic and hyperelastic constitutive models was more evident. For mean distractions of 17 and 33%, RMS errors were 34 and 39% and the most affected strain parameter was the transverse shear strain, which the linear elastic model underestimated by 6 and 20% strain, respectively. Since the distraction injury simulated using the full, linear elastic model had a mean distraction of 4%, it is inferred that the maximum strains predicted by this model were within 1% strain of those that would have been predicted by a hyperelastic model.

For the compression and dislocation injury mechanisms, the effect of the material model selection is more complicated to predict based on the information available. For the compression mechanism, the largest strain component was the dorsal-ventral strain, with a peak mean value of 12%. For the dislocation mechanism, the largest strain component was the sagittal shear strain, with a peak mean value of 14%. At these levels of strain, the material property sensitivity study would predict errors up to 6% strain in the calculated maximum strains. It is unknown which strain components would be most affected by the hyperelastic constitutive model in compression and dislocation.

The material model sensitivity study was limited since it was not known how accurately the hyperelastic model reproduces experimentally observed strain components. The uniaxial response of the material was fit to experimental data (Bilston and Thibault 1996), however there was no experimental data to validate the transverse shearing which was observed for higher levels of strain.

The hyperelastic study demonstrated that simple uniaxial tension applied to the spinal cord may result in significant shear strains at a local level. This effect was lost in the linear elastic finite element model of spinal cord tissue, which predicted the maximum transverse shear strain to be 8% of the maximum axial strain. For the hyperelastic model, the maximum transverse shear strain increased from 15% of the maximum axial strain (at a low strain level) to 70% of the maximum axial strain (for a large strain level).

Previous finite element modelling found a hyperelastic combined with a viscoelastic material model best represents spinal cord tissue, with the viscous effects being more important at lower rates (Bilston 1998). The loading rates applied in this study were very low (quasistatic) and the validation studies found the response to be linear, up to the strains applied (Hung, Lin et al. 1982). Therefore, the linear elastic constitutive model was deemed appropriate for the development of this geometrically complex model.

4.4 Modelling of Tissue Failure

Finite element modelling has been used in biomechanics to predict failure in trabecular and cortical bone (Cezayirlioglu, Bahniuk et al. 1985; Lotz, Cheal et al. 1991; Fenech and Keaveny 1999; Keaveny, Wachtel et al. 1999; Keyak and Rossi 2000). Failure mechanisms of bone are complex; they depend on the loading mode, architecture, and orientation of the tissue (Fenech and Keaveny 1999). The von Mises effective strain criteria, used in this study, was found to be the best indicator of bone yield and failure in a study of femoral fracture (Lotz, Cheal et al. 1991).

Due to the longitudinal nature of axons in white matter, an orthotropic failure criterion may be of use to compare strain distributions between the loading cases. The Tsai-Wu quadratic criterion (Tsai and Wu 1971) accounts for strength asymmetry (different tensile and compressive strengths), anisotropy, and interactions between strengths in the different loading directions. The Tsai-Wu failure criterion was found to be a reasonable predictor of multiaxial failure behaviour of trabecular bone (Keaveny, Wachtel et al. 1999). For this criterion to be applied, multiaxial failure stresses of spinal cord tissue must be known. Experimental data available were insufficient to consider the use of this failure criterion.

The current knowledge of axonal damage has been based on uniaxial tension. Axons may be morphologically damaged at 18% strain (Bain and Meaney 2000), electrophysiologically damaged at 21% strain (Bain and Meaney 2000), structurally damaged at 25% strain (Galbraith, Thibault et al. 1993), and severed at strains greater than 65% (Smith, Wolf et al. 1999). These tolerances have been determined through a variety of models each with their own conditions and limitations; tolerances are not

directly transferable to human SCI. The incorporation of data such as these to finite element models is limited; since axons in vivo have connections to the grey matter and failure of other components of spinal cord tissue (i.e. blood elements) may also lead to axonal disruption.

Finite element modelling has been applied in traumatic brain injury and shear strain was found to be a good predictor of diffuse axonal injury (DAI) (King, Ruan et al. 1995). DAI was found in regions where high shear strain persisted for longer periods during impact. Shear strain limits between 4 and 28% were related in injury. Regions with high strain but no DAI were all in grey matter (King, Ruan et al. 1995).

The tolerance of white and grey matter to strain may be significantly different. The elongation at failure of white matter sections from bovine spinal cord tissue was recently found to be 126%, while that of grey matter was 49% (Ichihara, Taguchi et al. 2001). This is the only such study; therefore more research in this area is required to determine the tolerance of spinal cord tissue to mechanical loading.

4.5 Experimental Relevance

4.5.1 Compression

The characteristic spinal cord contusion or compression lesion is characterised by a large central area of cavitation with a rim of preserved white matter (Blight and Decrescito 1986; Fehlings and Tator 1995). The histology of experimental spinal cord lesions are often studied several weeks after the animal has been injured (Bresnahan, Beattie et al. 1987; Noyes 1987; Bresnahan, Beattie et al. 1991; Behrmann, Bresnahan et al. 1992; Gruner, Yee et al. 1996). These results are difficult to compare to those from a FE model since by this time, a significant amount of secondary injury may have occurred that would further damage spinal cord tissue. Furthermore, many studies report the lesion volume, lesion length, or the tissue spared as a percentage of the cross sectional area of the spinal cord without reporting which columns are prominently spared or injured (Bresnahan, Beattie et al. 1987; Noyes 1987). In addition, differences in methodology, interpretation of changes in injury parameters, animal species, methods of applying loads,

and temporal characteristics of the loads and deformations make it difficult to compare studies.

The grey matter, which is located in the centre of the cord, is more extensively damaged in mild contusion injuries (Gruner, Yee et al. 1996). Evidence of damage has been found in the central grey matter and extending into the dorsal and ventral horns (Rosenberg and Wrathall 1997), although the tips of the dorsal horns are infrequently spared (Behrmann, Bresnahan et al. 1992). One study found that white matter damage in mild injuries is focused in the ventral portion of the dorsal funicular white matter (Rosenberg and Wrathall 1997), however another study using more severe injuries reported the dorsal columns to be best preserved with the dorsolateral region having the most destruction (Blight and Decrescito 1986). The overall shape of contusion lesion is biconical with extensions in the base of the dorsal funiculus (Bresnahan, Beattie et al. 1991). An interpretation of these experimental findings is illustrated in Figure 4.1.

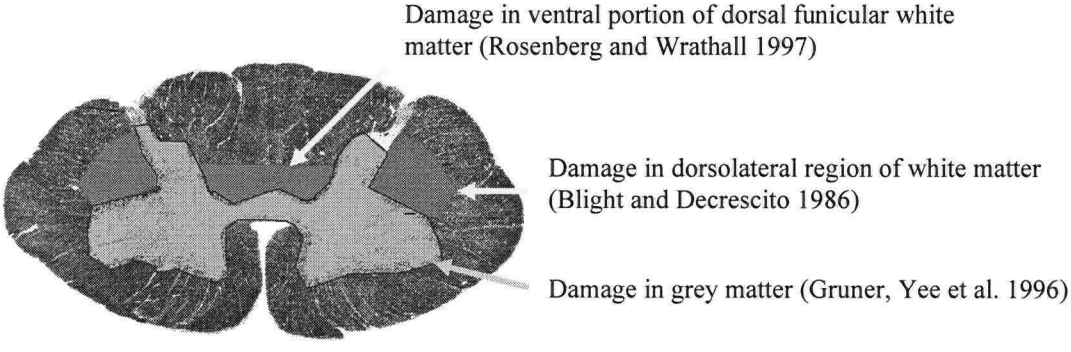

Figure 4.1: Interpretation of injured tracts in experimentally produced compression injury (Figure modified from Kiernan 1998)

The simulated compression injury constituted a mild injury, which may not have resulted in neurological injury. The only neuropathological findings reported were for more severe compression injuries in which mild oedema of white matter was found with normal neurons in the dorsal and ventral horns, or extensive necrosis of both white and grey matter (Hung, Lin et al. 1982).

The results of the FE model indicated that the dorsal, central, and ventral columns experienced more strains than the lateral columns. Characteristic strain components were

dorsal-ventral strain (Figure 4.2), transverse shear strain (Figure 4.3), and sagittal shear strain. Critical regions in the FE model were the dorsal column, under the indentor and the ventral column, at the level of the contacting vertebral body.

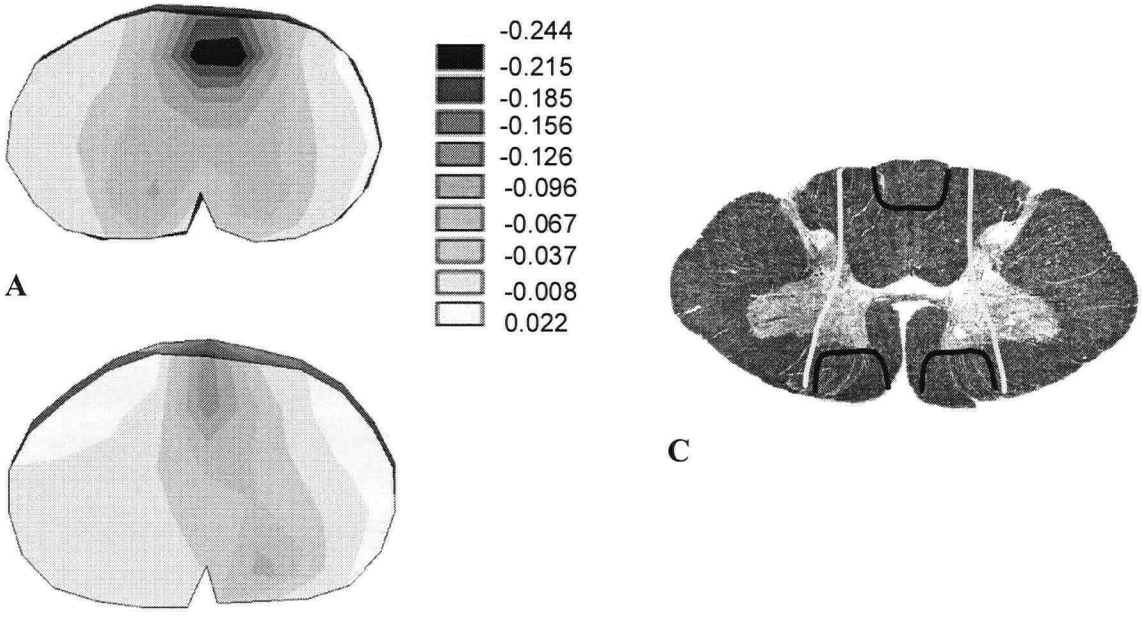

Figure 4.2: Predicted critical areas of strain in spinal cord transverse compression related to tracts in the spinal cord. Sample dorsal-ventral strain distribution for a compression injury at A) the level of the cranial tip of the indentor B) a more caudal level under the indentor. C) Interpretation of the critical areas in compression related to tracts in the spinal cord (Figure modified from Kiernan 1998). Black lines indicate critical regions of strain, while grey lines indicate the load path between critical regions.

Predicted critical regions of dorsal-ventral strain corresponded to the dorsal white funiculus (particularly the posterior portion of the fasciculus gracilis, which is an ascending tract) and the ventral white funiculus (containing ascending and descending fibres). The load path between these critical points also experienced larger strains. This path comprised the posterior and anterior portion of the fasciculus gracilis and cuneatus, medial portions of the dorsal, intermediate, and ventral horns of the grey matter, and the ventral white funiculus (Figure 4.2).

Predicted critical regions of transverse shear strain were slightly different from those of dorsal-ventral strain (Figure 4.3). The dorsal white funiculus had relatively higher strains in more lateral aspects, corresponding to the posterior portion of the fasciculus cuneatus.

The ventral white funiculus had relatively higher strains in more medial aspects. The load path between these critical points was wide in the dorsal aspect of the cord and closer to the median line in the more ventral aspect. This path consisted of similar tracts as that of dorsal-ventral strains, however an additional tract contained was the lateral corticospinal tract (a major descending tract which is involved in voluntary discrete skilled movements) (Figure 4.3).

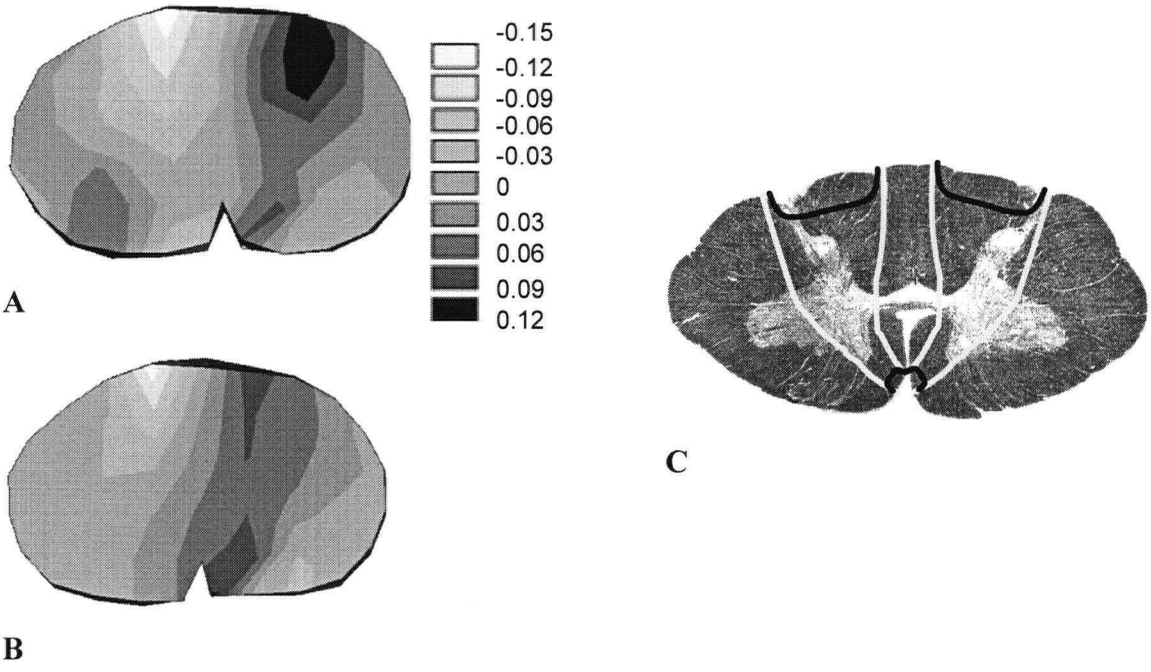

Figure 4.3: Predicted critical areas of strain in spinal cord transverse compression related to tracts in the spinal cord. Sample transverse shear strain distribution for a compression injury at A) the level of the cranial tip of the indentor B) a more caudal level under the indentor. C) Interpretation of the critical areas in compression related to tracts in the spinal cord (Figure modified from Kiernan 1998). Black lines indicate critical regions of strain, while grey lines indicate the load path between critical regions.

Although critical regions of dorsal-ventral and transverse shear strains do not correlate to experimental damage, the load paths of strain contain regions which are known to be damaged experimentally. For example, the central grey matter, ventral portion of the dorsal white funicular matter, and the medial portion of the dorsolateral white matter are contained in the load path and have been found to be damaged experimentally (Blight and Decrescito 1986; Gruner, Yee et al. 1996; Rosenberg and Wrathall 1997). However, damage to the posterior portion of the dorsal columns is not typically observed in

experimental spinal cord compression injury, which was the most critical region of strain in the FE model. This difference highlights the possibility of the preferential damage to the grey matter due to its mechanical or biological susceptibility, relative to that of white matter.

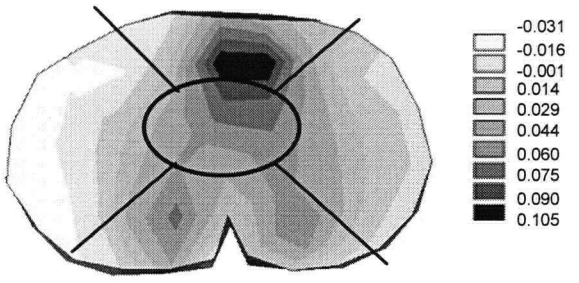

Figure 4.4: Lateral strain distribution in compression at the level of the cranial tip of the indentor

Although not one of the three characteristic strains of compression, the lateral strain was a maximum mean value in the central column (Figure 4.4). The central grey matter, which is injured first in compression injuries, roughly corresponds to the central column in the FE model. Therefore, in terms of the current knowledge of lesions in compressive injuries, the simulated lateral strain in the compression injury was the best indicator of neuronal damage. This parameter was greatest in the central column, in the region beneath the indentor. However, from a transverse section (Figure 4.4) it may be observed that the lateral strains are a maximum in the dorsal column, but due to smaller lateral strains at the lateral edges of the dorsal region, the central column has the maximum mean lateral strain. The damage seen experimentally in the central region may not be due to an increased strain in this region as many other factors may play a role: potential difference in material properties of grey matter, damaged blood supply, and secondary injury. Furthermore, if the spinal cord is assumed to behave as a fluid in a tube of pia mater, rather than a solid, contusion would produce the greatest movement centred in the middle of the tube (Blight and Decrescito 1986). Although nervous tissue does have a fluid element, it also has a solid element, which is represented in this FE model.

This FE model also highlighted the difference between dura mater displacement and cord compression produced in an experimental setting. For the simulated injury, a posterior displacement of 3.6 mm of the dura resulted in displacements of 2.1 mm of the posterior aspect of the spinal cord, due to the geometry and stiffness of the dural sheath. Due to

variation in the profile of the vertebral body, the anterior aspect of the cord displaced 0.5 to 1.6 mm, resulting in an average compression depth of 1.0 mm. This corresponded to a dorsal-ventral compression of 10% with a peak mean von Mises strain of 18% in the dorsal column.

4.5.2 Distraction

Compared to the compression mechanism, there is a scarcity of information regarding the effect of distraction on the vertebral column and cord. Histological and ultrastructural changes have been observed in animals surviving weeks after the injury (Sances, Myklebust et al. 1983; Myklebust, Maiman et al. 1988; Maiman, Myklebust et al. 1989), thus secondary injury would have complicated the effects of the initial mechanical insult. Studies examining the early response to stretching have not specified which columns were most injured; central haemorrhage was observed hours after the injury and evidence of cellular injury in the grey matter, myelin damage, and axonal stretching was demonstrated one day after injury (Myklebust, Maiman et al. 1988). The white matter columns exhibiting damage were not specified, however degeneration of the dorsal and lateral columns was found several weeks after the injury (Myklebust, Maiman et al. 1988).

Characteristic strain components for the distraction injury were axial strain, sagittal shear strain, and lateral strain. The dorsal column experienced the maximum mean absolute axial strain since it was on the most concave side of the initial curvature of the spinal column (Figure 4.5). However, all columns had normalized peak mean absolute strains of greater than 50%, indicating a generally common strain was applied to all columns.

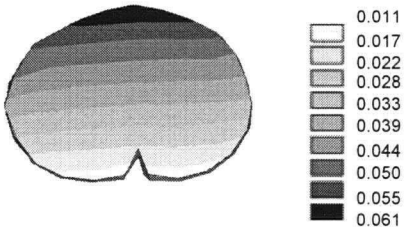

Figure 4.5: Axial strains for a distraction injury

Results from the FE model correlated well to the limited available experimental measures of injury. Regions of critical strain predicted by the FE model may not be compared to experimental findings, since the validation study did not include histological evaluation (Maiman,

Coats et al. 1989). Mild to moderate histological and neurological damage have been demonstrated (using similar methodology) with applied loads three to four times greater than those used in the simulated injury (Maiman, Myklebust et al. 1989). An increase in the disc space was found experimentally and reproduced in the FE model where strains in the disc and spinal ligament elements reached values up to 290%. All spinal cord columns were stretched axially and compressed in the dorsal-ventral and lateral directions. Strains were found to be more continuous along the length of the cord, compared to compression and dislocation in which strains reached a peak value near the imposing structures and reached lower values further away from these structures. This correlated with experimental studies which have found maximum displacements to occur at local levels in a contusion injury, whereas distraction injuries resulted in more extensive displacements and hence more extensive neurological damage (Maiman, Coats et al. 1989; Maiman, Myklebust et al. 1989).

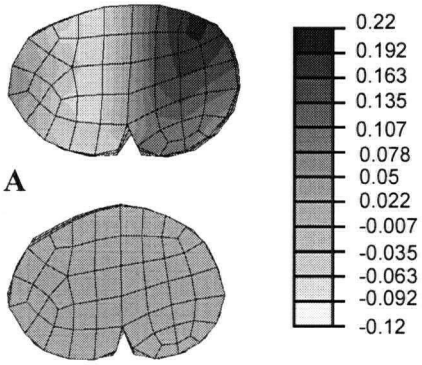

Figure 4.6: Transverse shear strains in 20 mm distraction. A) hyperelastic, B) linear elastic

The hyperelastic study demonstrated that simple uniaxial tension applied to the spinal cord may result in significant shear strains at a local level (Figure 4.6). This effect should be considered in experimental models of SCI induced by axial tension. Observed failures may be due to shearing of axons.

This FE study also highlighted the effect of spinal cord curvature on the distribution of strains in the cord during distraction. Since the ventral and dorsal columns were on the convex and concave side of the curve, respectively, strains were lowest in the ventral column, and largest in the dorsal column. However, this effect was less significant with the use of a hyperelastic material model which more accurately described the behaviour of spinal cord tissue.

4.5.3 Dislocation

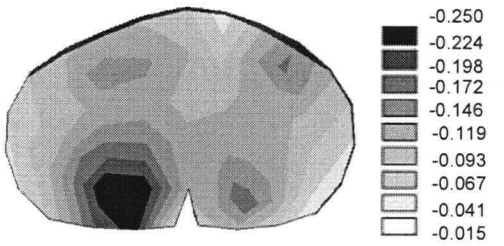

Figure 4.7: Sagittal shear strains at the level of contact with the lamina of C5 for a dislocation injury

Dislocation is not currently employed in producing experimental SCI; therefore comparisons to experimentally produced injuries may not be made. The most characteristic strain component of dislocation injury was the sagittal shear strain. The normalized peak mean sagittal shear strains were greater than 50% in all columns. A transverse section of the cord at the level of contact with the lamina of C5 illustrates critical regions at the ventral and dorsolateral edges of the cord (Figure 4.7). Sagittal shear strains were between 6 and 25% in almost the entire cross-section.

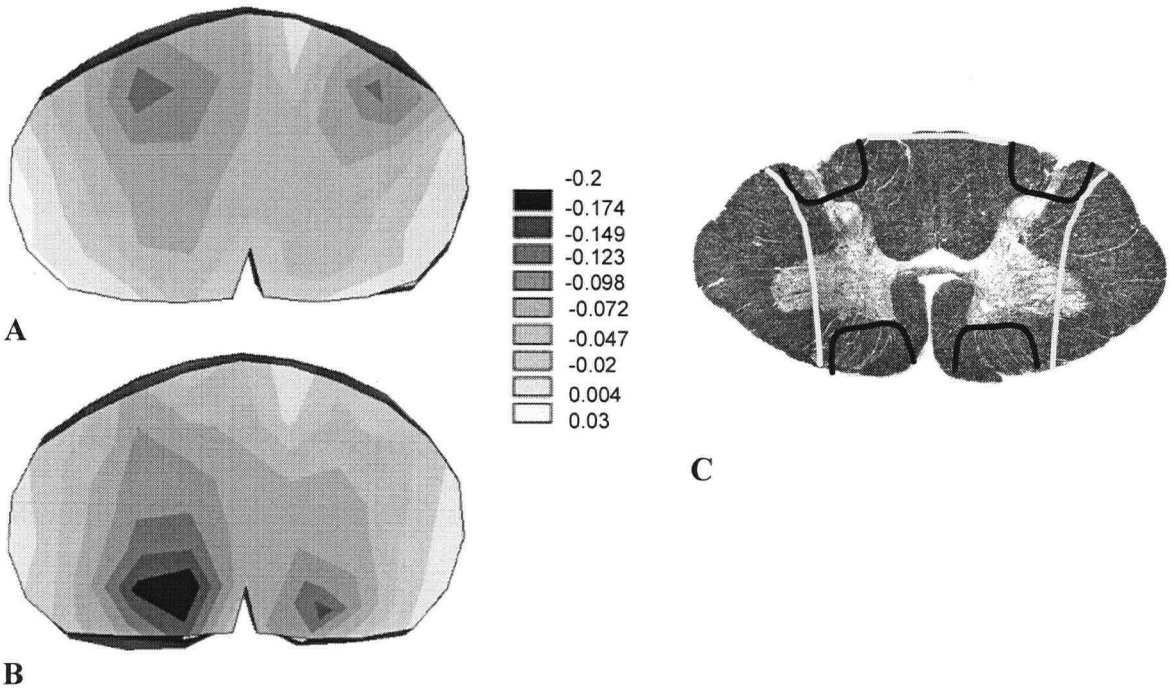

Figure 4.8: Predicted critical areas of dorsal-ventral strain in spinal cord compression related to tracts in the spinal cord. Sample dorsal-ventral strain distributions for a dislocation injury at A) the level of contact with the C5 lamina B) the level of contact with the C6 vertebral body. C) Interpretation of the critical areas in compression related to tracts in the spinal cord (Figure modified from Kiernan 1998). Black lines indicate critical regions of strain, while grey lines indicate the load path between critical regions.

Dorsal-ventral strains were also characteristic of the dislocation injury. Dorsal-ventral strains had normalized peak mean values greater than 50% for the ventral, dorsal, and central columns. Critical regions of dorsal-ventral strain were near the dorsal surface of the cord in the dorsolateral columns at the level of the contacting lamina, and in the ventral funiculus at the level of the contacting vertebral body (Figure 4.8). These regions correspond approximately with the dorsolateral tract of Lissauer (fibres ascending or descending several levels) and the ventral white funiculus, containing ascending and descending fibres. Most of the cross-section of the spinal cord, with the exception of the lateral columns, experiences strains through the load path from the dorsolateral contact points and the ventral contact points.

In comparing the mean strain distributions between columns, the lateral columns experience the least dorsal-ventral strains; however, all columns experienced similar axial and shear strains. These data suggest that the dislocation mechanism applies similar levels of strain to all columns, while the compression mechanism preferentially applies strain to particular columns.

A preliminary study in the Division of Orthopaedic Engineering Research compared experimentally produced contusion (rapid compression) and dislocation injuries with a small sample size. This work was performed by Anthony Choo. The contusion injury was found to have more immediate central grey matter damage, while the dislocation injury seemed to have less grey matter damage at an equal time point. Morphological white matter damage was central, for the contusion injured cords, while in dislocation, damage seemed to be focused in the dorsolateral and ventrolateral regions at the edges of the cord. These regions of damage correspond to critical regions of strain predicted by the finite element model; however further research is experimental required to determine the damaged zones with more certainty.

4.6 Clinical Relevance

Difficulties in determining the injury force vector, the compounding effect of secondary injury progression, and the lack of standards in reporting injured regions of the cord preclude the comparison of clinical results from injuries incurred by the three injury

mechanisms. Autopsy results from patients dying with acute SCI found specimens generally exhibited the most severe traumatic necrosis in the central grey matter and adjoining posterior columns of the cord with preserved continuity of a proportion of the lateral, anterior, and posterior white matter (Kakulas 1984). A review of 22 cases of human SCI found the rat contusion lesion to represent 5 (23%) of those lesions (Bunge, Puckett et al. 1993). Ninety percent of cervical spine injuries may be classified as anterior or central cord syndrome (Bosch, Stauffer et al. 1971).

Relationships between cord syndromes and column injury mechanisms are currently speculative (Allen, Ferguson et al. 1982). Finite element modelling of the spinal cord for various column injury mechanisms may advance understanding of these relationships.

The results of this study indicate that spinal cord compression, distraction, and dislocation result in different strain distributions throughout the cord, which may correspond to different distributions of neurological damage. The compression mechanism targeted tracts of tissue under the indentor, the distraction mechanism stretched all of the tracts similarly, and the dislocation mechanism targeted certain tracts between the two structures impeding the spinal canal, while applying shear strains to all tracts.

Knowledge of the cord regions which are affected by various components of strain may assist in the understanding and treating various types of injuries. At this stage, the tolerances of spinal cord tissue to dorsal-ventral, lateral, and axial strain as well as shear strain are not known. Therefore, it is difficult to conclude which tracts are likely to suffer neurological damage. It is hypothesized that, once the tolerance of spinal cord tissue is known for various modes of loading (i.e. tension, compression, shear), finite element modelling could prove to be indispensable in terms of its ability to predict strain distributions which may relate to neurological damage.

Several other important findings may be considered in terms of their clinical relevance. Mechanical loading of the spinal cord resulted in internal strains that were a function of the imposing structure and of the profile of the opposing surface of the vertebral canal. This implies that the shape of the bony fragment impinging the spinal canal may affect

the peak strains throughout the cord and the final neurological deficit. Results from this study also suggest that dislocation injuries may result in more extensive and widespread shear strains than burst fracture injuries, which result in one-sided contusion to the cord. Furthermore, the effects of distraction on the spinal cord extended over several segments and mechanically affected all columns of the cord. Extensive distraction resulted in local shear strains applied to the cord. Distraction has an important influence on the cord during the application of traction devices and surgical distractive tools; therefore its effect to the internal strains of the cord is of interest.

5 Conclusions

Strain distributions throughout the spinal cord were different for compression, distraction, and dislocation injury mechanisms. Sagittal shear strains were characteristic of all three injury mechanisms, while dorsal-ventral strains were characteristic of compression and dislocation injury mechanisms, and axial strains were characteristic of distraction and dislocation mechanisms. Strains throughout the cord induced by mechanical impact were a function of the imposing structure and of the profile of the opposing surface of the vertebral canal.

For the simulated compression injury, critical regions of strain were the dorsal column of the cord under the indentor (particularly the fasciculus gracilis) and the ventral white funiculus at the level of the opposing vertebral body. The load path between these contacting surfaces also experienced similar levels of strain and included the dorsal, central, and ventral funiculi. Although this distribution corresponded to some extent to damage observed in experimental and clinical settings, differences may be due to factors such as a mechanical or biological susceptibility of grey matter to loading, damaged blood supply, and secondary injury.

FE simulation indicated that tracts on the concave side of the spinal column curvature were most susceptible to damage in distraction, however strain distributions were most evenly spread throughout the columns and the length of the cord for this mechanism. The effects of distraction on the spinal cord extended over several segments and mechanically affected all columns of the cord. Extensive distraction, simulated with a hyperelastic constitutive model, resulted in significant shear strains at a local level. This may be of interest since distraction has an important influence on the cord during the application of traction devices and surgical distractive tools. This effect should be considered in experimental models of SCI induced by axial tension. Observed failures may be due to shearing of axons.

Dislocation of a vertebra resulted in different strain distributions than spinal cord compression. Critical regions of strain were the dorsolateral tracts of the cord

(particularly the dorsolateral tract of Lissauer) at the level of contact with the lamina, and the ventral white funiculus at the level of contact with the vertebral body. The load path between these critical points also experienced similar levels of strain and included the central column. Although the dorsal, ventral, and central columns experienced the greatest strains, all columns experienced similar sagittal shear strain, which was the most characteristic strain component of dislocation injury. Results from this study suggest that dislocation injuries may result in more extensive and widespread shear strains than burst fracture injuries, which result in one-sided contusion of the cord.

Linear elastic and hyperelastic constitutive models produced similar strain distributions (difference of less than 1% strain between each maximum component strain) for axial loading of the spinal cord up to 8% axial strain. Assuming the hyperelastic model best represents the behaviour of spinal cord tissue, the linear elastic model overestimated the range of axial strains and underestimated the dorsal-ventral and transverse shear strains for axial strains between 17 and 33%. The linear elastic model may be used for static FE modelling of the spinal cord at low strain levels (less than 8%). The linear elastic model is not appropriate for static loading of the cord at strains greater than 17%.

5.1 Future Directions

The development of this anatomically accurate FE model of the spinal cord and the surrounding structures provided a useful tool, which may be used in future studies to examine other aspects of SCI. Future studies would benefit from more experimental validation of the model. Several aspects of the model could be validated by different experiments. First, since the strain distributions and loading response is dependent upon variations in the profile of the vertebral canal, it would be ideal to study the spinal cord inside the human cervical spine. The FE model would be easier to validate with a fresh spinal cord from another large mammal (i.e. bovine) placed into a cadaveric cervical spine. Furthermore, a surrogate spinal cord could be useful for validation of this model. However experiments with in vitro or surrogate tissue are limited, since the response of live tissue could not be measured. Similar experiments could be carried out on rats to provide a picture of histological damage.

The next logical step for the model would be to include dynamic loading and material properties, since experimental data is available and no new elements would be required. Rate effects would be of interest to study the dynamic event of injury. Following this step, the grey and white matter should be modelled separately since variation in material properties between these two tissues could significantly affect the mechanical response of the spinal cord. Complications in experimental procedure have thus far precluded the determination of these properties. The interaction between the grey and white matter has not been mechanically defined and may be challenging to model. Nerve roots could also be included in the model as extensions of the dura mater into the IV foramina with link elements attaching the ends of the dura to the foramina. It would also be of interest to validate spinal column kinematics of the model. This would involve modelling contact of the facets and would require more complicated modelling of the IV discs. Several other additions to the model could provide further insight into the strain distributions of the cord during injury such as more complicated material models for the dura mater, a finer mesh of the spinal cord, and the addition of pia mater, nerve roots and rootlets. It would also be of interest to implement a biphasic, or porohyperelastic model for the spinal cord to simulate the motion of fluid within the cord, since both grey and white matter consist largely of water. However, limited knowledge of the required properties exist

Once the regions of the cord under high strain during primary injury are determined, these may be compared with histological results immediately following injury to determine the relationship between strain and tissue damage. These results may help elucidate the tolerance of axons to mechanical strain. This study could begin with the determination of the mechanical parameter most closely linked to damage in spinal cord tissue (i.e. axial tension, shear strain, anteroposterior or lateral strain). Following this knowledge, a maximum strain that may be tolerated by the tissue without resulting in damage may be determined. FE models of injury could then evaluate damage by finding regions of the cord that exhibit strains higher than the maximum tolerable value. These regions in the cord may be substantially different between injury mechanisms; which would imply that interventions and treatment should be targeted to different regions of the cord for different injury mechanisms. For example, contusion or compression may damage the central grey matter, while distraction and dislocation may result in tearing of

axons of the white matter. Targeted therapeutic interventions may then be developed to improve the pharmacological environment to minimize damage to axons and allow them to begin healing themselves. Therefore, finite element modelling has the potential to revolutionize the treatment of SCI.

6 References

Abaqus User's Manual version 6.3 (2002). Hibbitt, Karlsson & Sorensen Inc.

Allen, B. L., Jr., R. L. Ferguson, et al. (1982). "A mechanistic classification of closed, indirect fractures and dislocations of the lower cervical spine." Spine 7(1): 1-27.

Ansys User's Manual version 7.1 (2003). Pennsylvania, Swanson Analysis Inc.

Bain, A. C. and D. F. Meaney (2000). "Tissue-level thresholds for axonal damage in an experimental model of central nervous system white matter injury." J Biomech Eng 122(6): 615-22.

Behrmann, D. L., J. C. Bresnahan, et al. (1992). "Spinal cord injury produced by consistent mechanical displacement of the cord in rats: behavioral and histologic analysis." J Neurotrauma 9(3): 197-217.

Berkowitz, M., P. K. O'Leary, et al. (1998). Spinal Cord Injury: An Analysis of Medical and Social Costs. New York, Demos Medical Publishing, Inc.

Bilston, L. E. (1994). The biomechanics of the spinal cord during traumatic spinal cord injury. Bioengineering. Pennsylvania, University of Pennsylvania: 165.

Bilston, L. E. (1998). Finite Element Analysis of Some Cervical Spinal Cord Injury Modes. International Research Council on the Biomechanics of Impact Conference, Goteborg, Sweden.

Bilston, L. E., Z. Liu, et al. (1997). "Linear viscoelastic properties of bovine brain tissue in shear." Biorheology 34(6): 377-385.

Bilston, L. E., Z. Liu, et al. (2001). "Large strain behaviour of brain tissue in shear: some experimental data and differential constitutive model." Biorheology 38(4): 335-45.

Bilston, L. E. and L. E. Thibault (1996). "The mechanical properties of the human cervical spinal cord in vitro." Ann Biomed Eng 24(1): 67-74.

Blight, A. (1988). "Mechanical factors in experimental spinal cord injury." J Am Paraplegia Soc 11(2): 26-34.

Blight, A. and V. Decrescito (1986). "Morphometric analysis of experimental spinal cord injury in the cat: the relation of injury intensity to survival of myelinated axons." Neuroscience 19(1): 321-341.

Bosch, A., E. S. Stauffer, et al. (1971). "Incomplete traumatic quadriplegia. A ten-year review." Jama 216(3): 473-8.

Bozic, K. J., J. H. Keyak, et al. (1994). "Three-dimensional finite element modeling of a cervical vertebra: an investigation of burst fracture mechanism." J Spinal Disord 7(2): 102-10.

Breig, A. (1960). Biomechanics of the Central Nervous System. Chicago, The Year Book Publishers, Inc.

Breig, A. (1970). "Overstretching of and circumscribed pathological tension in the spinal cord--a basic cause of symptoms in cord disorders." J Biomech 3(1): 7-9.

Bresnahan, J. C., M. S. Beattie, et al. (1991). "Three-dimensional computer-assisted analysis of graded contusion lesions in the spinal cord of the rat." J Neurotrauma 8(2): 91-101.

Bresnahan, J. C., M. S. Beattie, et al. (1987). "A behavioral and anatomical analysis of spinal cord injury produced by a feedback-controlled impaction device." Exp Neurol 95(3): 548-70.

Brown, T., R. J. Hansen, et al. (1957). "Some mechanical tests on the lumbosacral spine with particular reference to the intervertebral disc." J Bone Joint Surg Am 39-A(5): 1135-1164.

Bunge, R. P., W. R. Puckett, et al. (1993). "Observations on the pathology of human spinal cord injury. A review and classification of 22 new cases with details from a case of chronic cord compression with extensive focal demyelination." Adv Neurol 59: 75-89.

Carlson, G. D., K. E. Warden, et al. (1997). "Viscoelastic relaxation and regional blood flow response to spinal cord compression and decompression." Spine 22(12): 1285-91.

Cezayirlioglu, H., E. Bahniuk, et al. (1985). "Anisotropic yield behavior of bone under combined axial force and torque." J Biomech 18(1): 61-9.

Chang, G. L., T. K. Hung, et al. (1981). "Stress-strain measurement of the spinal cord of puppies and their neurological evaluation." J Trauma 21(9): 807-10.

Chang, G. L., T. K. Hung, et al. (1988). "An in-vivo measurement and analysis of viscoelastic properties of the spinal cord of cats." J Biomech Eng 110(2): 115-22.

Chazal, J., A. Tanguy, et al. (1985). "Biomechanical properties of spinal ligaments and a histological study of the supraspinal ligament in traction." J Biomech 18(3): 167-76.

Clausen, J. D., V. K. Goel, et al. (1997). "Uncinate processes and Luschka joints influence the biomechanics of the cervical spine: quantification using a finite element model of the C5-C6 segment." J Orthop Res 15(3): 342-7.

Cusick, J. F., J. Myklebust, et al. (1982). "Effects of vertebral column distraction in the monkey." J Neurosurg 57(5): 651-9.

Cusick, J. F. and N. Yoganandan (2002). "Biomechanics of the cervical spine 4: major injuries." Clin Biomech (Bristol, Avon) 17(1): 1-20.

Dall, D. M. (1972). "Injuries of the cervical spine. I. Does the type of bony injury affect spinal cord recovery?" S Afr Med J 46(30): 1048-56.

De Jager, M., A. A. Sauren, et al. (1996). A global and detailed mathematical model for head-neck dynamics. 40th Stapp Car Crash Conference, Society of Automotive Engineers.

Dekutoski, M. and A. A. Cohen-Gadol (2003). Distractive Flexion Cervical Spine Injuries: A Clinical Spectrum. Fractures of the Cervical, Thoracic, and Lumbar Spine. A. R. Vaccaro. New York, Marcel-Dekker, Inc.: 751.

DeVivo, M. J., R. D. Rutt, et al. (1992). "Trends in spinal cord injury demographics and treatment outcomes between 1973 and 1986." Arch Phys Med Rehabil 73(5): 424-30.

Dixon, G. S., J. N. Danesh, et al. (1993). "Epidemiology of spinal cord injury in New Zealand." Neuroepidemiology 12(2): 88-95.

Donnelly, B. and J. Medige (1997). "Shear properties of human brain tissue." J Biomech Eng 119: 423-432.

Dryden, D. M., L. D. Saunders, et al. (2003). "The epidemiology of traumatic spinal cord injury in Alberta, Canada." Can J Neurol Sci 30(2): 113-21.

Evans, F. G. (1973). Mechanical Properties of Bone. Springfield, Illinois, Charles C Thomas.

Fehlings, M. G. and C. H. Tator (1995). "The relationships among the severity of spinal cord injury, residual neurological function, axon counts, and counts of retrogradely labeled neurons after experimental spinal cord injury." Exp Neurol 132(2): 220-8.

Fenech, C. M. and T. M. Keaveny (1999). "A cellular solid criterion for predicting the axial-shear failure properties of bovine trabecular bone." J Biomech Eng 121(4): 414-22.

Fife, D. and J. Kraus (1986). "Anatomic location of spinal cord injury. Relationship to the cause of injury." Spine 11(1): 2-5.

Fiford, R. J. and L. B. Bilston (1998). "Strain distribution and relaxation behaviour of rat spinal cord." Advances is Bioengineering (ASME) 39: 247-248.

Firoozbakhsh, K. K. and C. N. DeSilva (1975). "A model of brain shear under impulsive torsional loads." J Biomech 8(1): 65-73.

Gadea-Ciria, M., J. Gervas-Camacho, et al. (1975). "Water contents of various regions of the feline nervous system." Med Biol 53(6): 469-74.

Galbraith, J. A., L. E. Thibault, et al. (1993). "Mechanical and electrical responses of the squid giant axon to simple elongation." J Biomech Eng 115(1): 13-22.

Galford, J. E. and J. H. McElhaney (1970). "A viscoelastic study of scalp, brain, and dura." Journal of Biomechanics 3: 211-221.

Gerber, A. M. and W. S. Corrie (1979). "Effect of impounder contact area on experimental spinal cord injury." J Neurosurg 51(4): 539-42.

Girardi, F. P., S. N. Khan, et al. (2000). "Advances and strategies for spinal cord regeneration." Orthop Clin North Am 31(3): 465-72.

Goel, V. K. and J. D. Clausen (1998). "Prediction of load sharing among spinal components of a C5-C6 motion segment using the finite element approach." Spine 23(6): 684-91.

Goel, V. K. and G. O. Njus (1986). Stress-strain characteristic of spinal ligaments. Transactions of the 32nd annual meeting of the Orthopaedic Research Society, New Orleans, LA, Orthopaedic Research Society.

Griffin, M. R., W. M. O'Fallon, et al. (1985). "Mortality, survival and prevalence: traumatic spinal cord injury in Olmsted County, Minnesota, 1935-1981." J Chronic Dis 38(8): 643-53.

Griffin, M. R., J. L. Opitz, et al. (1985). "Traumatic spinal cord injury in Olmsted County, Minnesota, 1935-1981." Am J Epidemiol 121(6): 884-95.

Gruner, J. A., A. K. Yee, et al. (1996). "Histological and functional evaluation of experimental spinal cord injury: evidence of a stepwise response to graded compression." Brain Res 729: 90-101.

Guillaume, A., D. Osmont, et al. (1997). "Effects of Perfusion on the mechanical behaviour of the brain exposed to hypergravity." J Biomech 30(4): 383-389.

Halldin, P. H., K. Brolin, et al. (2000). "Investigation of Conditions that affect neck compression-flexion injuries using numerical techniques." Stapp Car Crash Journal 44: 127-138.

Hayashi, K., T. Yabuki, et al. (1977). "The anterior and the posterior longitudinal ligaments of the lower cervical spine." J Anat 124(3): 633-6.

Hirano, A. (1970). Neurofibrillary changes in conditions related to Alzheimer's disease. Alzheimer's Disease and RElated Conditions: A Ciba Founddation Symposium. W. G.E.W. and M. O'Connor. London, Churchill: 185-207.

Hirano, A. and J. F. Llena (1995). Morphology of central nervous system axons. The Axon. S. G. Waxman, J. D. Kocsis and P. K. Stys. New York, Oxford University Press: 49-67.

Holbourn, A. H. S. (1944). "The mechanics of trauma with special reference to herniation of cerebral tissue." J Neurosurg 1: 190-200.

Hosey, R. R. and Y. K. Liu (1982). A homeomorphic finite element model of the human head and neck. Finite Elements in Biomechanics. R. H. Gallagher, B. R. Simon, P. C. Johnson and J. F. Gross. New York, John Wiley & Sons, Ltd: 379-401.

Hung, T. K. and G. L. Chang (1981). "Biomechanical and neurological response of the spinal cord of a puppy to uniaxial tension." J Biomech Eng 103(1): 43-7.

Hung, T. K., G. L. Chang, et al. (1981). "Stress-strain relationship and neurological sequelae of uniaxial elongation of the spinal cord of cats." Surg Neurol 15(6): 471-6.

Hung, T. K., G. L. Chang, et al. (1987). "Studying animals to understand spinal cord injuries." SOMA: 40-44.

Hung, T. K., G. L. Chang, et al. (1981). "Stress-strain relationship of the spinal cord of anesthetized cats." J Biomech 14(4): 269-76.

Hung, T. K., H. S. Lin, et al. (1979). "The standardization of experimental impact injury to the spinal cord." Surg Neurol 11(6): 470-7.

Hung, T. K., H. S. Lin, et al. (1982). "Mechanical and neurological response of cat spinal cord under static loading." Surg Neurol 17(3): 213-7.

Ichihara, K., T. Taguchi, et al. (2003). "Mechanism of the spinal cord injury and the cervical spondylotic myelopathy: new approach based on the mechanical features of the spinal cord white and gray matter." J Neurosurg 99(3 Suppl): 278-85.

Ichihara, K., T. Taguchi, et al. (2001). "Gray matter of the bovine cervical spinal cord is mechanically more rigid and fragile than the white matter." J Neurotrauma 18(3): 361-7.

Jorst, R. and G. N. Nurick (1996). "Development of a finite element model of the human." International Journal of Crashworthiness 5(3): 259-69.

Kahn, E. A. (1947). "The role of dentate ligaments in spinal cord compression." J Neurosurg 4: 191-9.

Kakulas, B. A. (1984). "Pathology of spinal injuries." Cent Nerv Syst Trauma 1(2): 117-29.

Kearney, P. A., S. A. Ridella, et al. (1988). "Interaction of contact velocity and cord compression in determining the severity of spinal cord injury." J Neurotrauma 5(3): 187-208.

Keaveny, T. M., E. F. Wachtel, et al. (1999). "Application of the Tsai-Wu quadratic multiaxial failure criterion to bovine trabecular bone." J Biomech Eng 121(1): 99-107.

Keyak, J. H. and S. A. Rossi (2000). "Prediction of femoral fracture load using finite element models: an examination of stress- and strain-based failure theories." J Biomech 33(2): 209-14.

Kiernan, J. A. (1998). Barr's The Human Nervous System, seventh edition. Philadelphia, Lippincott Williams & Wilkins.

King, A. I., J. S. Ruan, et al. (1995). "Recent advances in biomechanics of brain injury research: a review." J Neurotrauma 12(4): 651-8.

Kraus, J. F., C. E. Franti, et al. (1975). "Incidence of traumatic spinal cord lesions." J Chronic Dis 28(9): 471-92.

Kubo, Y., S. Waga, et al. (1994). "Microsurgical anatomy of the lower cervical spine and cord." Neurosurgery 34(5): 895-90; discussion 901-2.

Kumaresan, S. and S. Radhakrishnan (1996). "Importance of partitioning membranes of the brain and the influence of the neck in head injury modelling." Med Biol Eng Comput 34(1): 27-32.

Kumaresan, S., N. Yoganandan, et al. (1999). "Finite element analysis of the cervical spine: a material property sensitivity study." Clin Biomech (Bristol, Avon) 14(1): 41-53.

Kwon, B. K., T. R. Oxland, et al. (2002). "Animal Models Used in Spinal Cord Regeneration Research." Spine 27(14): 1504-1510.

Lee, C. K., Y. E. Kim, et al. (2000). "Impact response of the intervertebral disc in a finite-element model." Spine 25(19): 2431-9.

Levine, D. N. (1997). "Pathogenesis of cervical spondylotic myelopathy." J Neurol Neurosurg Psychiatry 62: 334-340.

Lin, H. S., Y. K. Liu, et al. (1978). "Mechanical response of the lumbar intervertebral joint under physiological (complex) loading." J Bone Joint Surg Am 60(1): 41-55.

Lotz, J. C., E. J. Cheal, et al. (1991). "Fracture prediction for the proximal femur using finite element models: Part I--Linear analysis." J Biomech Eng 113(4): 353-60.

Maiman, D. J., J. Coats, et al. (1989). "Cord/spine motion in experimental spinal cord injury." J Spinal Disord 2(1): 14-9.

Maiman, D. J., J. B. Myklebust, et al. (1989). "Experimental spinal cord injury produced by axial tension." J Spinal Disord 2(1): 6-13.

Marar, B. C. (1974). "The pattern of neurological damage as an aid to the diagnosis of the mechanism in cervical-spine injuries." J Bone Joint Surg Am 56(8): 1648-54.

Markolf, K. L. (1972). "Deformation of the thoracolumbar intervertebral joints in response to external loads: a biomechanical study using autopsy material." J Bone Joint Surg Am 54(3): 511-33.

Maurel, N., F. Lavaste, et al. (1997). "A three-dimensional parameterized finite element model of the lower cervical spine. Study of the influence of the posterior articular facets." J Biomech 30(9): 921-31.

McElhaney, J. H., J. W. Melvin, et al. (1973). "Dynamic characteristics of the tissues of the head." Perspectives in Biomedical Engineering: 215-222.

Mendis, K., R. Stalnaker, et al. (1995). "A constitutive relationship for large deformation finite element modeling of brain tissue." J Biomech Eng 117: 279-285.

Mercer, S. and N. Bogduk (1999). "The ligaments and annulus fibrosus of human adult cervical intervertebral discs." Spine 24(7): 619-26; discussion 627-8.

Metz, H., J. McElhaney, et al. (1970). "A comparison of the elasticity of live, dead, and fixed brain tissue." J Biomech 3: 453-458.

Miller, K. (1999). "Constitutive model of brain tissue suitable for finite element analysis of surgical procedures." J Biomech 32(5): 531-7.

Miller, K. and K. Chinzei (2002). "Mechanical properties of brain tissue in tension." J Biomech 35(4): 483-90.

Miller, K., K. Chinzei, et al. (2000). "Mechanical properties of brain tissue in-vivo: experiment and computer simulation." J Biomech 33(11): 1369-76.

Mooney, M. (1940). "A theory of large elastic deformation." J Applied Physics 11: 582-592.

Moore, K. L. and A. F. Dalley (1999). Clinically oriented anatomy. Philadelphia, Lippincott Williams & Wilkins.

Moroney, S. P., A. B. Schultz, et al. (1988). "Load-displacement properties of lower cervical spine motion segments." J Biomech 21(9): 769-79.

Myers, B. S. and B. A. Winkelstein (1995). "Epidemiology, classification, mechanism, and tolerance of human cervical spine injuries." Crit Rev Biomed Eng 23(5-6): 307-409.

Myklebust, J. B., J. F. Cusick, et al. (1986). Closed distraction spinal cord injury model. Mechanisms of Head and Spine Trauma. A. Sances, Jr., D. Thomas, C. Ewing, S. J. Larson and F. Unterharnscheidt. New York, Aloray, Inc.: 441-475.

Myklebust, J. B., D. J. Maiman, et al. (1988). "Axial tension model of spinal cord injury." J Am Paraplegia Soc 11(2): 50-5.

Myklebust, J. B., F. Pintar, et al. (1988). "Tensile strength of spinal ligaments." Spine 13(5): 526-31.

Nachemson, A. L. and J. H. Evans (1968). "Some mechanical properties of the third lumbar inter-laminar ligament (ligamentum flavum)." J Biomech 1: 211-220.

Nauta, H. J., E. Dolan, et al. (1983). "Microsurgical anatomy of spinal subarachnoid space." Surg Neurol 19(5): 431-7.

Neumann, P., T. S. Keller, et al. (1994). "Effect of strain rate and bone mineral on the structural properties of the human anterior longitudinal ligament." Spine 19(2): 205-11.

Ng, H. W. and E. C. Teo (2001). "Nonlinear finite-element analysis of the lower cervical spine (C4-C6) under axial loading." J Spinal Disord 14(3): 201-10.

Noyes, D. H. (1987). "Correlation between parameters of spinal cord impact and resultant injury." Exp Neurol 95(3): 535-47.

Noyes, D. H. (1987). "Electromechanical impactor for producing experimental spinal cord injury in animals." Med Biol Eng Comput 25(3): 335-40.

O'Connor, P. (2002). "Incidence and patterns of spinal cord injury in Australia." Accid Anal Prev 34(4): 405-15.

Ommaya, A. K. (1968). "Mechanical properties of tissues of the nervous system." J Biomech 1: 127-138.

Ozawa, H., T. Matsumoto, et al. (2001). "Comparison of spinal cord gray matter and white matter softness: measurement by pipette aspiration method." J Neurosurg 95(2 Suppl): 221-4.

Pamidi, M. R. and S. H. Advani (1978). "Nonlinear constitutive relations for human brain tissue." J Biomech Eng 100: 44-48.

Panjabi, M. and A. White, 3rd (1988). "Biomechanics of nonacute cervical spinal cord trauma." Spine 13(7): 838-42.

Panjabi, M. M., T. R. Oxland, et al. (1991). "Quantitative anatomy of cervical spine ligaments. Part II. Middle and lower cervical spine." J Spinal Disord 4(3): 277-85.

Panjabi, M. M., D. J. Summers, et al. (1986). "Three-dimensional load-displacement curves due to forces on the cervical spine." J Orthop Res 4(2): 152-61.

Panjabi, M. M. and A. A. White, 3rd (1980). "Basic biomechanics of the spine." Neurosurgery 7(1): 76-93.

Park, J. B. and R. S. Lakes (1992). Biomaterials: An Introduction. New York, Plenum Press.

Parkin, I. G. and G. R. Harrison (1985). "The topographical anatomy of the lumbar epidural space." J Anat 141: 211-7.

Patin, D. J., E. C. Eckstein, et al. (1993). "Anatomic and biomechanical properties of human lumbar dura mater." Anesth Analg 76(3): 535-40.

Pech, P., K. Bergstrom, et al. (1987). "Attenuation values, volume changes and artifacts in tissue due to freezing." Acta Radiol 28(6): 779-82.

Peters, G., J. Meulman, et al. (1997). "The applicability of the time/temperature superposition principle to brain tissue." Biorheology 34(2): 127-138.

Pickett, W., K. Simpson, et al. (2003). "Traumatic spinal cord injury in Ontario, Canada. The epidemiology of traumatic spinal cord injury in Alberta, Canada." J Trauma 55(6): 1070-6.

Pintar, F. A., N. Yoganandan, et al. (1992). "Biomechanical properties of human lumbar spine ligaments." J Biomech 25(11): 1351-6.

Przybylski, G. J., G. J. Carlin, et al. (1996). "Human anterior and posterior cervical longitudinal ligaments possess similar tensile properties." J Orthop Res 14(6): 1005-8.

Przybylski, G. J., P. R. Patel, et al. (1998). "Quantitative anthropometry of the subatlantal cervical longitudinal ligaments." Spine 23(8): 893-8.

Rabin, Y., M. J. Taylor, et al. (1998). "Thermal expansion measurements of frozen biological tissues at cryogenic temperatures." J Biomech Eng 120(2): 259-66.

Reid, D. C. and L. Saboe (1989). "Spine fractures in winter sports." Sports Med 7(6): 393-9.

Reid, J. D. (1960). "Effects of flexion-extension movements of the head and spine upon the spinal cord and nerve roots." J Neurol Neurosurg Psychiatry 23: 214-221.

Rosenberg, L. J. and J. R. Wrathall (1997). "Quantitative analysis of acute axonal pathology in experimental spinal cord contusion." J Neurotrauma 14(11): 823-38.

Runza, M., R. Pietrabissa, et al. (1999). "Lumbar dura mater biomechanics: experimental characterization and scanning electron microscopy observations." Anesth Analg 88(6): 1317-21.

Sahay, K. B., R. Mehrotra, et al. (1992). "Elastomechanical characterization of brain tissues." J Biomech 25(3): 319-26.

Saito, T., T. Yamamuro, et al. (1991). "Analysis and prevention of spinal column deformity following cervical laminectomy. I. Pathogenetic analysis of postlaminectomy deformities." Spine 16(5): 494-502.

Sances, A., Jr., J. B. Myklebust, et al. (1983). Pathophysiology of cervical injuries. Proc. 26th Stapp Car Crash Conf, Warrendale, PA, Society of Automotive Engineers.

Sances, A., Jr., J. B. Myklebust, et al. (1984). "The biomechanics of spinal injuries." Crit Rev Biomed Eng 11(1): 1-76.

Scapinelli, R. (1990). "Anatomical and radiologic studies on the lumbosacral meningo-vertebral ligaments of humans." J Spinal Disord 3(1): 6-15.

Schneider, R. C., G. Cherry, et al. (1954). "The syndrome of acute central cervical spinal cord injury." J Neurosurg 20: 546-77.

Scifert, J., K. Totoribe, et al. (2000). Spinal cord deformation in flexion and extension - a finite element study. 22nd Annual EMBS International Conference, Chicago, IL.

Scion Image for Windows (2000). Frederick MD, Scion Corporation.

Sekhon, L. H. and M. G. Fehlings (2001). "Epidemiology, demographics, and pathophysiology of acute spinal cord injury." Spine 26(24 Suppl): S2-12.

Shields, C. L., J. M. Fox, et al. (1978). "Cervical cord injuries in sports." The physician and sports medicine 6(9): 71-76.

Shinomiya, K., T. Sato, et al. (1995). "Isolated muscle atrophy of the distal upper extremity in cervical spinal cord compressive disorders." J Spinal Disord 8(4): 311-6.

Shuck, L. and S. Advani (1972). "Rheological response of human brain tissue in shear." J Bas Eng 94: 905-911.

Silberstein, M. and K. McLean (1994). "Non-contiguous spinal injury: clinical and imaging features, and postulated mechanism." Paraplegia 32(12): 817-23.

Simpson, J. M., D. Sutton, et al. (1994). Traumatic injuries to the adult lower cervical spine. Surgery of the cervical spine. H. S. An and J. M. Simpson. Baltimore, Williams & Wilkins.

Smith, D. H., J. A. Wolf, et al. (1999). "High tolerance and delayed elastic response of cultured axons to dynamic stretch injury." J Neuroscience 19(11): 4263-4269.

Somerson, S. K. and B. T. Stokes (1987). "Functional analysis of an electromechanical spinal cord injury device." Exp Neurol 96(1): 82-96.

Spencer, D. L., G. S. Irwin, et al. (1983). "Anatomy and significance of fixation of the lumbosacral nerve roots in sciatica." Spine 8(6): 672-9.

Spitzer, V., M. J. Ackerman, et al. (1996). "The visible human male: a technical report." J Am Med Inform Assoc 3(2): 118-30.

Stokes, B. T., D. H. Noyes, et al. (1992). "An electromechanical spinal injury technique with dynamic sensitivity." J Neurotrauma 9(3): 187-95.

Stokes, B. T. and P. J. Reier (1992). "Fetal grafts alter chronic behavioral outcome after contusion damage to the adult rat spinal cord." Exp Neurol 116(1): 1-12.

Tator, C. H. (1983). "Spine-spinal cord relationships in spinal cord trauma." Clin Neurosurg 30: 479-94.

Tator, C. H., E. G. Duncan, et al. (1993). "Changes in epidemiology of acute spinal cord injury from 1947 to 1981." Surg Neurol 40(3): 207-15.

Tencer, A. F., B. L. Allen, Jr., et al. (1985). "A biomechanical study of thoracolumbar spine fractures with bone in the canal. Part III. Mechanical properties of the dura and its tethering ligaments." Spine 10(8): 741-7.

Tsai, S. W. and E. M. Wu (1971). "A general theory of strength for anisotropic materials." J Comp Mater 5: 58-80.

Tunturi, A. R. (1977). "Elasticity of the spinal cord dura in the dog." J Neurosurg 47: 391-396.

Tunturi, A. R. (1978). "Elasticity of the spinal cord, pia, and denticulate ligament in the dog." J Neurosurg 48: 975-979.

Tunturi, A. R. (1980). "Viscoelasticity of dog spinal cord." Physiol Chem Phys 12(4): 373-8.

Ugural, A. C. and S. K. Fenster (1995). Advanced Strength and Applied Elasticity. Upper Saddle River, New Jersey, Prentice-Hall PTR.

Vaccaro, A. R. (2003). Fractures of the cervical, thoracic, and lumbar spine. New York, Marcel Dekker, Inc.

Van der Horst, M. J., J. G. M. Thunnissen, et al. (1997). The influence of muscle activity on head-neck response during impact. 41st Stapp Car Crash Conference, Warrendale PA, Society of Automotive Engineers.

van Noort, R., M. M. Black, et al. (1981). "A study of the uniaxial mechanical properties of human dura mater preserved in glycerol." Biomaterials 2(1): 41-5.

van Noort, R., T. R. Martin, et al. (1981). "The mechanical properties of human dura mater and the effects of storage media." Clin Phys Physiol Meas 2(3): 197-203.

Voo, L. M., S. Kumaresan, et al. (1997). "Finite element analysis of cervical facetectomy." Spine 22(9): 964-9.

Wang, H. C. and A. S. Wineman (1972). "A mathematical model for the determination of viscoelastic behavior of brain in vivo. II. Relaxation response." J Biomech 5(6): 571-80.

Ward, C. C., P. E. Nikravesh, et al. (1978). "Biodynamic finite element models used in brain injury research." Aviat Space Environ Med 49(1 Pt. 2): 136-42.

White, A. and M. Panjabi (1990). Clinical Biomechanics of the Spine. Philadelphia, Lippincott.

Whyne, C. M., S. S. Hu, et al. (2003). "Burst fracture in the metastatically involved spine: development, validation, and parametric analysis of a three-dimensional poroelastic finite-element model." Spine 28(7): 652-60.

Wilcox, R. K., L. E. Bilston, et al. (2003). "Mathematical model for the viscoelastic properties of dura mater." J Orthop Sci 8(3): 432-4.

Wiltse, L. L., A. S. Fonseca, et al. (1993). "Relationship of the dura, Hofmann's ligaments, Batson's plexus, and a fibrovascular membrane lying on the posterior surface of the vertebral bodies and attaching to the deep layer of the posterior longitudinal ligament. An anatomical, radiologic, and clinical study." Spine 18(8): 1030-43.

Wrathall, J. R. (1992). "Spinal cord injury models." J Neurotrauma 9(Suppl 1): S129-34.

Yamada, H. (1970). Strength of Biological Materials. Baltimore, The Williams & Wilkins Company.

Yoganandan, N., M. Haffner, et al. (1989). Epidemiology and injury biomechanics of motor vehicle related trauma to the human spine. 33rd Stapp Car Crash Conference, Washington, D.C., Society of Automotive Engineers.

Yoganandan, N., S. Kumaresan, et al. (2000). "Geometric and mechanical properties of human cervical spine ligaments." J Biomech Eng 122(6): 623-9.

Yoganandan, N., S. Kumaresan, et al. (1996). "Finite element applications in human cervical spine modeling." Spine 21(15): 1824-34.

Yoganandan, N., S. C. Kumaresan, et al. (1996). "Finite element modeling of the C4-C6 cervical spine unit." Med Eng Phys 18(7): 569-74.

Yoganandan, N., D. Maiman, et al. (1990). "Cervical Spine Injuries from Motor Vehicle Accidents." J Clinical Engineering 15(6): 505-513.

Yoganandan, N., F. Pintar, et al. (1989). "Dynamic response of human cervical spine ligaments." Spine 14(10): 1102-10.

Yoganandan, N., L. Voo, et al. (1995). Finite element analysis of the cervical spine. Proceedings of Prevention Through Biomechanics Symposium, Detroit, Michigan, Wayne State University.

Young, W. (2002). "Spinal cord contusion models." Prog Brain Res 137: 231-55.

7 Glossary

Terms defining relative positions (Figure 7.1):

Anterior/Ventral – nearer to the front surface of the body

Posterior/Dorsal – nearer to the back of the body

Superior/Cranial – nearer to the topmost point of the body

Inferior/Caudal – nearer to the lowermost point of the body

Medial – nearer to the median plane of the body

Lateral – farther from the median plane of the body

Proximal – nearer the attachment or origin of a limb or structure

Distal – further from the attachment or origin of a limb or structure

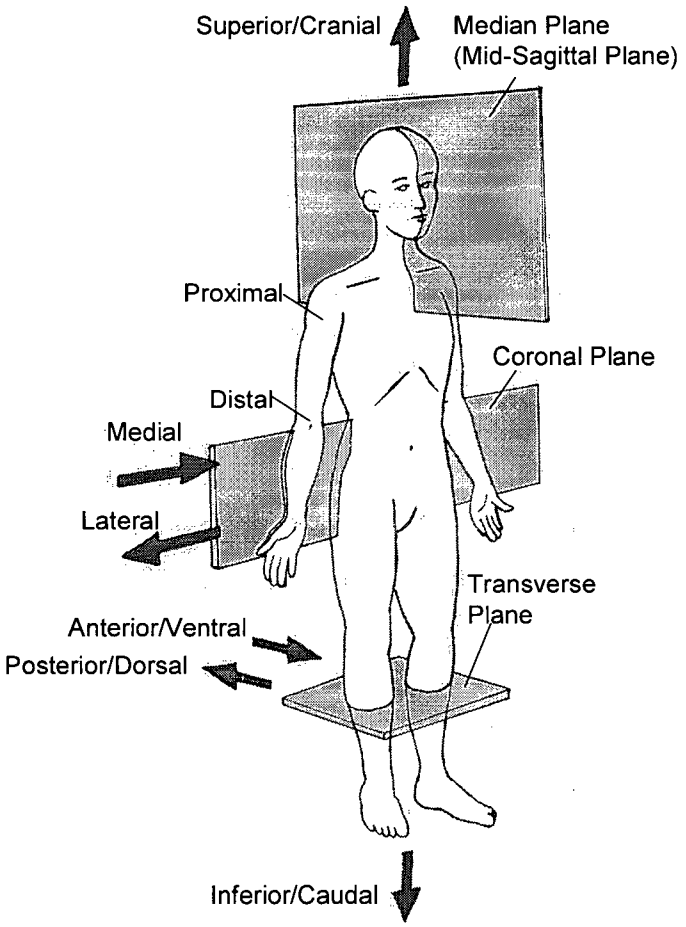

Figure 7.1: Description of anatomical terms

Anatomical Planes (Figure 7.1):

Median Plane – vertical plane passing longitudinally through the body, dividing it into left and right halves

Sagittal Planes – vertical planes parallel to the median plane

Coronal Planes – vertical planes passing longitudinally through the body, perpendicular to the median plane, dividing the body into front and back halves

Transverse Planes – horizontal planes passing through the body, perpendicular to the sagittal and coronal planes

Terms of Laterality:

Ipsilateral – occurring on the same side of the body

Contralateral – occurring on the opposite side of the body

Terms of Movement in reference to the cervical spine (Figure 7.2):

Flexion – movement occurring in an anterior direction

Extension – movement occurring in a posterior direction

Axial Rotation – turning of the head to the left or right side

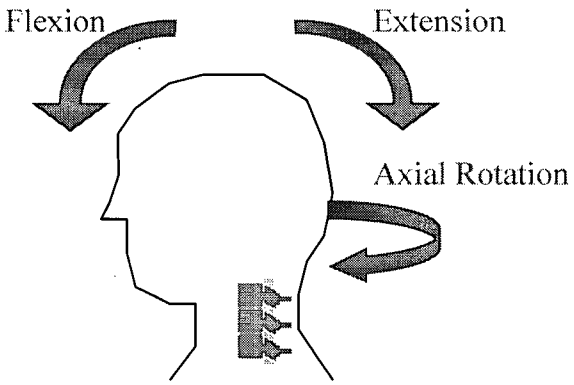

Figure 7.2: Terms of movement in the cervical spine

8 Appendices

Appendix A – Spinal Cord Contusion Experiments

Table A.1 Summary of sample spinal cord contusion experiments

	(Noyes 1987)	(Bresnahan, Beattie et al. 1987)	(Somerson and Stokes 1987)	(Stokes and Reier 1992)	(Stokes, Noyes, et al. 1992)
Species	Albino rats	Albino rats	Sprague-Dawley rats	Sprague-Dawley rats	Rodent
Number	17	24	not reported	21	not reported
Weight	136-259 g	136-325 g	250-375 g	250-375 g	not reported
Sex	Female	Female	Female	not reported	not reported
Age	Adult	Adult	Adult	Adult	not reported
Anesthetic	4% chloral hydrate, 2% magnesium sulphate, 1% sodium pentobarbital	4% choral hydrate, 2% MgSO4, 1% sodium pentobarbital	Ketamine HCl (60mg/kg), xylazine (10mg/kg)	HCl (80mg/kg), xylazine (10mg/kg)	Routinely anesthetized
Laminec-tomy	T6	T6, dura intact	T9, cord exposed by dural reflection	T8-T9, dura intact	T9, dura intact
Support	Pins inserted through paravertebral muscles and interspinous ligaments, pins attached to metal frame, rat in sling	2 18 gauge needles inserted in paravertebral muscles and interspinous ligaments, pins attached to metal frame, rat in sling	Spinal frame, clamps on spinous processes T8 & T10	Dorsal processes fixed (ref Somerson & Stokes 1987)	Allis clamps on spinous processes T8, T10 (part of spinal frame). Spinal frame is mounted on a machine tool table
Indentor tip	MMA, circular flat surface 2mm diameter	MMA, circular flat surface 2mm diameter		$7mm^2$	
Electromag netic driver	20-W speaker	20-W speaker	20-W speaker	Ling Shaker V203/S	Ling Shaker V203/S

	(Noyes 1987)	(Bresnahan, Beattie et al. 1987)	(Somerson and Stokes 1987)	(Stokes and Reier 1992)	(Stokes, Noyes, et al. 1992)
Force transducer	Semiconductor strain gauge	Semiconductor strain gauge	Semiconductor strain gauge		Piezoelectric
Disp. transducer	Non-contacting (KD-2300-8C, Kaman Sciences Corp)	Non-contacting	Non-contacting (KD-2300-8C, Kaman Sciences Corp)	Target device from Kaman instruments inc	Non-contacting (KD-2300-8C, Kaman Sciences Corp)
Dimpling force		0.01-0.015 N	0.01-0.015 N	0.03 N	0.03 N

Appendix B – Material Model Fit

Uniaxial test data for the model fit was obtained from experiments performed by Bilston (Bilston and Thibault 1996). Samples of human spinal cord tissue were acquired less than 24 hr from death. Twelve samples 3-7 cm in length were maintained at 100% humidity until testing. Before testing, the dura mater was removed and nerve roots were trimmed. The ends of the samples were fixed by drying and fixing to plastic plates with adhesive. Samples were loaded at 5 mm/min to a preload of 0.5 N. The testing protocol involved elongating specimens to preset maximum strains at set strain rates between 0.04 and 0.24 /s. Sample stress-strain curves were published for three strain rates. The slowest rate was selected for this FE model (0.048 /s), since static loading cases were examined.

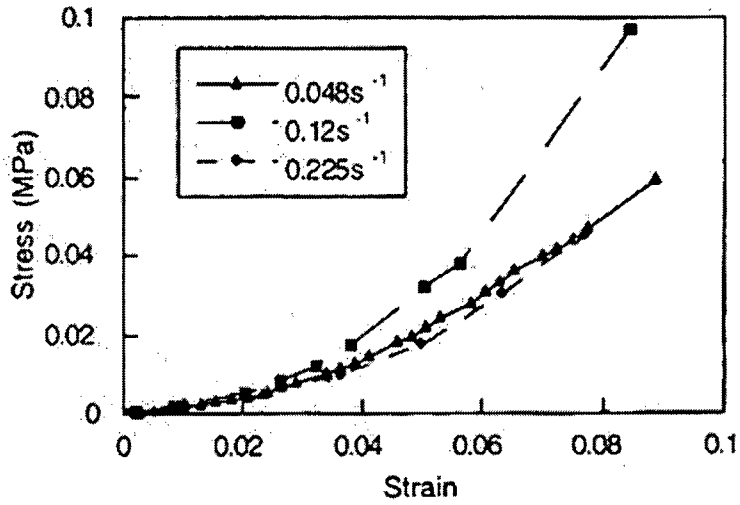

Figure B.1: Stress-strain curves of human spinal cord tissue (Figure from Bilston and Thibault 1992)

Data points were obtained from Figure B.1 at intervals of 0.005 strain and are listed in Table B.1.

Table B.1: Experimental stress-strain data

strain	stress (MPa)
0	0.000
0.005	0.001
0.01	0.003
0.015	0.004
0.02	0.006
0.025	0.007
0.03	0.009
0.035	0.012
0.04	0.015
0.045	0.017
0.05	0.022
0.055	0.026
0.06	0.031
0.065	0.036
0.07	0.040
0.075	0.046
0.08	0.051
0.0848	0.060

These data were fit to the hyperelastic constitutive model as follows. Principal stretch ratios ($\lambda_1, \lambda_2, \lambda_3$) are defined in terms of the principal strains ($\varepsilon_1, \varepsilon_2, \varepsilon_3$).

$$\lambda_1 = \varepsilon_1 + 1$$
$$\lambda_2 = \varepsilon_2 + 1$$
$$\lambda_3 = \varepsilon_3 + 1$$

Strain invariants (I_1, I_2, I_3) are defined as follows:

$$I_1 = \lambda_1^2 + \lambda_2^2 + \lambda_3^2$$
$$I_2 = \lambda_1^2\lambda_2^2 + \lambda_2^2\lambda_3^2 + \lambda_3^2\lambda_1^2$$
$$I_3 = \lambda_1^2\lambda_2^2\lambda_3^2$$

The Ogden form of the strain energy function (U) has been used in finite element models of the spinal cord (Bilston and Thibault 1996; Bilston 1998) and is defined as follows:

$$U = \frac{2\mu}{\alpha^2}(\lambda_1^\alpha + \lambda_2^\alpha + \lambda_3^\alpha - 3) + \frac{1}{d}(J_{elastic} - 1)^2$$

μ, α, and d are material constants, λ_1, λ_2, and λ_3 are principal stretch ratios, and $J_{elastic}$ is the elastic volumetric strain. Total volumetric strain is the change in volume per unit volume. The elastic volumetric strain follows from the total volumetric strain and the thermal volumetric strain.

$$J = \varepsilon_x + \varepsilon_y + \varepsilon_z$$

$$J = J_{elastic} J_{thermal}$$

$$J_{thermal} = (1 + \varepsilon_{thermal})^2$$

where $\varepsilon_{thermal}$ is the follows from the temperature and the coefficient of thermal expansion. This model assumes the material is isotropic and incompressible, or nearly incompressible. The parameter, d, defines the compressibility of the material and was set to zero for full incompressibility. The initial slope of the shear stress-shear strain curve is called the initial shear modulus (μ_o) and it is defined by:

$$\mu_o = \mu$$

The initial bulk modulus (K_o) is defined by:

$$K_o = \frac{2}{d}$$

With the parameter, d, set to zero, the initial bulk modulus is infinite.

For uniaxial loading, the experimental strains (ε_{exp}) are set to equal ε_1; therefore

$$\lambda_1 = \varepsilon_{exp} + 1 = \lambda_{exp}$$

which defined the first principal strain. Since spinal cord tissue is assumed to be incompressible, then

$$I_3 = \lambda_{exp}^2 \lambda_2^2 \lambda_3^2 = 1$$

The other principal strains were assumed to be equal ($\lambda_2 = \lambda_3$). Therefore,

$$1 = \lambda_{exp}^2 \lambda_2^4$$

$$\lambda_2 = \frac{1}{\sqrt{\lambda_{exp}}}$$

Substituting these relationships into the strain energy density,

$$U = \frac{2\mu}{\alpha}\left(\lambda_{exp}^{\alpha} + 2\lambda_{exp}^{-\frac{\alpha}{2}} - 3\right)$$

The uniaxial stress (T) may be calculated as follows:

$$T = \frac{\partial U}{\partial \lambda_{exp}}$$

$$T = \frac{2\mu}{\alpha^2}\left(\alpha\lambda_{exp}^{\alpha-1} + 2\left(\frac{-\alpha}{2}\right)\lambda_{exp}^{-\frac{\alpha}{2}-1}\right)$$

$$T = \frac{2\mu}{\alpha}\left(\lambda_{exp}^{\alpha-1} - \lambda_{exp}^{-\frac{\alpha}{2}-1}\right)$$

Thus the uniaxial stress is a non-linear function of the uniaxial stretch ratio. The initial Young's modulus may be calculated as

$$E = \left.\frac{\partial T}{\partial \lambda_{exp}}\right|_{\lambda_{exp}=1} = 3\mu$$

For the model fit, experimental strains were used along with randomly selected values for μ and α to calculate stresses. The calculated and experimental stresses were compared by squaring their difference, and summing these values. The total sum of the square of the differences was minimized by changing the values of μ and α, using the solver tool in Microsoft Excel. The calculated parameters were μ = 0.09 and α = 29.52, which corresponded to an initial Young's modulus of 0.27 MPa.

Appendix C – Matlab Code

C.1 readnodeleftright.m

```
%This file was created by Carolyn Greaves.
%Input: file containing spinal cord node numbers and co-ordinates
        (x,y,z)
%Purpose: Node numbers are organized by axial level (z value), sagittal
%         side (left or right), and column (ventral, central, dorsal,
%         lateral)
%Output: parameters to be used by following files
%        nventral, ncentral, ndorsal, nlateral - nodes of left side
%        mventral, mcentral, mdorsal, mlateral - nodes of right side
%Following files: loadresults, outputstrain

clear
fid=fopen('cordnodes2.txt','r');
line=fgetl(fid);
line=fgetl(fid);
line=fgetl(fid);
line=fgetl(fid);
coords=zeros(2501,4);

for i=1:125
   for j=1:20
      coords((i-1)*20+j,1:4)=fscanf(fid,'%f  %f %f %f',[1,4]);
   end
   line=fgetl(fid);
   line=fgetl(fid);
   line=fgetl(fid);
end

%read last node
i=i+1;
j=1;
coords((i-1)*20+j,1:4)=fscanf(fid,'%f  %f %f %f',[1,4]);

fclose(fid);

%************************************************
num=coords(:,1);
x=coords(:,2);
y=coords(:,3);
z=coords(:,4);
done=0;
total=0;
[zmin,i]=min(z); %find new minimum z (next z level)
zsort=sort(z);

maxnum=16;
nventral=zeros(1,maxnum);
ndorsal=zeros(1,maxnum);
ncentral=zeros(1,maxnum);
nlat=zeros(1,maxnum);
```

```
mventral=zeros(1,maxnum);
mdorsal=zeros(1,maxnum);
mcentral=zeros(1,maxnum);
mlat=zeros(1,maxnum);
car=1; %increment for number of z values

while done==0; %select z value
   zmin=zsort(1,1); %next z value (-34 to 26)

   j=1;
   ztot=0;
   for i=1:2501 %find all co-ords with same z coord
      if abs(z(i)-zmin)<0.02 %find new z co-ordinate, must be at least
0.02mm greater than last z co-ord
         index(j,1)=i;
         j=j+1; %number of co-ords with same z value = j-1
         ztot=ztot+z(i);
      end
   end
   zval(car,1)=ztot/(j-1); %average z value

   for i=1:(j-1) %select x, y, and node numbers for this z value
      xnew(i,1)=x(index(i,1));
      ynew(i,1)=y(index(i,1));
      numnew(i,1)=num(index(i,1));
   end

   [xsort,in]=sort(xnew); %sort by x
   k=1;
   for i=1:j-1 %select half of co-ords
      if i<=round((j-1)/2) %left half
         xh(i,1)=xnew(in(i),1);
         yh(i,1)=ynew(in(i),1);
         numh(i,1)=numnew(in(i),1);
      else %right half
         xr(k,1)=xnew(in(i),1);
         yr(k,1)=ynew(in(i),1);
         numr(k,1)=numnew(in(i),1);
         k=k+1;
      end
   end


dl=1;
dr=1;
vl=1;
vr=1;
cl=1;
cr=1;
ll=1;
lr=1;
ventral=[0 0 0];
central=[0 0 0];
dorsal=[0 0 0];
lat=[0 0 0];

nums(car,1)=round((j-1)/2);
```

```
maxleft=round((j-1)/2);

for i=1:j-1 %select node - left side of cord
   if i<=round((j-1)/2) %if on left side
      xtemp=xh;
      ytemp=yh;
      numtemp=numh;
      right=0;
      in=i;
   else %if on right side
      xtemp=xr;
      ytemp=yr;
      numtemp=numr;
      right=1;
      in=i-maxleft;
   end
      yrange=max(ytemp)-min(ytemp);
      xrange=max(xtemp)-min(xtemp);
      xmin=min(xtemp);
      xmax=max(xtemp);
      ymin=min(ytemp);
      ymax=max(ytemp);
      ymean=mean(ytemp);
      xmean=mean(xtemp);

   if right==0 %left side equations
      topx=(ytemp(in,1)-ymean)*(xmin-xmax)/(ymax-ymean)+xmax;
      botx=(ytemp(in,1)-ymean)*(xmax-xmin)/(ymean-ymin)+xmax;
      circx=-(xrange*0.55)*sqrt(1-(ytemp(in,1)-
ymean)^2/(yrange*0.25)^2)+xmax;
      if abs(imag(circx))>0
         circx=500;
      end
   else %right side equations
      topx=((ytemp(in,1)-ymean)*(xmax-xmin)+(ymax-ymean)*xmin)/(ymax-
ymean);
      botx=(ytemp(in,1)-ymean)*(xmax-xmin)/(ymin-ymean)+xmin;
      circx=(xrange*0.4)*sqrt(1-(ytemp(in,1)-
ymean)^2/(yrange*0.25)^2)+xmin;
      if abs(imag(circx))>0
         circx=-500;
      end
   end %end of equations

    if ytemp(in,1)>=ymean %choose top half
       if right==0 %LEFT side
          if xtemp(in,1)>circx
            central(cl,1)=numtemp(in,1);
            central(cl,2)=xtemp(in,1);
            central(cl,3)=ytemp(in,1);
            cl=cl+1;
          elseif xtemp(in,1)<topx
             lat(ll,1)=numtemp(in,1);
             lat(ll,2)=xtemp(in,1);
             lat(ll,3)=ytemp(in,1);
             ll=ll+1;
          else
```

```
            dorsal(dl,1)=numtemp(in,1);
            dorsal(dl,2)=xtemp(in,1);
            dorsal(dl,3)=ytemp(i,1);
            dl=dl+1;
        end
      else %RIGHT side
         if xtemp(in,1)<circx
           central(cr,1+3)=numtemp(in,1);
           central(cr,2+3)=xtemp(in,1);
           central(cr,3+3)=ytemp(in,1);
           cr=cr+1;
         elseif xtemp(in,1)>topx
            lat(lr,1+3)=numtemp(in,1);
            lat(lr,2+3)=xtemp(in,1);
            lat(lr,3+3)=ytemp(in,1);
            lr=lr+1;
         else
            dorsal(dr,1+3)=numtemp(in,1);
            dorsal(dr,2+3)=xtemp(in,1);
            dorsal(dr,3+3)=ytemp(in,1);
            dr=dr+1;
         end
     end
else %start 'if less than ymean group'
   if right==0 %LEFT side
      if xtemp(in,1)>circx
         central(cl,1)=numtemp(in,1);
         central(cl,2)=xtemp(in,1);
         central(cl,3)=ytemp(in,1);
         cl=cl+1;
      elseif xtemp(i,1)<botx
         lat(ll,1)=numtemp(in,1);
         lat(ll,2)=xtemp(in,1);
         lat(ll,3)=ytemp(in,1);
         ll=ll+1;
      else
         ventral(vl,1)=numtemp(in,1);
         ventral(vl,2)=xtemp(in,1);
         ventral(vl,3)=ytemp(in,1);
         vl=vl+1;
      end
   else %RIGHT side
       if xtemp(in,1)<circx
         central(cr,1+3)=numtemp(in,1);
         central(cr,2+3)=xtemp(in,1);
         central(cr,3+3)=ytemp(in,1);
         cr=cr+1;
      elseif xtemp(in,1)>botx
         lat(lr,1+3)=numtemp(in,1);
         lat(lr,2+3)=xtemp(in,1);
         lat(lr,3+3)=ytemp(in,1);
         lr=lr+1;
      else
         ventral(vr,1+3)=numtemp(in,1);
         ventral(vr,2+3)=xtemp(in,1);
         ventral(vr,3+3)=ytemp(in,1);
         vr=vr+1;
```

```
      end
    end %end of side selection
 end %end of 'greater than or less than ymean' selection


end
%*************************************************************************
%Option to output nodes at each level to verify column designations
  %  car-1
  %  mean(yh)
  %  input('ok?');
  %
plot(ventral(:,2),ventral(:,3),'+',dorsal(:,2),dorsal(:,3),'d',lat(:,2)
,lat(:,3),'+',central(:,2),central(:,3),'*');
  %  plot(ventral(1:vr-1,5),ventral(1:vr-1,6),'+',dorsal(1:dr-
1,5),dorsal(1:dr-1,6),'d',lat(1:lr-1,5),lat(1:lr-1,6),'+',central(1:cr-
1,5),central(1:cr-1,6),'*');
  %
plot([ventral(:,2);ventral(:,5)],[ventral(:,3);ventral(:,6)],'+',[dorsa
l(:,2);dorsal(:,5)],[dorsal(:,3);dorsal(:,6)],'d',[lat(:,2);lat(:,5)],[
lat(:,3);lat(:,6)],'+',[central(:,2);central(:,5)],[central(:,3);centra
l(:,6)],'*');
  %  legend('ventral','dorsal','lat','cent');
%*************************************************************************
dr=dr-1;
dl=dl-1;
vr=vr-1;
vl=vl-1;
cr=cr-1;
cl=cl-1;
ll=ll-1;
lr=lr-1;

    if
(((dr>maxnum)|(dl>maxnum))|((vr>maxnum)|(vl>maxnum))|((cr>maxnum)|(cl>m
axnum))|((lr>maxnum)|(ll>maxnum)))
       car
       lr
       ll
    end
for i=1:maxnum
    if i<vl
        ventralrow(1,i)=ventral(i,1);
    else
        ventralrow(1,i)=0;
     end
    if i<vr
        ventralrowr(1,i)=ventral(i,4);
    else
        ventralrowr(1,i)=0;
    end
    if i<dl
        dorsalrow(1,i)=dorsal(i,1);
    else
        dorsalrow(1,i)=0;
     end
    if i<dr
```

```
        dorsalrowr(1,i)=dorsal(i,4);
    else
        dorsalrowr(1,i)=0;
    end
    if i<ll
        latrow(1,i)=lat(i,1);
    else
        latrow(1,i)=0;
     end
    if i<lr
        latrowr(1,i)=lat(i,4);
    else
        latrowr(1,i)=0;
    end
    if i<cl
        centralrow(1,i)=central(i,1);
    else
        centralrow(1,i)=0;
    end
   if i<cr
        centralrowr(1,i)=central(i,4);
    else
        centralrowr(1,i)=0;
    end

end


nventral=[nventral;ventralrow]; %LEFT nodes
ndorsal=[ndorsal;dorsalrow];
ncentral=[ncentral;centralrow];
nlat=[nlat;latrow];

mventral=[mventral;ventralrowr]; %RIGHT nodes
mdorsal=[mdorsal;dorsalrowr];
mcentral=[mcentral;centralrowr];
mlat=[mlat;latrowr];

car=car+1;
if car==43
   done=1;
else
   [b c]=size(zsort);
   zsort=zsort((j-1):b,1);

end

end

nventral=nventral(3:43,:);
ndorsal=ndorsal(3:43,:);
ncentral=ncentral(3:43,:);
nlat=nlat(3:43,:);

mventral=mventral(3:43,:);
mdorsal=mdorsal(3:43,:);
mcentral=mcentral(3:43,:);
```

```
mlat=mlat(3:43,:);

zval=zval(2:42,1);
```

C.2 loadresults.m

```
%This file was created by Carolyn Greaves
%Input: File containing spinal cord element strains
%Purpose: Mean strains are calculated for each of five columns at 41
%         axial levels
%Output: Mean strains xst, yst, zst, xyst, yzst, xzst
%Previous files:  readnodeleftright
%Following files: outputstrain

%fid=fopen('cont_c5_estrain.txt','r');
%fid=fopen('dist_col7_estrain.txt','r');
fid=fopen('shear_8_estrain.txt','r');

for i=1:14
   line=fgetl(fid);
end


for i=1:640
   for k=1:3
      for j=1:8
         strains((i-1)*24+(k-1)*8+j,1:7)=fscanf(fid,'%f  %f %f %f %f %f %f',[1,7]);
      end
      if k<=2
         for j=1:4
            line=fgetl(fid);
         end
      end
   end
   for j=1:14
      line=fgetl(fid);
   end

end

%node, x, y, z, xy, yz, xz

fclose(fid);

sorts=sortrows(strains,1);
k=1;
strain=zeros(2501,7);
tot=zeros(1,6);
numb=0;
for i=1:15359
   tot=tot+sorts(i,2:7);
   numb=numb+1;
   if sorts(i,1)~=sorts(i+1,1);
      if numb~=0;
         strain(k,1)=sorts(i,1);
         strain(k,2:7)=tot/numb;
```

```
      else
         strain(k,1:7)=sorts(k,1:7);
      end
      k=k+1;
      numb=0;
      tot=zeros(1,6);
   end
end
tot=tot+sorts(15360,2:7);
numb=numb+1;
strain(k,1)=sorts(i,1);
strain(k,2:7)=tot/numb;
strains=strain;

for i=1:2501 %calculate von mises strain
   matrix=[strains(i,2) strains(i,5) strains(i,7);strains(i,5)
strains(i,3) strains(i,6);strains(i,7) strains(i,6) strains(i,4)];
   eigs=eig(matrix);
   vm(i)=sqrt(((eigs(1)-eigs(2))^2+(eigs(2)-eigs(3))^2+(eigs(1)-
eigs(3))^2)/2);
end

strains=[strains vm'];

v=1;
d=1;
c=1;
ll=1;
lr=1;
vmst=zeros(41,5);
xst=zeros(41,5);
yst=zeros(41,5);
zst=zeros(41,5);
xyst=zeros(41,5);
yzst=zeros(41,5);
xzst=zeros(41,5);
for i=1:41 %41 z values
    for j=1:maxnum %select first node in the region
        vdone=0;
        ddone=0;
        cdone=0;
        lldone=0;
        vrdone=0;
        drdone=0;
        crdone=0;
        lrdone=0;
        for k=1:2501
           if ((nventral(i,j)~=0 & (strains(k,1)==nventral(i,j))) &
vdone==0) %LEFT NODES
              xs(v,1)=strains(k,2);
              ys(v,1)=strains(k,3);
              zs(v,1)=strains(k,4);
              xys(v,1)=strains(k,5);
              yzs(v,1)=strains(k,6);
              xzs(v,1)=strains(k,7);
              vms(v,1)=strains(k,8);
              v=v+1;
```

```
            vdone=1;
        end
        if ((ndorsal(i,j)~=0 & (strains(k,1)==ndorsal(i,j))) &
ddone==0)
            xs(d,2)=strains(k,2);
            ys(d,2)=strains(k,3);
            zs(d,2)=strains(k,4);
            xys(d,2)=strains(k,5);
            yzs(d,2)=strains(k,6);
            xzs(d,2)=strains(k,7);
            vms(d,2)=strains(k,8);
            d=d+1;
            ddone=1;
        end
        if ((ncentral(i,j)~=0 & (strains(k,1)==ncentral(i,j))) &
cdone==0)
            xs(c,3)=strains(k,2);
            ys(c,3)=strains(k,3);
            zs(c,3)=strains(k,4);
            xys(c,3)=strains(k,5);
            yzs(c,3)=strains(k,6);
            xzs(c,3)=strains(k,7);
            vms(c,3)=strains(k,8);
            c=c+1;
            cdone=1;
        end
        if ((nlat(i,j)~=0 & (strains(k,1)==nlat(i,j))) & lldone==0)
            xs(ll,4)=strains(k,2);
            ys(ll,4)=strains(k,3);
            zs(ll,4)=strains(k,4);
            xys(ll,4)=strains(k,5);
            yzs(ll,4)=strains(k,6);
            xzs(ll,4)=strains(k,7);
            vms(ll,4)=strains(k,8);
            ll=ll+1;
            lldone=1;
        end

        if ((mventral(i,j)~=0 & (strains(k,1)==mventral(i,j))) &
vrdone==0) %RIGHT NODES
            xs(v,1)=strains(k,2);
            ys(v,1)=strains(k,3);
            zs(v,1)=strains(k,4);
            xys(v,1)=strains(k,5);
            yzs(v,1)=strains(k,6);
            xzs(v,1)=strains(k,7);
            vms(v,1)=strains(k,8);
            v=v+1;
            vrdone=1;
        end
        if ((mdorsal(i,j)~=0 & (strains(k,1)==mdorsal(i,j))) &
drdone==0)
            xs(d,2)=strains(k,2);
            ys(d,2)=strains(k,3);
            zs(d,2)=strains(k,4);
            xys(d,2)=strains(k,5);
            yzs(d,2)=strains(k,6);
```

```
                xzs(d,2)=strains(k,7);
                vms(d,2)=strains(k,8);
                d=d+1;
                drdone=1;
            end
            if ((mcentral(i,j)~=0 & (strains(k,1)==mcentral(i,j))) &
crdone==0)
                xs(c,3)=strains(k,2);
                ys(c,3)=strains(k,3);
                zs(c,3)=strains(k,4);
                xys(c,3)=strains(k,5);
                yzs(c,3)=strains(k,6);
                xzs(c,3)=strains(k,7);
                vms(c,3)=strains(k,8);
                c=c+1;
                crdone=1;
            end
            if ((mlat(i,j)~=0 & (strains(k,1)==mlat(i,j))) & lrdone==0)
                xs(lr,5)=strains(k,2);
                ys(lr,5)=strains(k,3);
                zs(lr,5)=strains(k,4);
                xys(lr,5)=strains(k,5);
                yzs(lr,5)=strains(k,6);
                xzs(lr,5)=strains(k,7);
                vms(lr,5)=strains(k,8);
                lr=lr+1;
                lrdone=1;
            end

        end %end of k loop
    end %end of j loop for node in the region

    vdcl=[v-1 d-1 c-1 ll-1 lr-1];
    for k=1:5
        xst(i,k)=mean(abs(xs(1:vdcl(k),k))); %substitute 'max' for
        xsd(i,k)=std(xs(1:vdcl(k),k));       %'mean' to find max
        yst(i,k)=mean(abs(ys(1:vdcl(k),k)));  %absolute nodal strain
        ysd(i,k)=std(ys(1:vdcl(k),k));
        zst(i,k)=mean(abs(zs(1:vdcl(k),k)));
        zsd(i,k)=std(zs(1:vdcl(k),k));
        xyst(i,k)=mean(abs(xys(1:vdcl(k),k)));
        xysd(i,k)=std(xys(1:vdcl(k),k));
        yzst(i,k)=mean(abs(yzs(1:vdcl(k),k)));
        yzsd(i,k)=std(yzs(1:vdcl(k),k));
        xzst(i,k)=mean(abs(xzs(1:vdcl(k),k)));
        xzsd(i,k)=std(xzs(1:vdcl(k),k));
        vmst(i,k)=mean(abs(vms(1:vdcl(k),k)));
        vmsd(i,k)=std(vms(1:vdcl(k),k));
    end
    v=1;
    d=1;
    c=1;
    ll=1;
    lr=1;
end %end of i loop

figure(1);
```

```
plot(zval+3.915,xst(:,1),'b',zval+3.915,xst(:,2),'g',zval+3.915,xst(:,3
),'r',zval+3.915,xst(:,4),'c',zval+3.915,xst(:,5),'m',[5.085 5.085],[-
0.1 0.1],'k--',[-5.085 -5.085],[-0.1 0.1],'k--')
legend('ventral','dorsal','central','left lateral','right lateral');
title('X Component of Strain (Lateral) for a Contusion Injury');
grid on;
xlabel('Caudal-Rostral Distance From C5 (mm)');
ylabel('Mean Strain');
axis([-30 30 -0.07 0.07]);

figure(2);
plot(zval+3.915,yst(:,1),'b',zval+3.915,yst(:,2),'g',zval+3.915,yst(:,3
),'r',zval+3.915,yst(:,4),'c',zval+3.915,yst(:,5),'m',[5.085 5.085],[-
0.1 0.1],'k--',[-5.085 -5.085],[-0.1 0.1],'k--')
legend('ventral','dorsal','central','left lateral','right lateral');
title('Y Component of Strain (A-P) for a Contusion Injury');
xlabel('Caudal-Rostral Distance From C5 (mm)');
ylabel('Mean Strain');
grid on;
axis([-30 30 -0.12 0.07]);

figure(3);
plot(zval+3.915,zst(:,1),'b',zval+3.915,zst(:,2),'g',zval+3.915,zst(:,3
),'r',zval+3.915,zst(:,4),'c',zval+3.915,zst(:,5),'m',[5.085 5.085],[-
0.1 0.1],'k--',[-5.085 -5.085],[-0.1 0.1],'k--')
legend('ventral','dorsal','central','left lateral','right lateral');
title('Z Component of Strain (Axial) for a Contusion Injury');
grid on;
xlabel('Caudal-Rostral Distance From C5 (mm)');
ylabel('Mean Strain');
axis([-30 30 -0.07 0.07]);
```

C.3 outputstrain.m

```
%This file was created by Carolyn Greaves
%Input: Mean (and standard deviation) column strains
%Purpose: Output mean strains to a text file
%Output:  Mean column strains and standard deviations
%Previous files:  readnodeleftright, loadresults

%fid=fopen('cont_c5_mean.txt','w');
%fid=fopen('dist_col7_mean.txt','w');
fid=fopen('shear_8_mean.txt','w');
fprintf(fid,'z vonmises            x              y              z
             xy             yz             xz\n');
fprintf(fid,'  ventral  dorsal   central  leftlateral rightlateral
   ventral  dorsal   central  leftlateral rightlateral   ventral
   dorsal   central  leftlateral rightlateral   ventral  dorsal
   central  leftlateral rightlateral   ventral  dorsal   central
   leftlateral rightlateral   ventral  dorsal   central  leftlateral
   rightlateral   ventral  dorsal   central  leftlateral
   rightlateral\n');
for i=1:41
   fprintf(fid,'%f   %f %f %f %f %f %f %f %f %f %f %f %f %f %f %f %f
               %f %f %f %f %f %f %f %f %f %f %f %f %f %f %f %f %f %f
```

```
   %f\n',zval(i,1)+3.915,vm(i,1),vm(i,2),vm(i,3),vm(i,4),vm(i,5),xst(i,
1),xst(i,2),xst(i,3),xst(i,4),xst(i,5),yst(i,1),yst(i,2),yst(i,3),yst(i
,4),yst(i,5),zst(i,1),zst(i,2),zst(i,3),zst(i,4),zst(i,5),xyst(i,1),xys
t(i,2),xyst(i,3),xyst(i,4),xyst(i,5),yzst(i,1),yzst(i,2),yzst(i,3),yzst
(i,4),yzst(i,5),xzst(i,1),xzst(i,2),xzst(i,3),xzst(i,4),xzst(i,5));
end
fclose(fid);

%fid=fopen('cont_c5_sd.txt','w');
%fid=fopen('dist_col7_sd.txt','w');
fid=fopen('shear_8_sd.txt','w');
fprintf(fid,'z x                y               z               xy
      yz              xz\n');
fprintf(fid,'  ventral  dorsal   central  leftlateral rightlateral
   ventral  dorsal   central  leftlateral rightlateral   ventral
   dorsal   central  leftlateral rightlateral   ventral  dorsal
   central  leftlateral rightlateral   ventral  dorsal   central
   leftlateral rightlateral   ventral  dorsal   central  leftlateral
   rightlateral\n');
for i=1:41
   fprintf(fid,'%f   %f %f %f %f %f %f %f %f %f %f %f %f %f %f %f %f %f
%f %f %f %f %f %f %f %f %f %f %f %f %f
   %f\n',zval(i,1)+3.915,xsd(i,1),xsd(i,2),xsd(i,3),xsd(i,4),xsd(i,5),y
sd(i,1),ysd(i,2),ysd(i,3),ysd(i,4),ysd(i,5),zsd(i,1),zsd(i,2),zsd(i,3),
zsd(i,4),zsd(i,5),xysd(i,1),xysd(i,2),xysd(i,3),xysd(i,4),xysd(i,5),yzs
d(i,1),yzsd(i,2),yzsd(i,3),yzsd(i,4),yzsd(i,5),xzsd(i,1),xzsd(i,2),xzsd
(i,3),xzsd(i,4),xzsd(i,5));
end
fclose(fid);
```